AD-A034 535 DAVID W TAYLOR NAVAL SHIP RESEARCH AND DEVELOPMENT CE--ETC F/G 20/4
LOW FROUDE NUMBER HYDRODYNAMIC PERFORMANCE OF A FLAT PLATE HYDR--ETC(U)
DEC 76 M B WILSON, J R KELLEY

UNCLASSIFIED SPD-743-01 NL

1 OF 2
AD
A034535

DAVID W. TAYLOR NAVAL SHIP
RESEARCH AND DEVELOPMENT CENTER
Bethesda, Md. 20084

12

LOW FROUDE NUMBER HYDRODYNAMIC PERFORMANCE OF A FLAT PLATE HYDROFOIL

by

Michael B. Wilson

and

Jerry R. Kelley

SHIP PERFORMANCE DEPARTMENT

DEPARTMENTAL REPORT

December 1976 SPD-743-01

MAJOR DTNSRDC ORGANIZATIONAL COMPONENTS

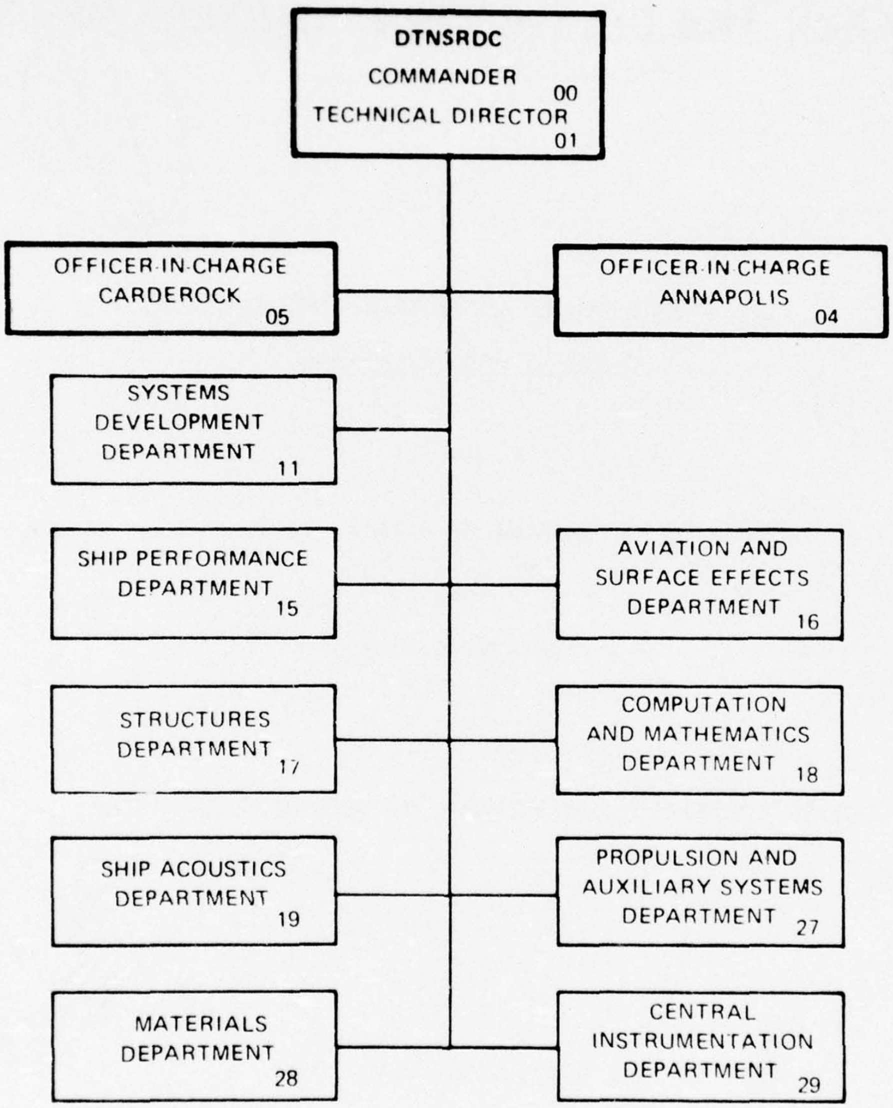

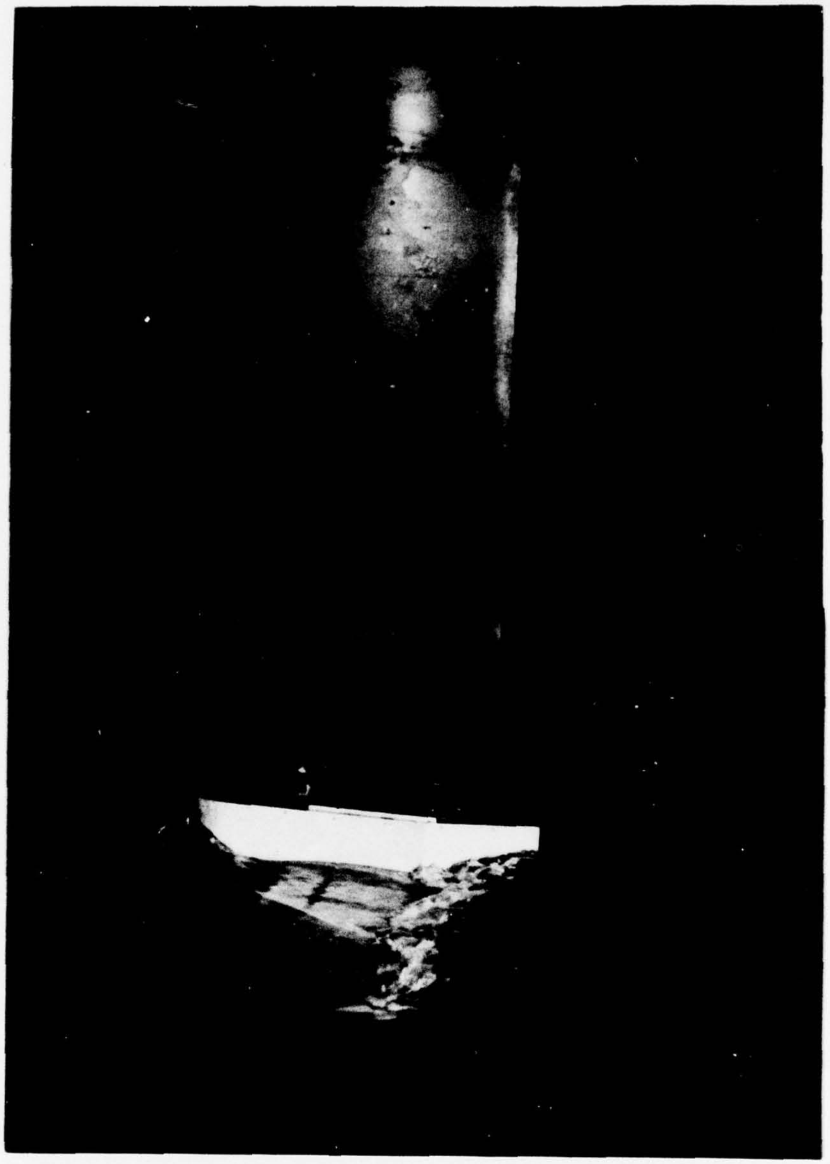

Flat plate hydrofoil mounted on its strut-shroud support, moving at chord Froude number $F_c = 0.5$ at submergence ratio $f/c = 0.25$ and angle of attack $\alpha = 6^o$. The shroud shown piercing through the free surface at this submergence is 6.125 inches(0.1556m) wide compared with the 8-foot (2.438m) span of the hydrofoil.

UNCLASSIFIED

SECURITY CLASSIFICATION OF THIS PAGE (When Data Entered)

REPORT DOCUMENTATION PAGE		READ INSTRUCTIONS BEFORE COMPLETING FORM
1. REPORT NUMBER SPD-743-01	2. GOVT ACCESSION NO. Departmental rept.	3. RECIPIENT'S CATALOG NUMBER
4. TITLE (and Subtitle) LOW FROUDE NUMBER HYDRODYNAMIC PERFORMANCE OF A FLAT PLATE HYDROFOIL		5. TYPE OF REPORT & PERIOD COVERED
		6. PERFORMING ORG. REPORT NUMBER
7. AUTHOR(s) Michael B. Wilson Jerry R. Kelley		8. CONTRACT OR GRANT NUMBER(s) 1-1861-014-44 1-1102-003-44 1-1500-100-13
9. PERFORMING ORGANIZATION NAME AND ADDRESS David W. Taylor Naval Ship R&D Center Bethesda, Maryland 20084		10. PROGRAM ELEMENT, PROJECT, TASK AREA & WORK UNIT NUMBERS Task Areas SS H15002 and SF 43 421 202
11. CONTROLLING OFFICE NAME AND ADDRESS Advanced Naval Vehicles Concepts Eval. Project and Naval Sea Systems Command, Washington, D.C. 20350		12. REPORT DATE December 1976
		13. NUMBER OF PAGES 110
14. MONITORING AGENCY NAME & ADDRESS (if different from Controlling Office) 112p.		15. SECURITY CLASS. (of this report) UNCLASSIFIED
		15a. DECLASSIFICATION/DOWNGRADING SCHEDULE
16. DISTRIBUTION STATEMENT (of this Report) APPROVED FOR PUBLIC RELEASE: DISTRIBUTION UNLIMITED		
17. DISTRIBUTION STATEMENT (of the abstract entered in Block 20, if different from Report) SSH15, F43421		
18. SUPPLEMENTARY NOTES SSH15002, SF43421202		
19. KEY WORDS (Continue on reverse side if necessary and identify by block number) Hydrofoil, Low Froude Number, Lift, Drag, Moment, Center of Pressure, Near-Surface Effect, Lift-Dependent Drag 740,000 - 5,200,000.		
20. ABSTRACT (Continue on reverse side if necessary and identify by block number) Results of towing tank experiments are presented for lift, drag, moment, and center of pressure of an aspect ratio 4, rectangular planform, 5.21 % thick, flat plate hydrofoil attached to a large strut and pod and operated beneath the free surface of water. The nominal range of the chord Froude number was 0.5 to 3.5 with corresponding chord Reynolds numbers of 0.74×10^6 to 5.2×10^6. Tests included seven foil submergence depths ranging from 0.25 to 3.5 chord lengths, and foil angles of attack varying		

DD FORM 1 JAN 73 1473 EDITION OF 1 NOV 65 IS OBSOLETE
S/N 0102-014-6601

i

UNCLASSIFIED

SECURITY CLASSIFICATION OF THIS PAGE (When Data Entered)

389 694

20. Abstract - Continued

from 0 to 8 degrees.

These unique data help to fill an important gap in our experimental knowledge of near-surface, low speed hydrofoil performance. This speed range has only recently attracted attention because of the large sizes of projected hydrofoil lift systems. The present experiments indicate that there are significant changes in lift and drag for operation at shallow and moderate submergences in the low chord Froude number range, especially in the vicinity of 0.75 to 1.5.

A prediction of the residual drag coefficients for an 18-foot-chord hydrofoil operating at constant lift shows that the wavemaking drag is significant and that the trend of the increase in the residual drag at Froude numbers ranging from 3.5 down to 1.75 appears to be roughly parallel to the trend of the induced drag alone. However, the magnitudes of the residual drag coefficients are rather large, and there are indications that interference wave drag due to the presence of a strut and a pod are an important feature of the low speed drag variation.

TABLE OF CONTENTS

LIST OF FIGURES

Page

Page

LIST OF TABLES

NOTATION

A	Aspect ratio = $b^2/S = b/c$ (rectangular planform)
b	Hydrofoil span
c	Hydrofoil chord
C_D	Hydrofoil drag coefficient = $D/\frac{1}{2}\rho U^2 S$
C_{D_f}	Friction drag coefficient based on S = $D_f/\frac{1}{2}\rho U^2 S$
C_{D_i}	Induced drag coefficient including biplane effect = $D_i/\frac{1}{2}\rho U^2 S$
$(C_{D_i} + C_W)$	Total lift-dependent (inviscid) drag coefficient; induced + biplane + wavemaking
$C_{D_{visc}}$	Total viscous drag coefficient
$C_{D_{vp}}$	Viscous pressure drag coefficient (form drag)
C_L	Hydrofoil lift coefficient = $L/\frac{1}{2}\rho U^2 S$
C_{L_α}	Lift-curve slope = $(\partial C_L/\partial\alpha)_{\alpha=o}$
C_M	Moment coefficient (about quarter-chord) = $M_{(c/4)}/\frac{1}{2}\rho U^2 Sc$
C_R	Residual drag coefficient = $D_R/\frac{1}{2}\rho U^2 S$
C_W	Wavemaking drag coefficient = $D_W/\frac{1}{2}\rho U^2 S$
D	Total drag force on model hydrofoil
f	Depth of submergence to quarter-chord of foil
F_c	Chord Froude number = $U/\sqrt{gc}$
F_f	Depth Froude number = $U/\sqrt{gf}$
g	Acceleration of gravity

L	Total lift force on hydrofoil
$M_{(c/4)}$	Pitching moment about hydrofoil quarter-chord (positive nose up)
R_c	Reynolds number based on foil chord = Uc/ν
S	Foil planform area = bc
t	Foil thickness
U	Freestream velocity
V_K	Freestream velocity in knots
X	Force measured along foil chord line; $X_{total} = X_1 + X_2$ (see Figure 2)
x_{cp}	Distance to foil center of pressure, measured from leading edge
Y	Force measured perpendicular to foil chord line; $Y_{total} = Y_1 + Y_2$ (see Figure 2)
α	Geometric angle of attack
α_o	Angle of attack for zero lift
δ	Glauert planform factor (=0.03 for a rectangular planform with A = 4)
λ	Ratio of depth of submergence-to-semi span = $f/(0.5b)$
ν	Kinematic viscosity
ρ	Water density
$\sigma(\lambda)$	Prandtl biplane factor for induced drag

ABSTRACT

Results of towing tank experiments are presented for lift, drag, moment, and center of pressure of an aspect ratio 4, rectangular planform, 5.21 percent thick, flat plate hydrofoil attached to a large strut and pod and operated beneath the free surface of water. The nominal range of the chord Froude number was 0.5 to 3.5 with corresponding chord Reynolds numbers of 0.74×10^6 to 5.2×10^6. Tests included seven foil submergence depths ranging from 0.25 to 3.5 chord lengths, and foil angles of attack varying from 0 to 8 degrees.

These unique data help to fill an important gap in our experimental knowledge of near-surface, low speed hydrofoil performance. This speed range has only recently attracted attention because of the large sizes of projected hydrofoil lift systems. The present experiments indicate that there are significant changes in lift and drag for operation at shallow and moderate submergences in the low chord Froude number range, especially in the vicinity of 0.75 to 1.5.

A prediction of the residual drag coefficients for an 18-foot-chord hydrofoil operating at constant lift shows that the wavemaking drag is significant and that the trend of the increase in the residual drag at Froude numbers ranging from 3.5 down to 1.75 appear to be roughly parallel to the trend of the induced drag alone. However, the magnitudes of the residual drag coefficients are rather large, and there are indications that interference wave drag due to the presence of a strut and a pod are an important feature of the low speed drag variation.

ADMINISTRATIVE INFORMATION

This work was sponsored in part by the Advanced Naval Vehicles Concepts Evaluation (ANVCE) Project, Task Area SS H15002, Work Units 1-1861-014-44 and 1-1102-003-44, and by the Naval Sea Systems Command, Task Area SF 43 421 202, Work Unit 1-1500-100-13.

INTRODUCTION

As the displacement and size of proposed subcavitating hydrofoil-supported ships have grown larger and larger in recent years, the physical sizes of the foils required for these designs have naturally also grown considerably. For typical speeds near takeoff, at around 20 to 25 knots, the corresponding chord Froude number range of interest has shifted to values lower than are available in the existing data base of hydrofoil hydrodynamic characteristics. Chord Froude numbers approaching $F_c = 2$ or 1.5 are now not unreasonable values to consider as extremes for takeoff performance of very large hydrofoil systems.

The distinctive features of the hydrodynamic forces on a hydrofoil traveling near a free surface at low Froude numbers are a rapid rise in the curve of induced plus wavemaking drag coefficient accompanied by a dip in the lift coefficient. These properties had been revealed long ago by calculations using linearized potential theory as presented for example by Nishiyama, summarized in Reference 1, by Wu[2] and by Breslin.[3] For instance, Figure 1 displays the predicted behavior for lift and total inviscid drag coefficients, as determined in computations by Nishiyama[4] for a rectangular planform wing with a foil submergence ratio $f/c = 0.59$. In these plots, the C_L is the resultant lift coefficient for the foil operating in the presence of the free surface, C_{L_∞} is the reference lift coefficient for the same foil in an unbounded flow, and $(C_{D_i} + C_W)$ is the total induced drag (including biplane effect) plus the wavemaking drag coefficient.

The general trends of these predicted features have been partially verified experimentally down to $F_c = 1$ at $f/c = 0.84$ for an aspect ratio 10 hydrofoil as pointed out by Breslin[3] in comparing his theory with the results of tests on rectangular planform hydrofoils presented by Wadlin, et al.[5] It may be noted that the low speed end of the test results reported in Reference 5 are somewhat suspect because the section drag coefficients (total viscous drag) are clearly smaller than the turbulent flat plate friction line. Guaranteeing that the measured friction drag always falls on the same transition curve between laminar and predominately turbulent flow is a notoriously troublesome experimental problem for experiments conducted at Reynolds numbers in the range 5×10^5 to 6×10^6 without turbulence stimulation.

Most hydrofoil experiments are designed to cover relatively high Froude numbers. For example, the extensive hydrofoil test program reported on by Feldman[6] produced data for the combination of a foil plus strut(s) for rectangular planform hydrofoils having six different aspect ratios, at six depths of submergence, with chord Froude numbers ranging between 2.06 and 9.63. More recently, Layne[7] has performed experiments on tapered planform hydrofoils similar to the forward foil of the PCH having two different NACA section shapes. The chord Froude number range covered was 7.44 to 23.2.

As far as is known, there exists no systematic data for hydrofoil performance at speeds spanning the low Froude number range where the most dramatic speed-dependent changes occur. The experiments reported on here have been planned to provide an initial body of information specifically for the low Froude number speed regime.

DESCRIPTION OF MODEL AND APPARATUS

HYDROFOIL

The hydrofoil model built for these experiments was made intentionally simple for ease of manufacture and low cost. It consisted of a rectangular planform, flat plate of 6061-T6 aluminum having a thickness of 1.25 inches (0.03175 m) with a 0.625 inch (0.0159 m) leading edge radius and a wedge-shaped afterportion tapered to a sharp trailing edge having an included angle of 21.8 degrees. With a span of 8 feet (2.438 m), the plate had simple squared-off tips. The 2 foot (0.6096 m) chord length was chosen to provide the desired Froude number range using the useful speed capability of the towing carriage, and it allowed reasonable Reynolds numbers (with turbulence stimulation) at the lowest speeds, while at the same time keeping the span at a manageable size. It also limited the magnitude of the largest expected lift forces to values that could be handled with available block gauges. The foil surface had a rolling mill finish, and the regions near the machined leading and trailing edges were smoothed with emery cloth. Table 1 summarizes the main features of the flat plate hydrofoil geometry.

In order to insure fully turbulent boundary layer flow throughout the speed range, wire trips were placed at the nose of the foil, extending from tip to tip across the entire span on both the top and bottom sides. It was felt that the turbulence stimulators should be located somewhat forward of the most likely position of flow separation which for an isolated circular cylinder is known to occur at about 81 degrees along the arc of the surface.[8] The two trip wires were placed nominally at ± 60 degrees along the nose radius, or at a distance of 0.312 inch (0.00794 m) back from the leading edge. The standard criterion for sizing a turbulence trip wire called for a wire diameter of about 0.011 inch (0.28 mm). This was an odd size and since there was a large quantity of 0.012 inch (0.305 mm) piano wire available, the latter was the best choice. Lengths of the wires were fastened with screws at the foil tips, and each one was held down by counter sunk screws at two points one-fourth of the span inboard from each tip. With these few connection points, each wire was free to strum. This appeared to help its effectiveness.

BLOCK GAUGE DYNAMOMETER AND INSTRUMENTATION

It was decided to measure the total forces and moment directly, rather than having to run the test matrix twice in order to determine

TABLE 1 - FLAT PLATE HYDROFOIL GEOMETRY

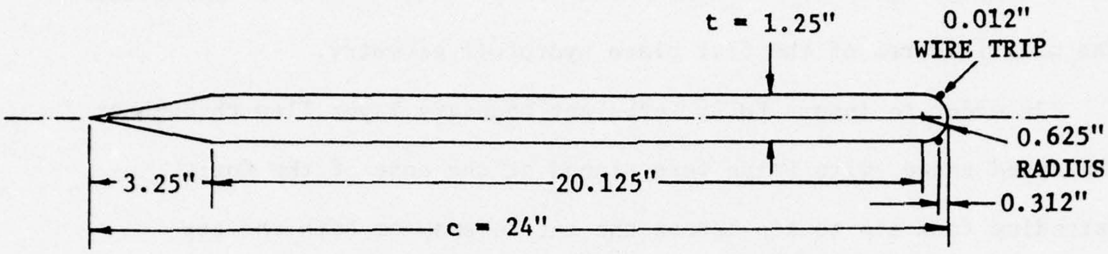

Aspect ratio	A = 4
Thickness ratio	t/c = 0.05208
Span	b = 8 ft = 2.438 m
Chord	c = 2 ft = 0.6096 m
Planform area	S = 16 ft^2 = 1.486 m^2
Wetted area (excluding portion covered by bottom connecting plate)	31.68 ft^2 = 2.943 m^2
Ratio of foil wetted area to planform area	1.98
Cross section area moment of inertia about centerline	I = 3.468 $inch^4$ = 1.44 x 10^{-6} m^4
Turbulence stimulator wires	diameter = 0.012 inch = 0.305 mm

the strut tare forces. This was accomplished by positioning the dynamometer between the foil and the base of the supporting strut. A system of four, standard 4-inch DTNSRDC block gauges was arranged such that two 1000-pound gauges and two 200-pound gauges were used for the Y-force and X-force measurements, respectively. To help reduce the influence of unmeasured moments in this system, pin joint hinges separated each of the pairs of stacked X- and Y-force gauges. The hinges were located chordwise so that the line of force of each of the Y-force gauges was equidistant from the quarter-chord of the foil. Since the expected center of pressure of a thin, uncambered, and unswept foil is at the quarter-chord, each Y-force gauge could be expected to share about half the vertical force. The entire assemblage was bounded below by a 1.25 inch (0.03175 m) thick, 5.25 inch (0.1334 m) wide bottom connecting plate that was bolted firmly to the hydrofoil at midspan, and was bounded above by a similar 1.25 inch (0.03175 m) thick upper connecting plate that in turn was attached to the base of the standard 9-foot (2.743 m) long strut. The robust nature of the connecting plates gave the entire block gauge system a virtual stiffness that exceeded the stiffness properties of the individual block gauges. Figure 2 is a schematic of the main parts of the assembled block gauge dynamometer.

Instrumentation for the collection of the four channels of force data consisted of ENDEVCO signal conditioners for the differential reluctance block gauges and DANA amplifiers. The voltage output from the amplifiers was digitized using ANALOGIC analog-to-digital converters. All the data were processed on-line using an Interdata Model 4 computer, with automatic data storage on magnetic tape using a Tri-Data Cartifile recorder. Hard copies of the data were available from a teletype machine which was used interactively to carry out the data collection procedure.

SHROUD

A sheet metal shroud fabricated from 0.25 inch (6.35 mm) thick aluminum enclosed the block gauge assemblage and was bolted to the upper connecting plate leaving a 1/8 inch (3.175 mm) gap between the bottom edge of the shroud and the upper surface of the foil. There was a similar size gap between the inner sides of the shroud and the side edges of the bottom connecting plate. The shroud had the external appearance both from the side and from the front of a rectangular pod, 6.125 inches (0.1556 m) wide, 10.5 inches (0.2667 m) high including the gap at the bottom edge, and 42.125 inches (1.07 m) long overall. Although this pod-like structure was not streamlined in the usual sense of a nacelle shape, it was faired in the longitudinal direction with a 2:1 elliptic nose and a straight wedge tail having an included angle of 26 degrees. Figure 3 is a sketch of the shroud geometry.

Since the shroud was attached to the upper connecting plate only, and did not touch the foil or bottom connecting plate, no hydrodynamic forces on it were transferred to the foil or to the floating portion of the dynamometer. Thus, aside from hydrodynamic interference effects, the hydrofoil was isolated from the other parts of the strut-shroud system exposed to the streamflow. The volume inside the shroud was flooded so the block gauges were operated wet. The block gauge core assemblies and electrical cables were completely waterproof, the latter were collected together in a bundle and led out through the interior of the strut via access holes.

The shroud represents a discontinuity in the strut geometry. For the particular case of foil submergence f/c = 0.25 it pierces through the free surface, and therefore plays the role of the strut in that situation.

STRUT

The strut had a chord length of 30 inches (0.762 m), was 3 inches (0.0762 m) thick, and had a simple ogive thickness variation in the longitudinal direction. The top end of the strut was attached to a turntable assembly that was held in a support frame that could be raised and lowered on the vertical rails of the towing carriage. Tilting the turntable assembly provided the means of changing angle of attack of the foil. A portable inclinometer was used to measure the angle of attack and a scale fixed to the vertical rails made it possible to fix the foil depth of submergence. Figure 4 is a sketch of the entire foil-strut-support system pictured with the hydrofoil at a positive angle of attack. Note that the Y-force and X-force values were measured in a coordinate system that rotated with the foil.

CALIBRATION

The foil-block gauge-strut arrangement was hung on a test stand for calibration. Each of the block gauges had been calibrated individually before assembly so that the sensitivities of the two X-gauges and the two Y-gauges, respectively, had been preset as closely as possible. The final force-to-voltage slopes of the complete dynamometer were determined, however, in the assembled condition.

ERRORS AND INTERACTIONS

Inaccuracies in the force and moment data are inherent to the mechanical/electrical system employed and are also caused by load distortions of both the model and/or force gauge system. Quantitative estimates of these errors are outlined here.

Measurement errors in the values of the forces manifest themselves in small scatter in the instrument readings of the block gauge outputs during calibration. For both the X- and Y-forces, these errors appeared to be always less than $\pm$ 0.01 of the applied load over the entire load range. Angle of attack values α were determined to within $\pm$ 0.02 degrees so that the relative error at $\alpha>2$ degrees was less than or equal to $\pm$ 0.01. Depth of submergence was accurate to within about $\pm$ 0.01 foot ($\pm$ 0.003048 m) so that for the submergence range tested, the relative angle error was less than or equal to $\pm$ 0.04.

Elastic deflections of the model hydrofoil under steady hydrodynamic loads undoubtedly altered the geometry of the lifting surface. Two categories of simple distortions have been estimated: vertical deflection associated with the spanwise bending caused by the Y-force loading, and twisting deflection due to the hydrodynamic pitching moment. The case of bending deflection has been computed using the assumption that an elliptic distribution of vertical loading acted over the entire hydrofoil span and that the hydrofoil half-span was a straight beam of constant section properties, cantilevered from the edge of the bottom connecting plate. The maximum deflection that occurred at each wing tip under the most extreme loading encountered was predicted using elementary strength of materials to be about 0.424 inch (0.01077 m) which is approximately 1/3 the plate thickness.

The torsional deflection was estimated using an approximate method for computing the angle of twist for rectangular cross section bars, as outlined by Seely and Smith.[9] The pitching moment taken about the quarter-chord axis was transferred to the mid-chord axis, and was assumed to be distributed elliptically across the span. For a rectangular beam of constant section properties having the same thickness-to-chord ratio as the hydrofoil model, the most extreme test condition was predicted to produce a maximum wing tip twist of about 0.24 degrees.

Elastic distortions within the force gauge arrangement itself were also responsible for errors in the final measured results, since each block gauge is in fact a deflection measuring device. Unlike the spurious character of the calibration scatter mentioned previously, the interaction errors of the block gauge were uni-directional. That is, the relative errors were always plus or always minus, rather than the ± values typical of calibration error bounds. Interactions of Y-force into the X-readings, and X-forces into the Y-readings were carefully determined during the calibration phase of the test. The influence of Y-force on the X-readings was found to be the larger, so the strongest interaction errors occurred for the foil at the largest angles of attack. Typical maximum values of the net relative corrections predicted for the most extreme test conditions were about -0.006 for the lift force and +0.015 for the drag force. Since the interaction slopes were themselves subject to calibration errors roughly of the order of ± 0.01 of the applied load (same as the pure force calibration errors), it was felt that such small adjustments to the measured values were not justified at this time.

None of the data presented in this report have been corrected or altered for any of the errors described above.

EXPERIMENTAL PROCEDURES

Experiments were carried out on Carriage II in the David Taylor Model Basin at the David W. Taylor Naval Ship R&D Center, Carderock facility. This deep water towing tank has a water depth of 22 feet (6.706 m) with a width of 51 feet (15.54 m). The measured water temperature was a constant 68°F (20°C), so the density and kinematic viscosity values used in data reduction were ρ = 1.9367 slug/foot^3 (998.13 kg/m^3) and $\nu = 1.0836 \times 10^{-5}$ foot^2/second (1.0067×10^{-6} m^2/s), respectively. The nominal test matrix for the data presented in this report is given in Table 2. At the low speeds of these experiments, no cavitation was ever observed to occur, even at the highest angles of attack.

A typical test run was made with fixed submergence depth f and angle of attack α. Several passes down the basin were necessary to complete all the speeds desired. After zeros were collected at the beginning of each pass, the carriage was brought up to speed and five channels of data were taken: the velocity, and the output voltages of X_1, X_2, Y_1, and Y_2. These were collected, averaged over a 10 second continuous record for each measured point, and processed onboard the carriage for both teletype output and tape storage as described earlier.

When changing angle of attack, appropriate changes had to be made for the vertical setting of the support bracket along the vertical rails so as to maintain a constant depth of submergence from the undisturbed free surface to the foil quarter-chord.

Since the X- and Y-forces were measured in the foil coordinate system, they were resolved into the desired drag and lift components (forces parallel and perpendicular to the free stream direction) using the formulas

TABLE 2

NOMINAL TEST MATRIX FOR LOW FROUDE NUMBER HYDROFOIL EXPERIMENTS

Parameter	Range
1. Speed	U = 4, 6, 8, 10, 12, 16, 20, 24, 28, ft/sec
	U = 1.22, 1.83, 2.44, 3.05, 3.66, 6.1, 7.32, 8.53, m/s
Chord Froude Number	$F_c \simeq$ 0.5, 0.75, 1.0, 1.5, 2.0, 2.5, 3.0, 3.5
Chord Reynolds Number	$R_c/10^6$ = 0.738, 1.11, 1.48, 1.85, 2.21, 2.95, 4.43, 5.17
2. Angle of Attack	α = 0, 2, 4, 6, 8 degrees
3. Depth of Submergence (to foil quarter-chord)	f = 0.5, 1.0, 1.5, 2.0, 3.0, 4.0, 7.0 ft
	f = 0.152, 0.305, 0.457, 0.61, 0.91, 1.22, 2.13 m
Submergence Ratio	f/c = 0.25, 0.5, 0.75, 1.0, 1.5, 2.0, 3.5

$$D = (X_1 + X_2)\cos\alpha + (Y_1 + Y_2)\sin\alpha$$
$$L = (Y_1 + Y_2)\cos\alpha - (X_1 + X_2)\sin\alpha \qquad (1)$$

where here $(X_1 + X_2)$ and $(Y_1 + Y_2)$ denote the sums of the block gauge outputs converted to forces using the calibration slopes. The hydrodynamic pitching moment, in foot-pounds, measured about the foil quarter-chord (positive for nose up) was determined from the expression

$$M_{(c/4)} = 0.708333\ (Y_1 - Y_2) \qquad (2)$$

where Y_1 and Y_2 represent the weighted force values of the forward and after Y-force gauges, respectively. The two force-to-voltage slopes for Y_1 and Y_2 were determined during calibration to satisfy simultaneously both the applied moment as well as the net applied vertical force, and therefore properly account for slight differences in the actual sensitivities of the two Y-gauges in the assembled system.

The distance to the center pressure x_{cp}, measured from the leading edge of the foil was determined from

$$x_{cp} = -\frac{M_{(c/4)}}{L} + \frac{c}{4} \qquad (3)$$

Nondimensional coefficient forms of the drag, lift, moment and center of pressure location are defined in the usual fashion as noted in the list of notation.

RESULTS AND DISCUSSION

Tables of the measured force and moment data reduced to coefficient form are presented in Appendix A. For purposes of this discussion, a considerable amount of cross plotting and further analysis has been carried out.

EFFECT OF FROUDE NUMBER ON DRAG AND LIFT

Curves of total measured drag coefficient and lift coefficient are plotted versus chord Froude number in Figures 5 through 11 for constant submergence ratios of f/c = 0.25 through 3.5, respectively. The contours are for constant geometric angle of attack α. It is evident that as the foil operates closer to the surface, the effects of speed (Froude number) become more and more pronounced. The curves of C_L versus Froude number are nearly flat at the deeper submergences (as they should be). For the foil operated nearer the surface, the dip in lift coefficient in the vicinity of $F_c \simeq 1$ becomes increasingly exaggerated.

At the shallowest submergence of f/c = 0.25, the hydrofoil experiences negative lift throughout the tested speed range at a geometric angle of attack, $\alpha = 0$, and displays intervals of negative lift for certain Froude numbers even up to an angle of attack of $\alpha = 4°$. For the $\alpha = 0$ case, the miminum point of the C_L curve has a value of $C_L = -0.21$ at a Froude number $F_c = 0.75$ ($F_f = 1.5$). With the f/c = 3.5 curves of Figure 11 as a measure of wave-free performance, it can be seen that this foil requires nearly a 4 degree angle of attack in order to reach a positive $C_L \approx 0.21$. Therefore, at $f/c = 0.25$ for a speed near $F_c = 0.75$, the foil apparently sees a net or averaged flow angle of almost minus 4 degrees. It is not known definitely by separate experiment or by calculation whether such a downwash flow could be generated by a 5.2 percent thick plate alone. At the shallowest submergence of $f/c = 0.25$, the plate thickness-to-depth ratio is only $t/f = 0.2083$, and the foil probably experiences some wavemaking drag due to thickness as well as wave-induced negative velocities produced by thickness across the entire span.

Of course, strut- and pod-induced downwash must alter the flow angle of attack locally near the center span region. However, it seems unlikely that a net minus 4 degrees could be induced across the 8 foot (2.44 m) span. Unfortunately, there are no computation procedures currently available for estimating the strut- and pod-induced downwash velocities at the intermediate values of Froude number of interest here. Such calculations could allow the best possibility of isolating the foil-alone performance from the present data.

The stong dip in the C_L variation with speed for the smallest submergence cases is present for all values of α tested, with the curves moving up in parallel contours for various angles.

Regarding the drag coefficient variation versus speed in Figures 5 through 11, it can be seen that for operation nearer and nearer the surface the drag coefficient curves steepen considerably.

This reflects the increasing amount of hydrofoil wavemaking drag. It is reasonable to suspect that a portion of this is caused by wavemaking due to thickness effects and some interference effects due to induced downwash flow from the strut and pod.

For reference, in each of Figures 5 through 11, the 1957 International Towing Tank Conference[10] (ITTC) turbulent friction correlation line is plotted, converted to a friction drag coefficient based on the planform area.

EFFECT OF FOIL SUBMERGENCE ON DRAG AND LIFT

Curves of total measured drag and lift coefficients are plotted versus submergence ratio in Figures 12 through 15 for the constant chord Froude numbers of F_c = 0.5, 0.75, 1.0, and 2.0, respectively. The contours are for constant angle of attack. Interesting changes in the characteristics occur at the low Froude numbers. These are especially noticeable in comparing the F_c = 0.5 case with the other three cases. The F_c = 2 curves in Figure 15 are typical of the expected behavior of drag and lift coefficients with depth of submergence at large Froude numbers: both force coefficients fall off with decreasing submergence depth, with the lift coefficient suffering the most rapid decrease. As the Froude number is decreased down to F_c = 0.75, the characteristic curves are similar to the F_c = 2 case, but display tendencies to remain level or have slight humps in the drag and lift coefficients before the final rapid descent at submergence ratios below 0.75. At $F_c = 0.5$ there is a definite difference. The drag coefficients actually increase with small f/c ratios, and the lift coefficients rise to rather sharp peaks before falling off below $f/c < 0.5$. Evidently an important change in the flow occurs for shallow submergences in the Froude number range between $F_c = 0.5$ and 0.75. From visual observations of the free surface, this change is manifest in a spanwise breaking wave or hydraulic jump that appears over the foil in this speed range. The photograph included in the frontispiece of this report shows the spanwise wave disturbance observed at $f/c = 0.25$ and $F_c = 0.5$. The dip the C_L versus F_c curves mentioned earlier also occurs in the same Froude number range as the appearance of the breaking waves.

It is interesting to note at this point that in two-dimensional hydrofoil experiments described by Parkin, et al,[11] similar waves were encountered and were shown to have a drastic effect on the pressure distribution over the foil surface. For the particular case of a 12 percent thick Joukowski profile hydrofoil at $\alpha = 5$ degrees and with the trailing edge submerged a distance of 0.25c, the character of the measured pressure distributions in Reference 11 showed a remarkable transformation at about $F_c = 0.61$. For Froude numbers higher than 0.61 the pressure distributions resembled those of a hydrofoil at deep submergence. At Froude numbers below $F_c = 0.61$, the upper surface negative pressure peak was suddenly shifted to near the rear of the foil with a strong positive pressure occurring at the nose.

This dramatic change was definitely associated with a hydraulic jump that appeared over the hydrofoil.

In the present finite aspect ratio experiments, the apparent shift in flow character occurs between $F_c = 0.5$ and 0.75 and the effects are noticeable in the character of the net hydrodynamic forces. While interference effects from the strut and pod could account for some of the changes, it appears that the primary influence is the breaking wave surface disturbance which was observed to occur across the entire span of the foil.

EFFECT OF ANGLE OF ATTACK ON DRAG AND LIFT

Graphs of drag and lift coefficients plotted versus angle of attack are given in Figures 16 through 21 for constant submergence ratios of f/c = 0.25, 0.5, 0.75, 1.0, 1.5, and 2.0, respectively. The contours are for selected values of chord Froude number $F_c = 0.5$, 0.75, 1.0, and 3.0. Froude number effects are evident at the low speeds in the separation of curves and variation of lift-curve slope for various Froude numbers.

MOMENT AND CENTER OF PRESSURE

Curves of the pitching moment coefficient about the quarter-chord C_M and the center of pressure ratio x_{cp}/c are plotted versus chord Froude number in Figures 22 through 28 for constant submergence ratios of f/c = 0.25 through 3.5, respectively. The contours are for constant geometric angle of attack.

As expected, the influence of the Froude number is more dramatic for the shallow submergence cases, with the moment coefficient having a strong dip centered near $F_c = 0.5 - 0.75$. The minimum point moves to higher Froude numbers with increasing f/c. The noteworthy changes in the sign and magnitude of the moment in the Froude number range of $F_c = 0.5 - 1.0$ are associated with the observed spanwide breaking wave, and can be explained qualitatively in terms of the pressure distribution results mentioned earlier.[11]

The center of pressure location also reflects the exaggerated Froude number effects in the vicinity of $F_c = 0.5$ to 1.5. Movement of the center of pressure off the foil is a common feature of the effect of camber at low angles of attack (see, for example Von Mises[12]). Although the foil itself is uncambered, there are clearly vertical velocities induced by the free surface and by the presence of the strut and pod. These create a Froude-dependent camber-like effect.

For the deepest submergence case, in Figure 28, the center of pressure ratio appears to settle down roughly in the neighborhood of the anticipated value of $x_{cp}/c \simeq 0.25$, although there is still an effect of angle of attack that moves the center of pressure aft for increasing α. It is interesting that for the larger values of α, the curves of center of pressure ratio versus Froude number seem to level off at roughly the same value of $x_{cp}/c \simeq 0.22$ even at the shallower submergences, and despite the dip occurring near $F_c = 0.75$.

LIFT-CURVE SLOPE

Figures 29 and 30 show, respectively, the influence of Froude number and depth of submergence on the lift-curve slope. The curves of C_{L_α} versus F_c with contours of submergence ratio in Figure 29 indicate that in the low Froude number range near $F_c = 1$, the corresponding dips in the plots of C_L versus F_c are brought about not only by an overall shift in the net angle of attack seen by the foil, but also by a reduction in the lift-curve slope. This is probably caused by a camber or flow curvature effect due to the observed spanwise broken waves occurring in this speed range at the shallowest submergences, and due to interference velocities from the strut and pod. In any case, this graph shows that in addition to submergence ratio, Froude number must also be considered in determining lift-curve slopes.

In Figure 30, the reference value of lift-curve slope for the present data is that for the deepest submergence and highest speed

$$C_{L_{\alpha(REF)}} = C_{L_\alpha} (f/c = 3.5,\ F_c = 3.5) = 0.0617 \text{ deg}^{-1} \qquad (4)$$

The solid line curve in Figure 30 is taken from the experimental results of Wadlin, et al[5] for a rectangular planform, aspect ratio 4 hydrofoil at chord Froude numbers $F_c > 3.24$. The distorting effect of small Froude number is evident here in the curves for $F_c = 1$ and 2. There is good correspondence between the present lift-slope ratio results at $F_c = 3$ and the results of the previous experiments.

COMPARISON OF LIFT RESULTS

The low speed end of the NACA experiments of Reference 5 can also be used in a comparison of lift at similar Froude numbers and submergences. Comparison plots of lift coefficient versus angle of attack measured from zero lift are given in Figures 31 through 34 with the present data at $F_c = 3.0$ and $f/c = 0.5$, 1, 2, and 3.5, respectively. The NACA data are for a constant $F_c = 3.24$ and $f/c = 0.59$, 1.09, 2.09, and 3.09/4.09, respectively. It can be seen that absolute values of lift-curve slopes for the flat plate foil appear to be somewhat less than those for the NACA 64A412 section used in Reference 5. The discrepancies may be due to the poor section properties of the faired flat plate, but the differences in the C_{L_α} values decrease with increasing submergence to about 6 percent at the deepest cases shown.

RESIDUAL DRAG COEFFICIENTS

An attempt has been made to extract the induced-plus-wave drag from the measured values of total drag. In the present work, the residual drag coefficient is defined as

$$C_R = C_D - C_{D_{visc}} (R_c) \tag{5}$$

where $C_{D_{visc}}$ is the estimated total viscous drag given by

$$C_{D_{visc}} (R_c) = C_{D_f} (R_c) + C_{D_{vp}} \tag{6}$$

Here C_{D_f} denotes the flat plate friction drag coefficient based on planform area, R_c is the foil chord Reynolds number, and $C_{D_{vp}}$ denotes the viscous pressure or "form" drag. It was decided to use the ITTC 1957 friction correlation curve for the flat plate friction drag instead of the usual practice of using the Schoenherr line. Recent work by Granville[13] has shown that at low turbulent flow Reynolds numbers ($5 \times 10^5 < R_c < 10^7$), the ITTC line turns out to be very close to the best semi-empirical flat plate friction line. It is therefore preferable to the Schoenherr curve in the range of the present experiments and becomes indistinguishable from the Schoenherr values at Reynolds numbers greater than 10^7.

For the deepest submergences tested (f/c = 2 and 3.5), at the highest speeds, and at zero angle of attack the drag coefficients are observed to level out on a curve parallel to the ITTC 1957 line. Since at these depths the C_L curve for $\alpha = 0$ is flat and very near zero, the difference between the measured total drag coefficient and the flat plate friction value is assumed to be the viscous pressure drag, entirely free of lift-dependent wavemaking effects. The result is an estimate for the form drag coefficient of

$$C_{D_{vp}} \simeq 0.005 \qquad (7)$$

This is assumed to be a function of shape only, independent of Reynolds number so that all the Reynolds number variation in $C_{D_{visc}}$ is contained in C_{D_f} of Equation (6).

Inclusion of the viscous pressure drag in the definition of residual drag is somewhat unusual, since the typical practice is to absorb any small form drag into the total pressure drag category. The definition in Equation (6) is desirable here because the idea of the present experiments was to remove the section-shape-dependent drag as completely as possible, leaving only the Froude-dependent drag variation. The form drag of this section was determined to be rather large, and therefore an important contributor to total section drag. This is not an unexpected result for the drag on a faired flat plate of the type used here. One set of examples can be found in a NACA report by Wadlin, et al,[14] with results of experiments on three flat plate hydrofoils of small aspect ratio having 2:1 elliptical noses and straight wedge tails, with thickness ratios of 1.0, 1.3, and 2.7 percent. The measured drag coefficients at the deepest submergence cases, taken at zero lift, were typically 0.004 to 0.0025 above the ITTC 1957 friction line in the same Reynolds number range of the present experiments. Such values of form drag for very thin plates lend confidence in the $C_{D_{vp}}$ value determined in the present experiments.

Curves of measured C_R/C_L^2 versus chord Froude number are plotted in Figures 35 through 41 for submergence ratios of f/c = 0.25 through 3.5, respectively. The contours are for constant angle of attack. As noted earlier, the residual drag coefficients C_R should be a close approximation to the Froude-dependent variation of $(C_{D_i} + C_W)$ which is the sum of total induced drag plus wavemaking drag. For a hydrofoil near the free surface, the total induced drag consists of the unbounded flow plus the biplane induced drag.

For reference, the proper limits of $(C_{D_i} + C_W)/C_L^2$ at infinitely large and zero Froude numbers are indicated in the Figures 35 through 41 as horizontal dash-dot lines at the extremes of the speed range. In the limit of infinitely large Froude number, the wavemaking drag disappears and all that remains is the total induced drag including the biplane effect of the free surface. Thus

$$\frac{(C_{D_i} + C_W)}{C_L^2} \rightarrow \frac{1 + \delta + \sigma(\lambda)}{\pi A} \qquad (8)$$

where δ = Glauert planform factor for non-elliptic planforms[15]

$\sigma(\lambda)$ = Prandtl biplane factor, which is strictly a function of the submergence-to-semi span ratio λ

A discussion of the biplane function $\sigma(\lambda)$ can be found in von Kármán and Burgers.[16]

In the limit of zero Froude number, the free surface acts as a rigid wall. The sign of the biplane induced drag must be reversed from the high Froude number case, since the flow is now symmetrical about the free surface plane. For vanishing Froude number, the wavemaking drag goes to zero, leaving the total induced drag at the low speed extreme expressed as

$$\frac{(C_{D_i} + C_W)}{C_L^2} \rightarrow \frac{1 + \delta - \sigma(\lambda)}{\pi A} \qquad (9)$$

The factor δ is equal to 0.03 for a rectangular planform, aspect ratio 4 lifting foil. Numerical values of $\sigma(\lambda)$ valid for an elliptic load distribution, and values of the two limits of $(C_{D_i} + C_W)/C_L^2$ that appear in Figures 35 through 41 are given in the table of Appendix B.

A rough comparison between a theoretical prediction of $(C_{D_i} + C_W)/C_L^2$ and measured C_R/C_L^2 versus F_c is shown in Figure 42. The theory curve is from Nishiyama[4] for A = 4, and applies to a submergence ratio of f/c = 0.59. The two experimental curves are for f/c = 0.5 and 0.75, at angle of attack $\alpha = 8°$ only. This indicates that at least for large lift, there is a measure of correspondence between the experiments and the analytical results of linear potential theory. The same cannot be said for smaller angles of attack.

It can be seen from Figures 35 through 41 that the curves of C_R/C_L^2 versus F_c for various angles of attack do not fall on the same curve, although the spread becomes considerably smaller as the depth of submergence is increased, and at the larger angles of attack for any given submergence. The prediction of linear potential theory (Breslin[3], Nishiyama[4]) is that there is <u>one</u> curve of $(C_{D_i} + C_W)/C_L^2$ for an isolated hydrofoil of a given planform shape and depth of submergence, regardless of angle of attack. One explanation of the divergence between the experimental results and the theory is that the linear theory may be inadequate to describe the flow phenomena at low chord Froude numbers, especially at the shallowest submergences where spanwide breaking waves are observed to occur in just the Froude number range of the most exaggerated differences. Another possibility is that the present measurements include Froude- and depth-dependent interference drag components caused by the strut and pod.

A complementary viewpoint of the variation of residual drag coefficient is afforded in Figures 43 through 46 for submergence ratios of f/c = 0.25, 0.5, 0.75, and 1.0, respectively. In these graphs, C_R is plotted versus positive lift coefficient squared to the right of zero, and versus negative lift coefficient squared to the left. The contours are for chord Froude number equal to 0.5, 0.75, 1.0, and 3.0. From the linear theory, the expected variation of $(C_{D_i} + C_W)$ versus $(\pm C_L)^2$ for a given Froude number consists of a straight line in each quadrant, extending from zero in the positive C_R direction. For large C_L values, the curves do appear to settle onto straight lines. Near zero lift, however, there is a mixture of nonlinear lift-, Froude-, and depth-dependent drag revealed by the rapidly changing slopes and the non-zero values of C_R at $C_L = 0$. These drag effects are accentuated at shallow submergences, and seem to diminish in magnitude as the submergence depth is increased.

Although it is not possible to separate out all the drag components that are present in the C_R values of these experiments, it is fair to say that the drag due-to-lift of a hydrofoil at low Froude numbers is distinctly influenced by the presence of a strut and pod. These factors should be better understood both from a point of view of designing future experiments and for estimating drag on large prototype hydrofoil systems.

APPLICATION OF THE MEASURED DATA

An example application of the model drag and lift data is presented here for the performance of a hypothetical large hydrofoil system consisting of three, aspect ratio 4, rectangular planforms operated at constant lift. If a length scaling ratio of 9 is used, then the prototype chord length is 18 feet (5.486 m), and the prototype speed interval corresponding to a chord Froude number range of F_c = 1.75 to 3.5 is V_K = 25 to 50 knots. This is a reasonable speed range for operation between takeoff and cruise.

Several questions can be investigated:

1. What is the predicted breakdown of drag for a large-chord hydrofoil operated at constant lift in a practical range of subcavitating speeds? Is the wavemaking portion of the drag significant?

2. How does the trend of measured residual drag versus Froude number compare with the trend of induced drag alone?

3. What is the effect of lift loading on the residual drag?

With the available lift coefficients of these experiments, the attainable lift loadings are limited to about L/S = 800 pound/foot^2 (38304 N/m^2) or smaller, in the speed range $V_K \leq 50$ knots. Unfortunately, this does not match with the usual requirements of L/S = 1200 to 1400 pounds/foot^2 (57456 to 67032 N/m^2), but such lift loadings can only be achieved with cambered foils and/or with flaps. This illustrative example is worked using only the measured data.

The case of $f/c = 1$ is considered as representative. With a lift loading of $L/S = 800$ pounds/foot^2, the total weight supported by all three hydrofoils, each one having a planform area of 1296 foot^2 (120.4 m^2), is 1389 long tons (1411 m.tonne). Measured model lift coefficients and deduced residual drag coefficients are assumed to apply at the same Froude numbers for the prototype. Lift coefficients corresponding to constant lift loading on each foil are calculated, and cross plots of C_L and C_R versus α are used to find the required C_R values at constant lift by interpolation. Friction drag coefficients at the prototype Reynolds numbers are determined from the ITTC 1957 correlation line. Wavemaking drag is found by deducting the total induced drag from the residual drag as follows

$$C_W = C_R - C_{D_i} \tag{10}$$

where

$$C_{D_i} = \frac{C_L^2}{\pi A}[1 + \delta + \sigma(\lambda)] = (0.1004)C_L^2 \qquad \text{for } A = 4,\ f/c = 1$$

Then the total projected drag coefficient for each hydrofoil is estimated by

$$C_{D_t} = C_R + C_{D_f} \tag{11}$$

Table 3 contains the numerical results of this procedure, with the drag coefficient breakdown versus Froude number plotted in Figure 47. It can be seen from this extrapolation of measured model drag data that, the wavemaking drag is a significant portion of the residual

TABLE 3 - ESTIMATED DRAG BREAKDOWN OF AN ASPECT RATIO 4 HYDROFOIL AT f/c = 1.0 OPERATING AT CONSTANT L/S = 800 pounds/foot^2

F_c	V_K (knots)	R_c (prototype)	C_{D_f} (ITTC)	C_R (interpolated)	C_L (calculated)	C_{D_i}	C_W	C_{D_t} (one foil)
3.5	49.9	1.33×10^8	.004	.0039	.1134	.001291	.00261	.0079
3.0	42.78	1.14×10^8	.004088	.007	.1544	.002393	.00461	.01109
2.5	35.64	9.52×10^7	.004196	.0133	.2224	.004966	.00833	.0175
2.0	28.52	7.62×10^7	.004336	.0303	.3474	.01212	.0182	.03464
1.75	24.95	6.66×10^7	.004424	.0502	.4538	.02068	.0295	.05462

Drag Components in Pounds (Each Foil)

V_K	Friction D_f	Residual D_R	Total Induced D_i	Wavemaking D_W	Total D_t
49.9	36,562	35,648	11,800	23,848	72,210
42.78	27,455	47,012	16,071	30,941	74,467
35.64	19,565	62,015	23,156	38,859	81,580
28.52	12,941	90,429	36,172	54,257	103,370
24.95	10,107	114,686	47,245	67,441	124,793

drag, and of the total hydrofoil drag as well, especially at low Froude numbers.

The drag of three foils is taken as simply three times the drag on one. The resulting lift-to-drag ratio for the foils alone is plotted versus Froude number in Figure 47. There is a noticeable reduction of lift-to-drag ratio at the lower speeds for operation at constant lift at f/c = 1.

It is interesting to compare the relative trends of the residual drag and the induced drag as functions of speed. Figure 48 is a plot of C_R/C_R (F_c = 3.5) and C_{D_i}/C_{D_i} (F_c = 3.5) versus chord Froude number for constant f/c = 1. The reference values for C_R and C_{D_i} are taken at V_K = 49.9 knots (F_c = 3.5) for a c = 18 ft hydrofoil. With the simple expressions for C_{D_i} given previously, the induced drag ratio at constant lift loading, for any speed V_K, is

$$\frac{C_{D_i}}{C_{D_i}\ (F_c = 3.5)} = \left(\frac{49.9}{V_K}\right)^4 = \left(\frac{3.5}{F_c}\right)^4 \qquad (12)$$

The C_R values were obtained at various lift loadings by simple interpolations as described earlier. The contours are for prototype values of L/S = 600, 800, and 900 pounds/foot^2. Figure 48 indicates that the relative rise of measured residual drag is slightly milder than the relative rise of induced drag, at least for the prototype loadings covered by the present data. It is also noted that the relative rise of the measured C_R steepens for larger lift loadings.

CONCLUSIONS AND RECOMMENDATIONS

1. Unique force and moment data are presented for low Froude number operation of near-surface hydrofoils.

2. At shallow submergences ($f/c \sim 0.25$) there are remarkable changes in the character of forces and moments that occur in the range of $F_c = 0.5$ to 0.75. These are associated with a spanwide hydraulic jump or breaking wave that occurs over the foil, which in turn appears to be caused by foil thickness as well as angle of attack. These changes may be of more than academic interest when consideration is given to schemes for partial hydrofoil support systems of large ships.

3. The measured values of residual drag contribute significantly to the total drag at low Froude number on an aspect ratio 4 foil at constant lift, as determined from an example estimation for an 18-foot-chord hydrofoil operating at $f/c = 1$.

4. The variation of hydrofoil drag at low Froude numbers apparently includes important contributions due to the presence of a strut and pod. These should be better understood, both experimentally and theoretically.

5. Additional low Froude number experiments should be conducted with forward-leading sting(s) support in order to better isolate the lifting planform from interference drag effects caused by the strut and pod.

6. A cambered foil shape should be used in order to achieve maximum lift coefficients on the order of 0.8 or higher. The planform should have an aspect ratio of 5 or 6, and some consideration should be given to other aspect ratios as well.

7. Negative angles of attack should be included in any future test program.

8. Analytical methods and computer programs to implement them should be developed for the prediction of wavemaking drag on hydrofoil-pod-strut systems at arbitrary Froude number. These would be useful for the extraction of foil-only data from experiments and for possible optimization of very large hydrofoil support systems.

ACKNOWLEDGEMENTS

Douglas L. Gregory served as co-principal investigator on this project. His continuous participation and guidance has been essential to the successful completion of the experiment.

The authors acknowledge gratefully the work of Dennis R. Mullinix for his preparation of the computer programs for data acquisition and for his advice and help throughout the test program. The assistance during calibration by Jack J. Gordon and Gary A. Hampton is also much appreciated.

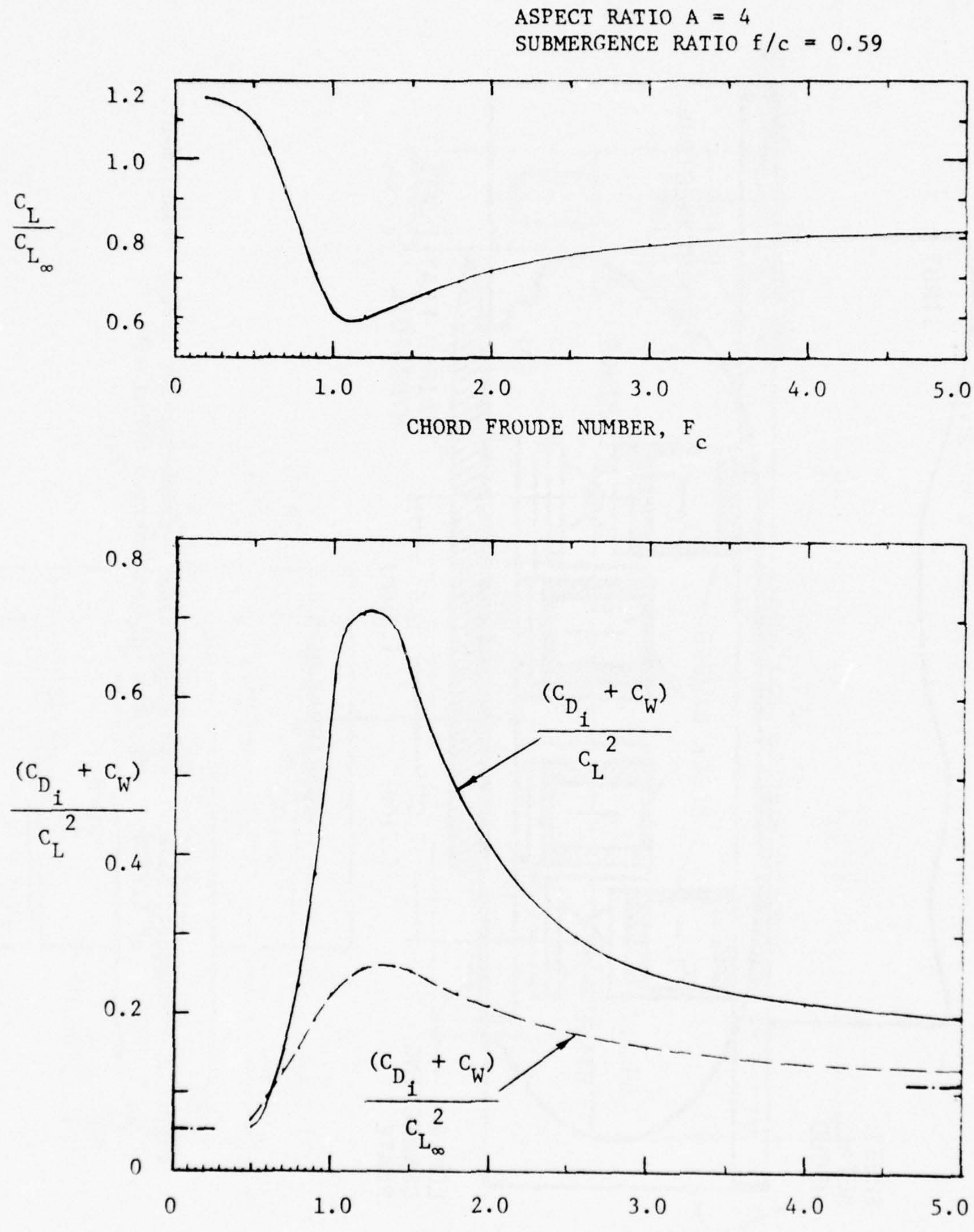

Figure 1 - Predicted Behavior for Lift and Inviscid Drag Coefficients Determined by Nishiyama[4] for Rectangular Planform Hydrofoil

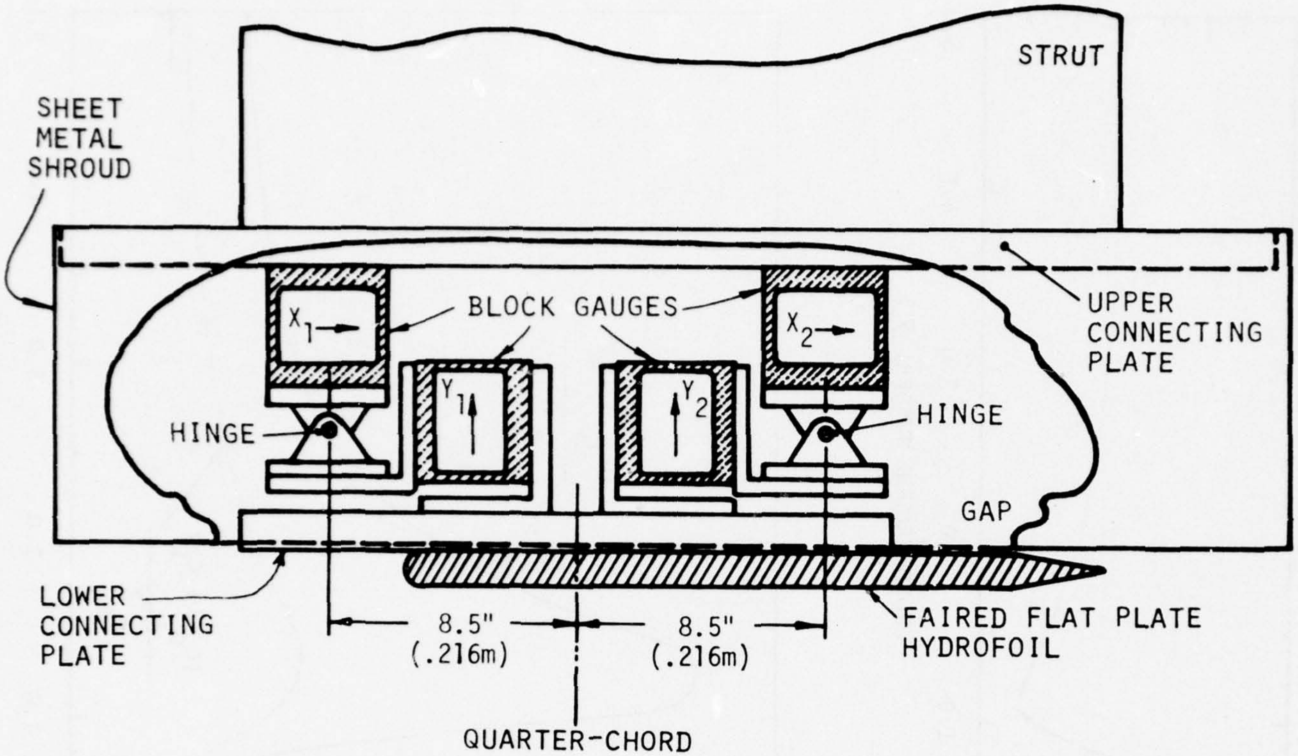

Figure 2 - Schematic Side View of Block Gauge Dynamometer for Direct Measurement of Lift and Drag on a Fully Submerged Hydrofoil

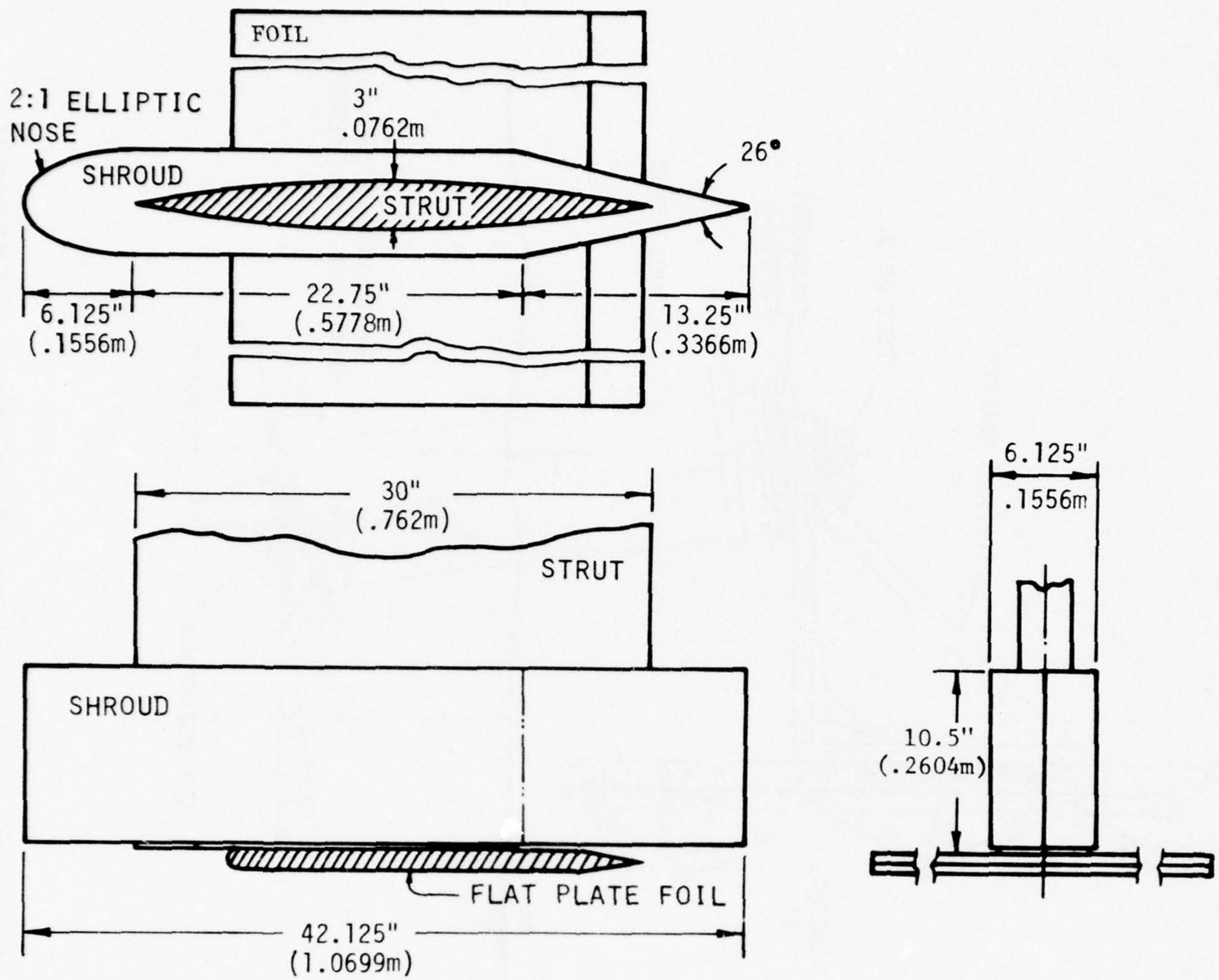

Figure 3 - Geometry of the Shroud and Strut

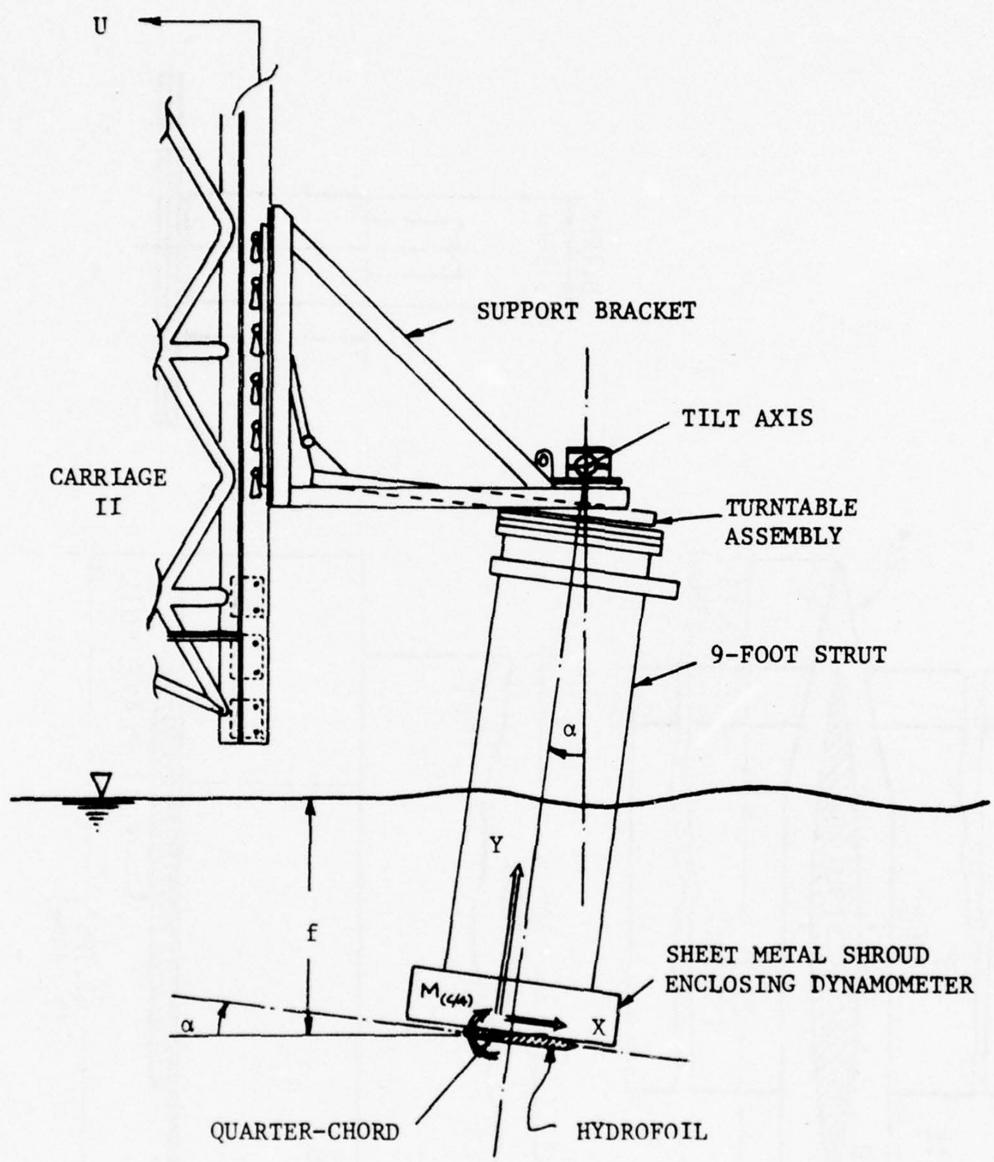

Figure 4 - Sketch of Experimental Setup Mounted to Carriage II

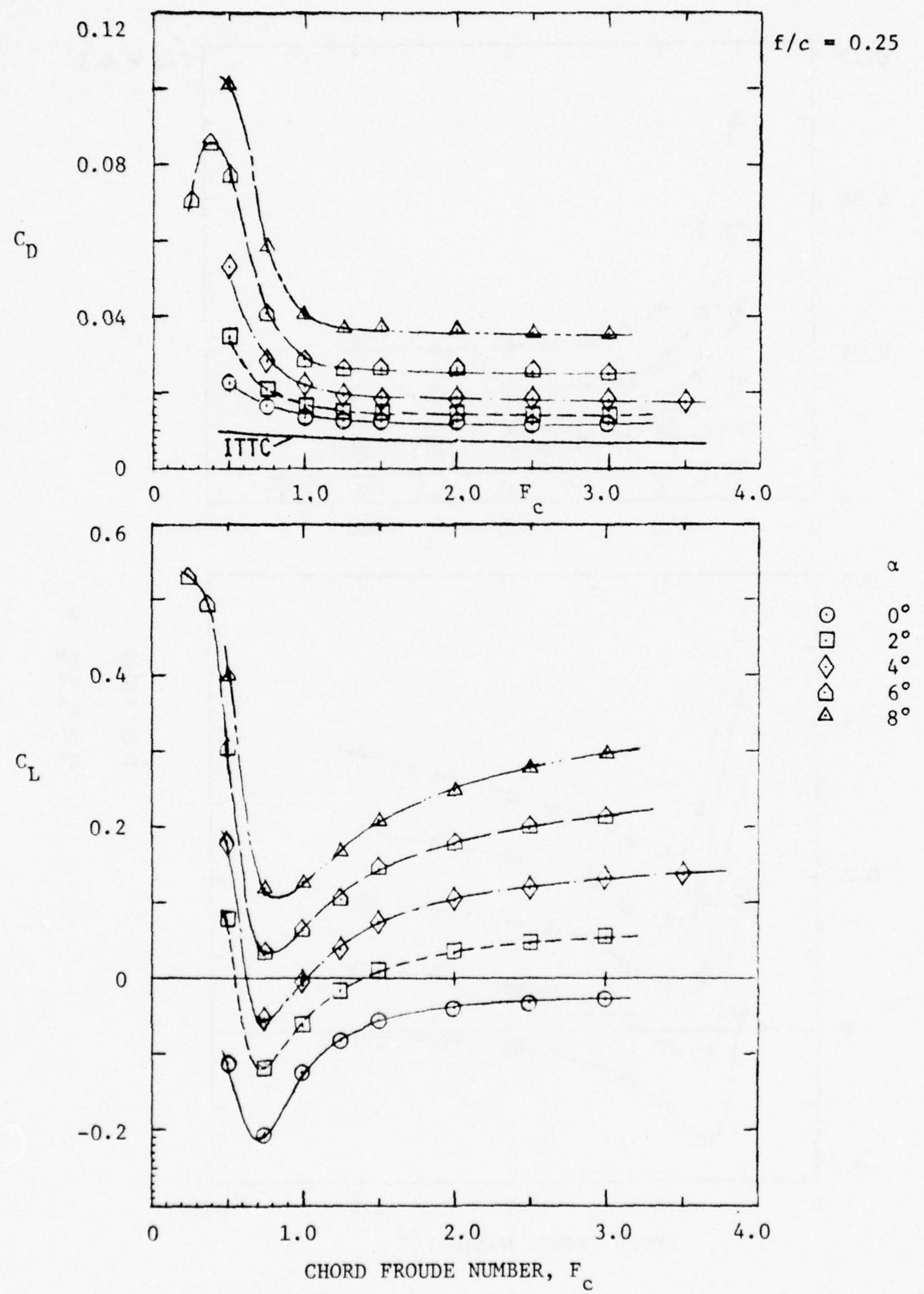

Figure 5 - Measured Drag and Lift Coefficients Versus Chord Froude Number for Submergence Ratio f/c = 0.25

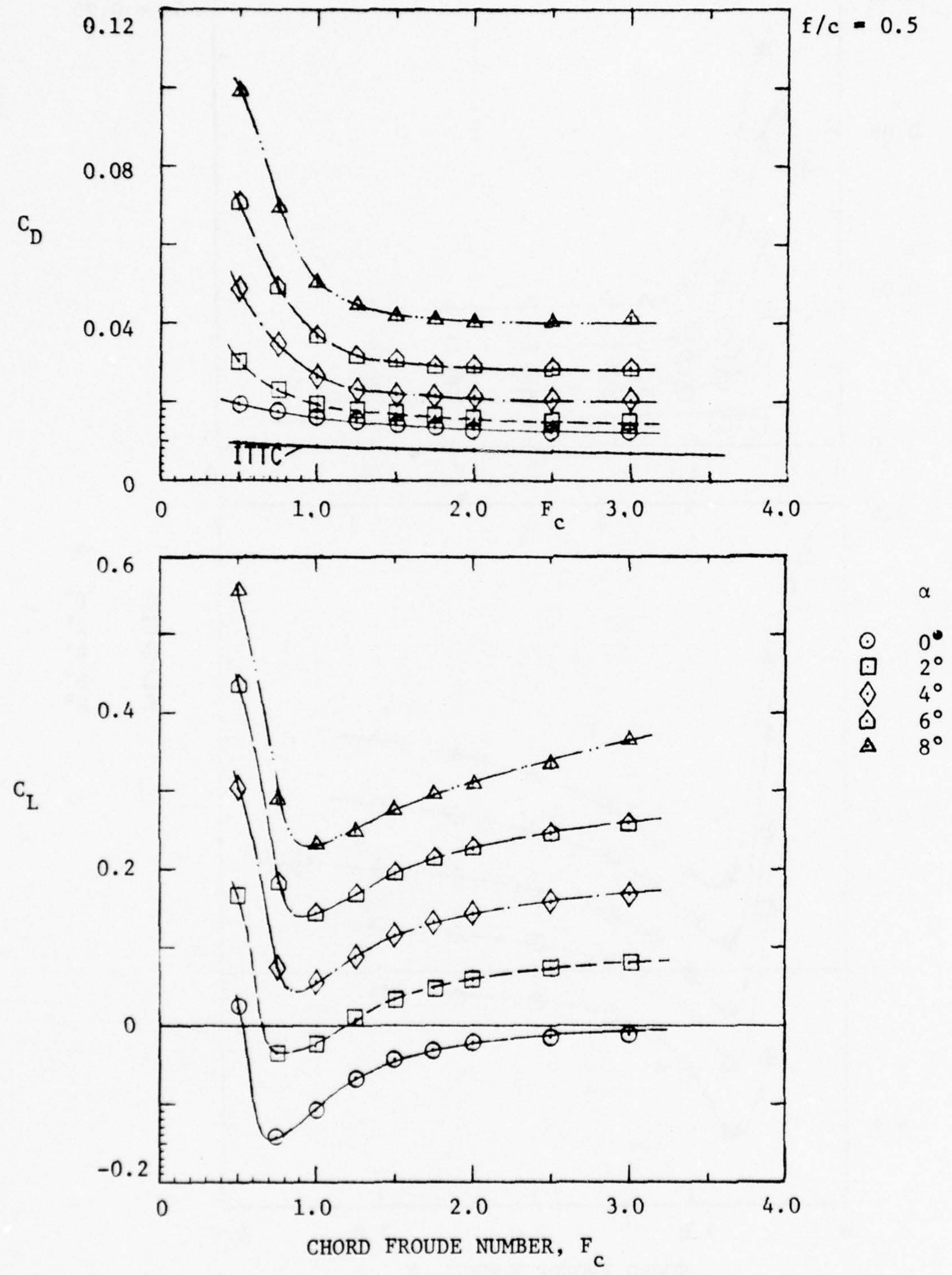

Figure 6 - Measured Drag and Lift Coefficients Versus Chord Froude Number for Submergence Ratio f/c = 0.5

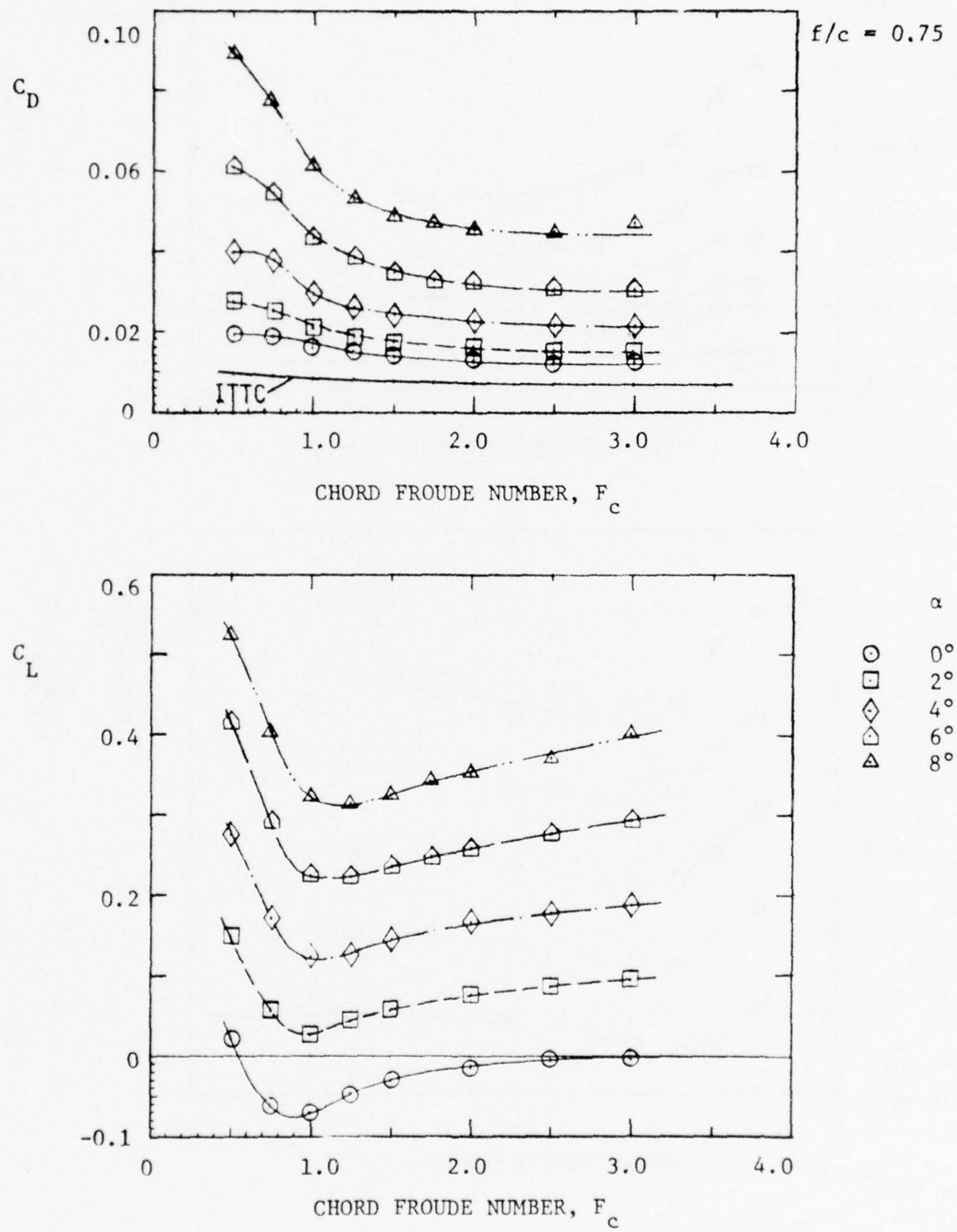

Figure 7 - Measured Drag and Lift Coefficients Versus Chord Froude Number for Submergence Ratio f/c = 0.75

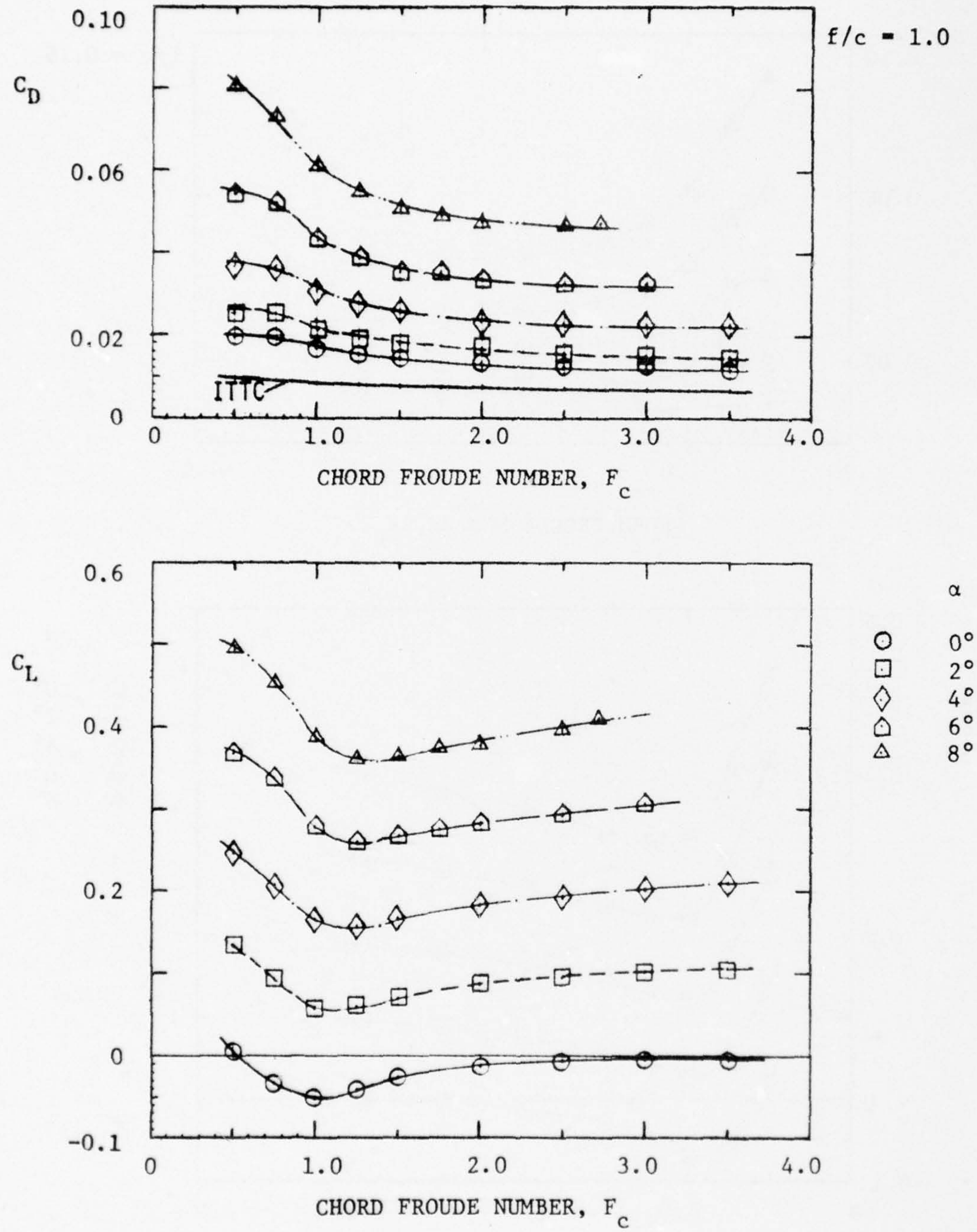

Figure 8 - Measured Drag and Lift Coefficients Versus Chord Froude Number for Submergence Ratio f/c = 1.0

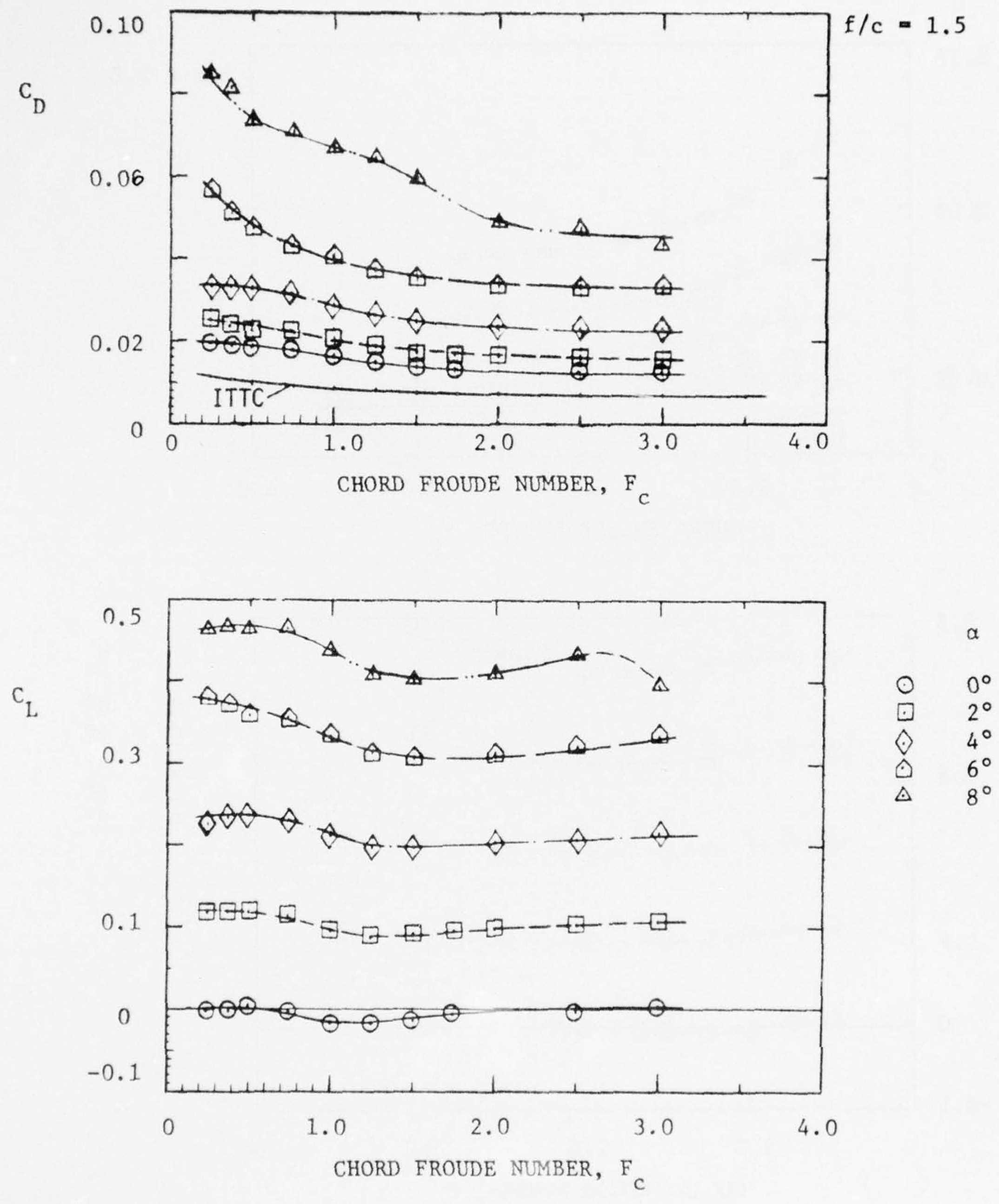

Figure 9 - Measured Drag and Lift Coefficients Versus Chord Froude Number for Submergence Ratio f/c = 1.5

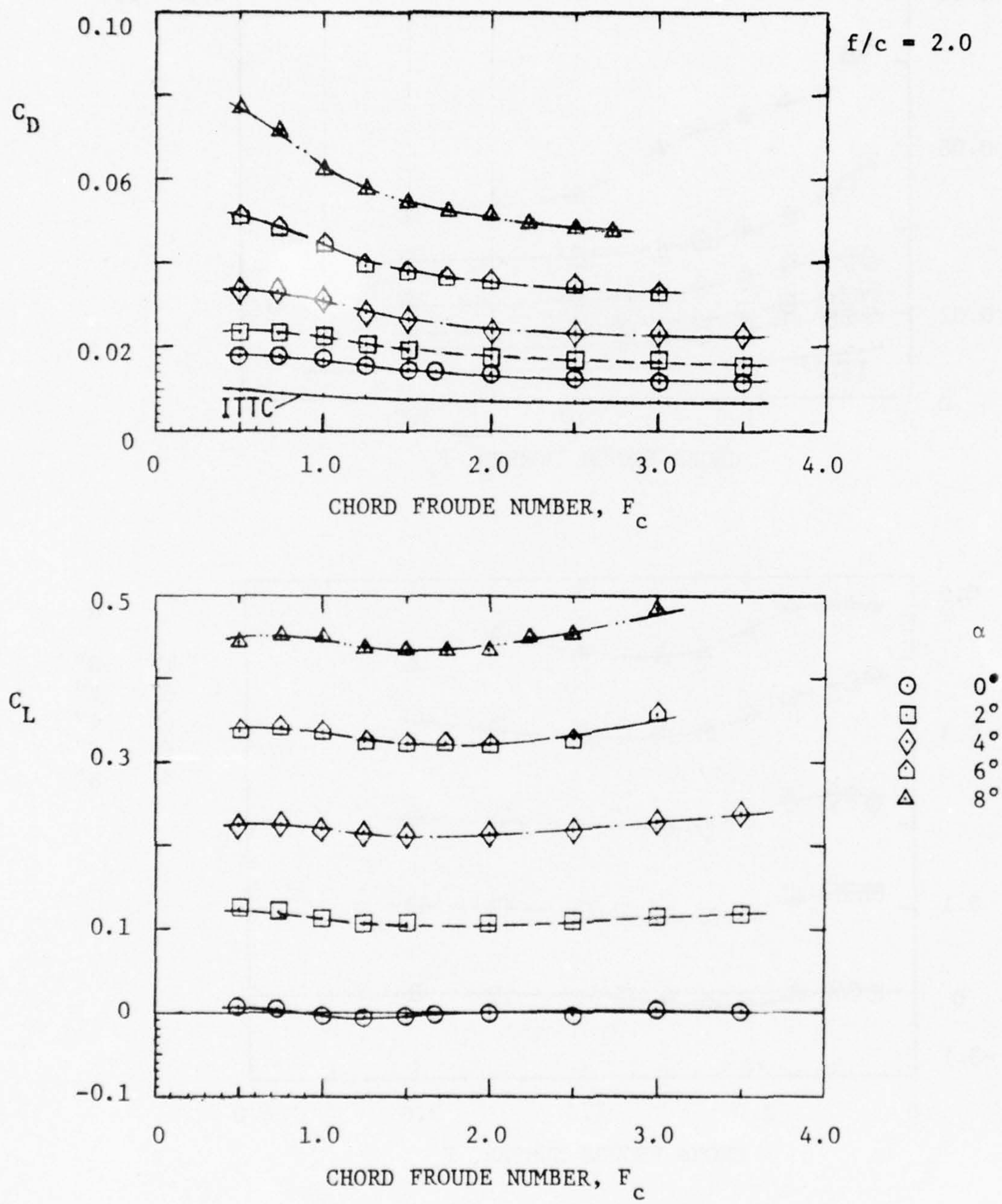

Figure 10 - Measured Drag and Lift Coefficients Versus Chord Froude Number for Submergence Ratio f/c = 2.0

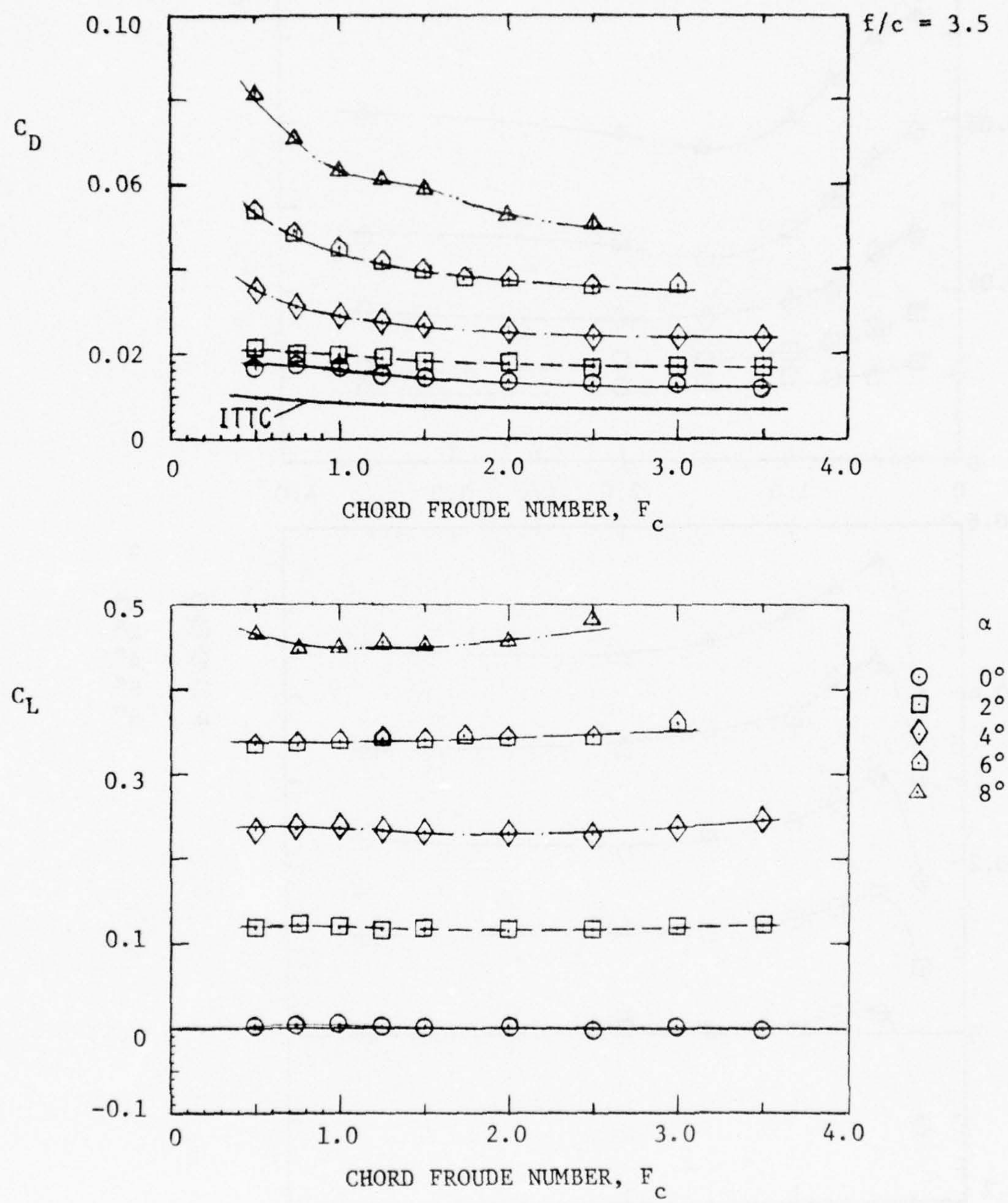

Figure 11 - Measured Drag and Lift Coefficients Versus Chord Froude Number for Submergence Ratio f/c = 3.5

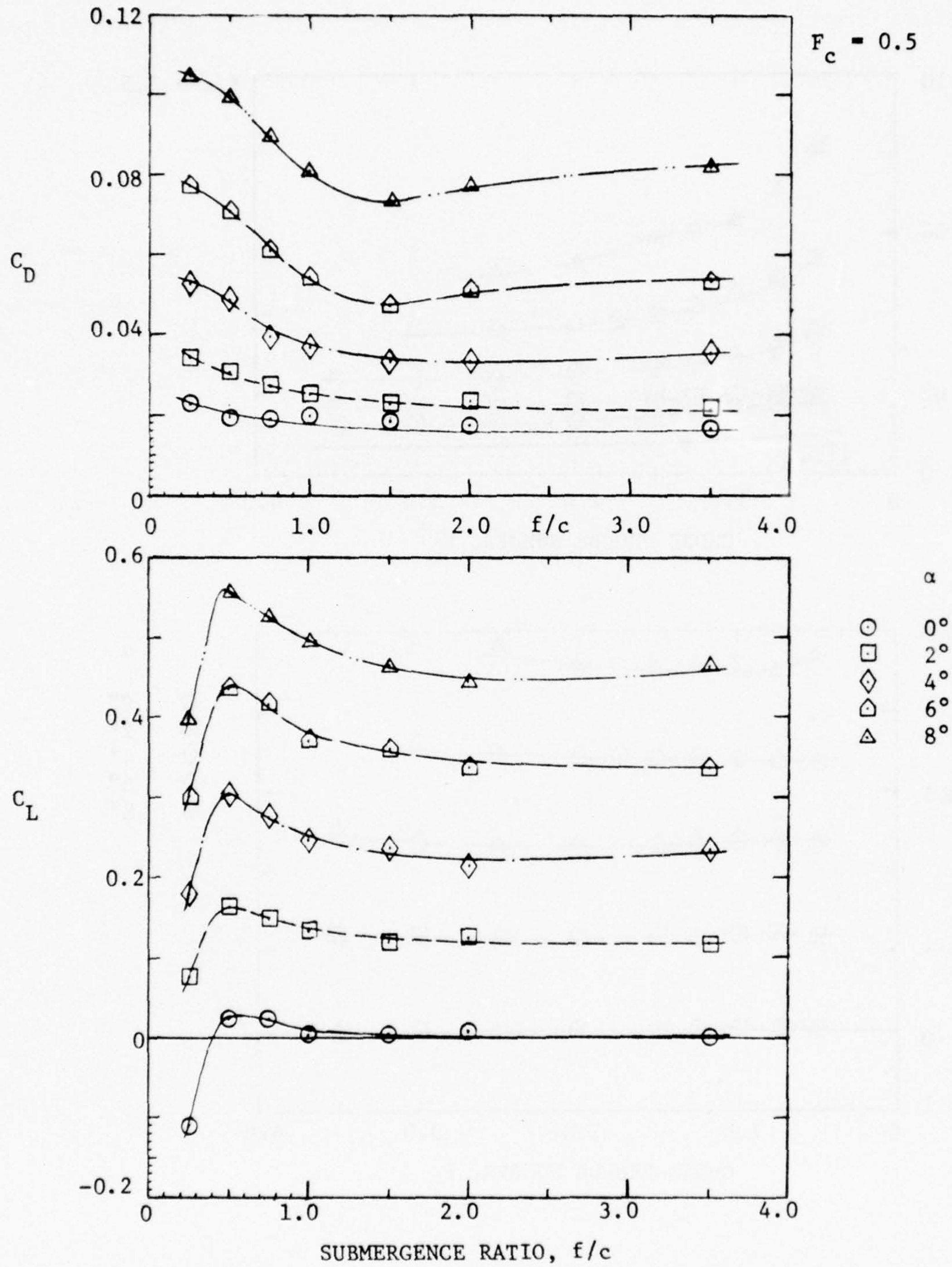

Figure 12 - Measured Drag and Lift Coefficients Versus Submergence Ratio for Chord Froude Number F_c = 0.5

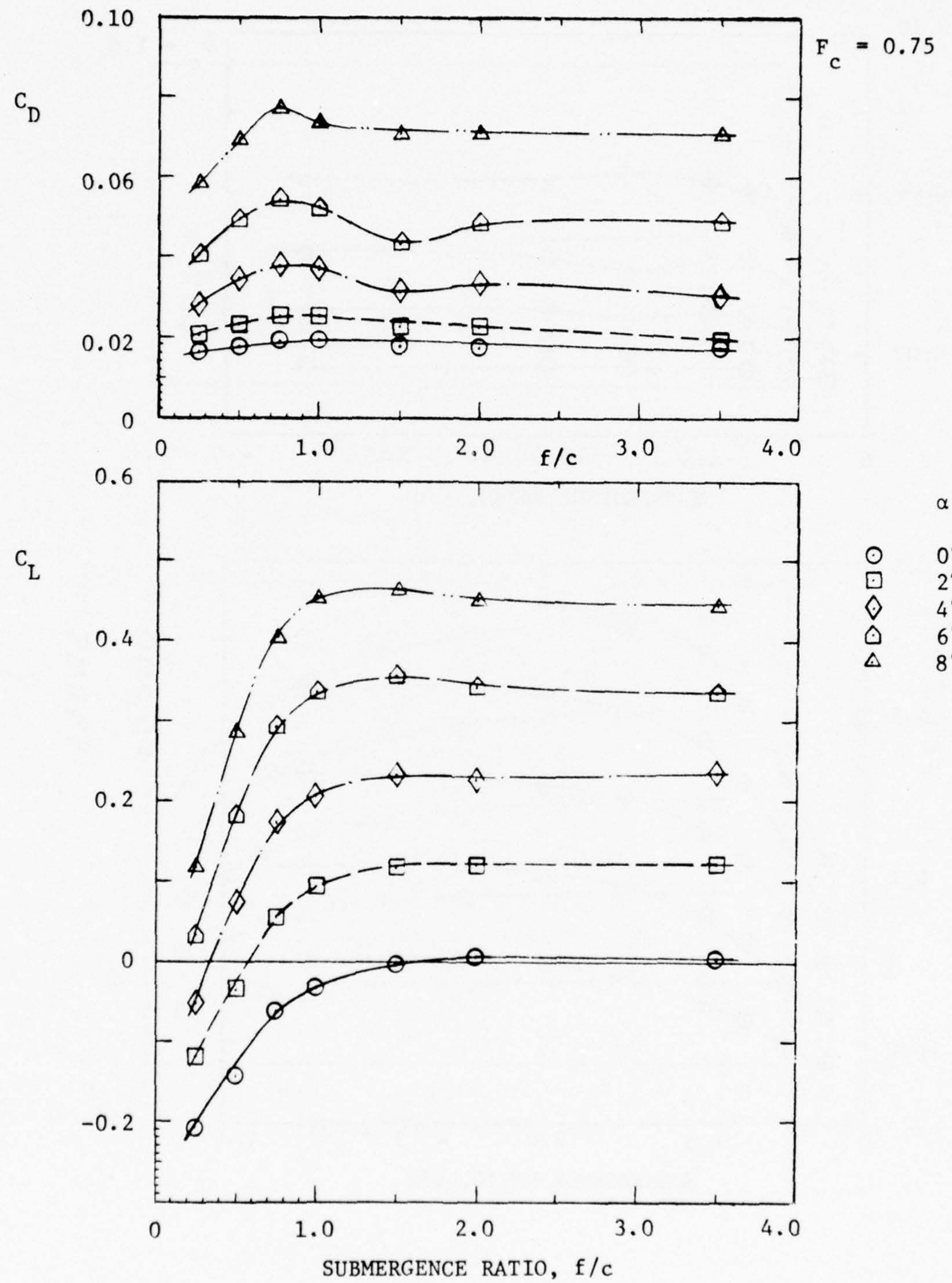

Figure 13 - Measured Drag and Lift Coefficients Versus Submergence Ratio for Chord Froude Number F_c = 0.75

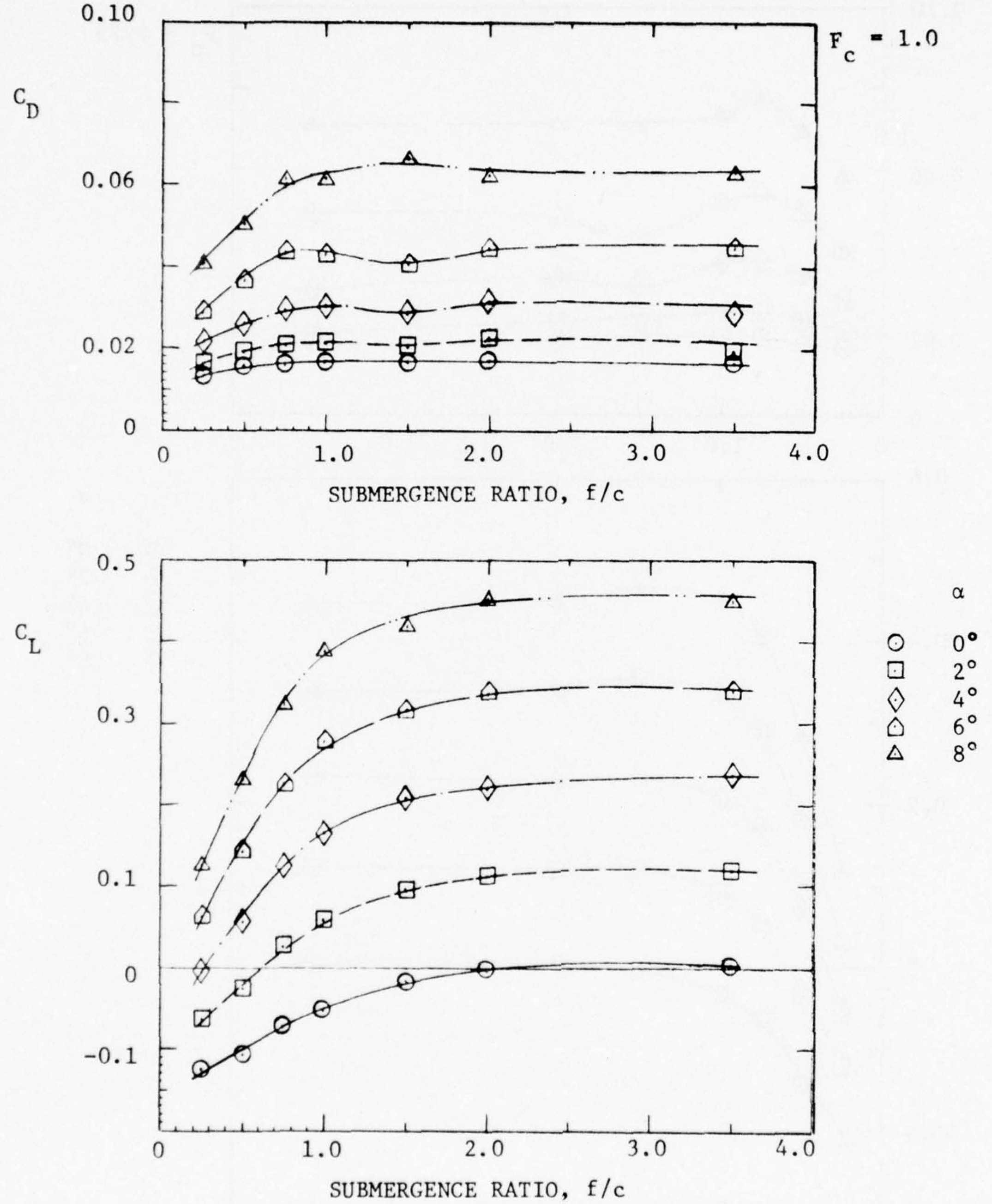

Figure 14 - Measured Drag and Lift Coefficients Versus Submergence Ratio for Chord Froude Number F_c = 1.0

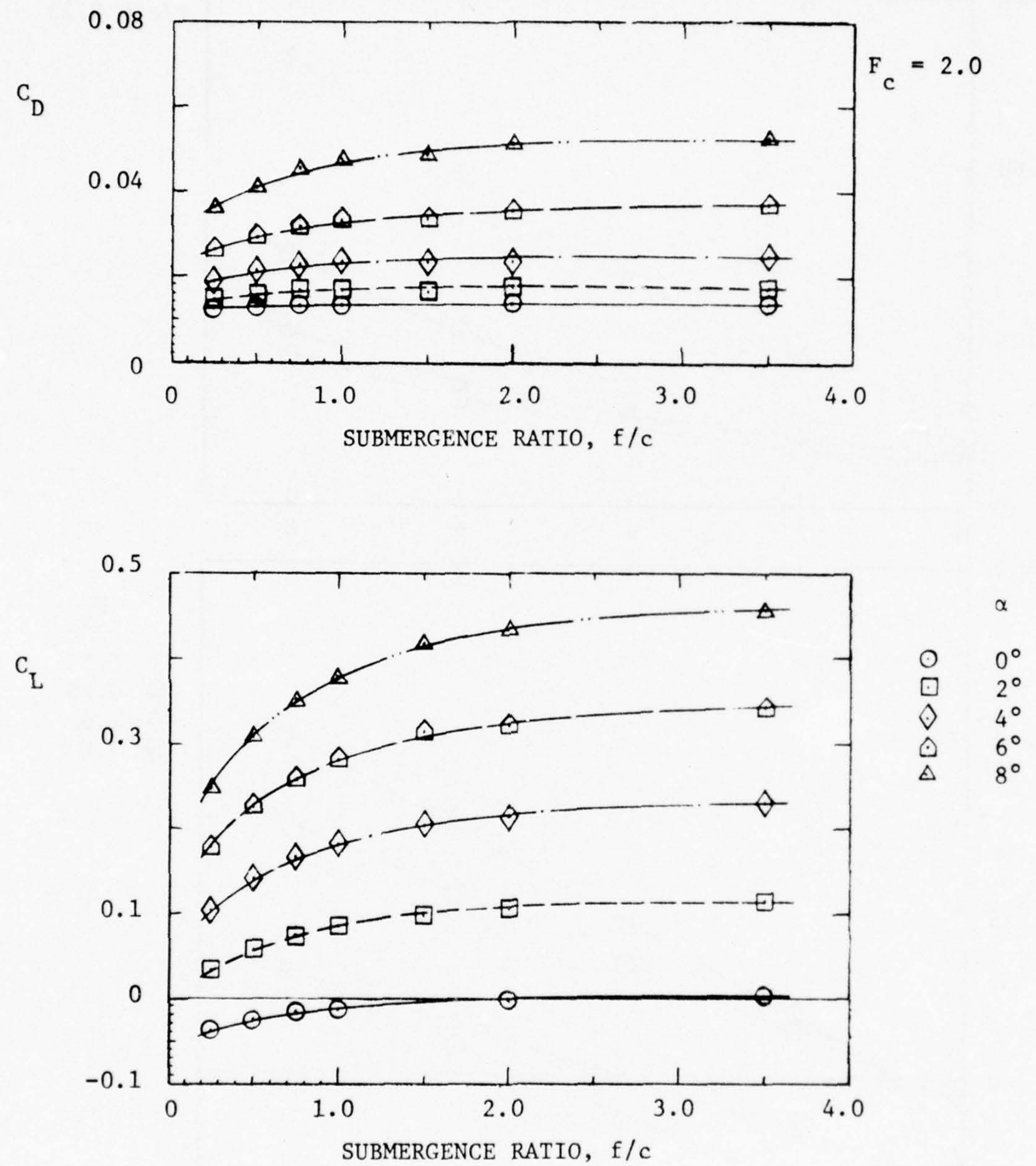

Figure 15 - Measured Drag and Lift Coefficients Versus Submergence Ratio for Chord Froude Number F_c = 2.0

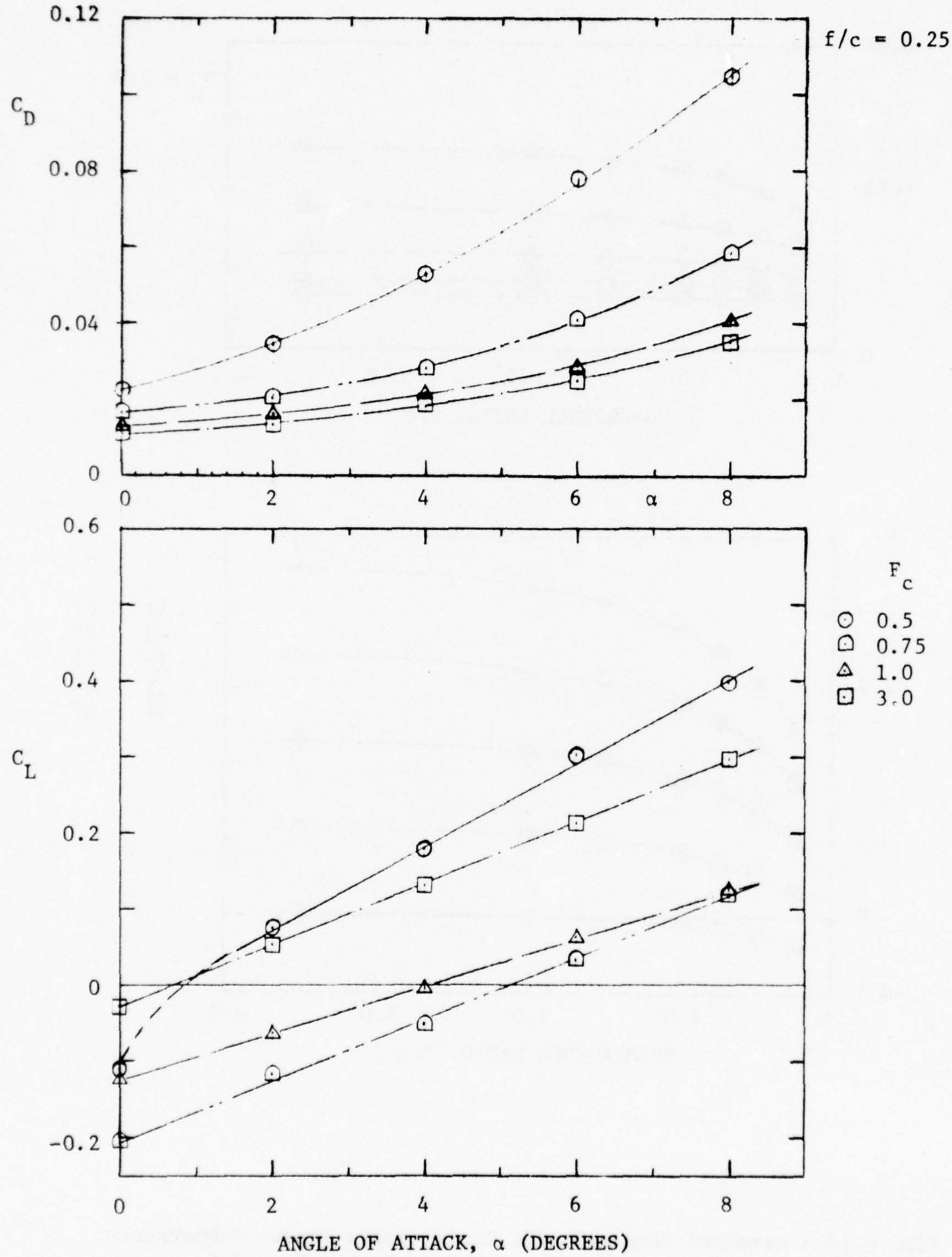

Figure 16 - Measured Drag and Lift Coefficients Versus Angle of Attack for Submergence Ratio f/c = 0.25

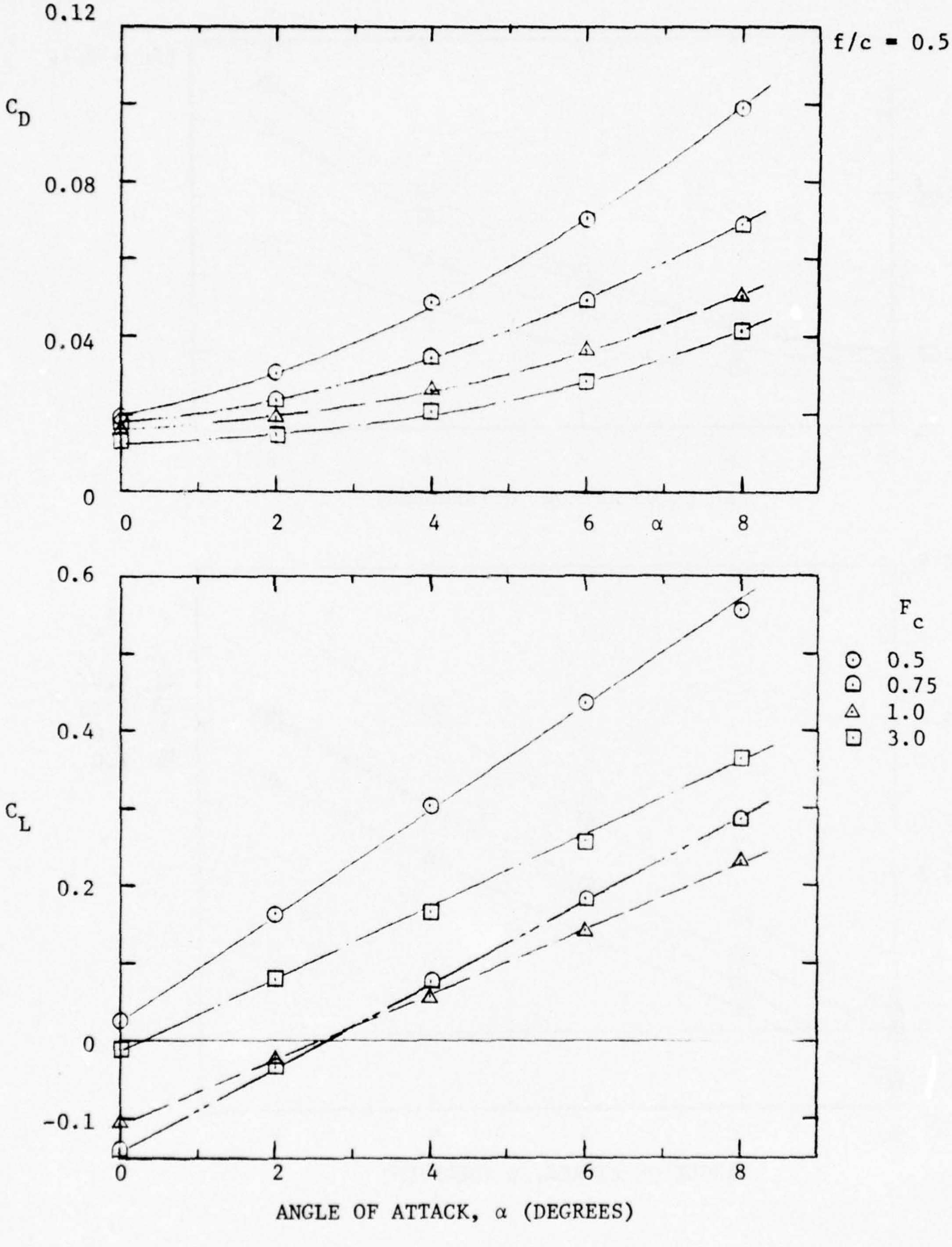

Figure 17 - Measured Drag and Lift Coefficients Versus Angle of Attack for Submergence Ratio f/c = 0.5

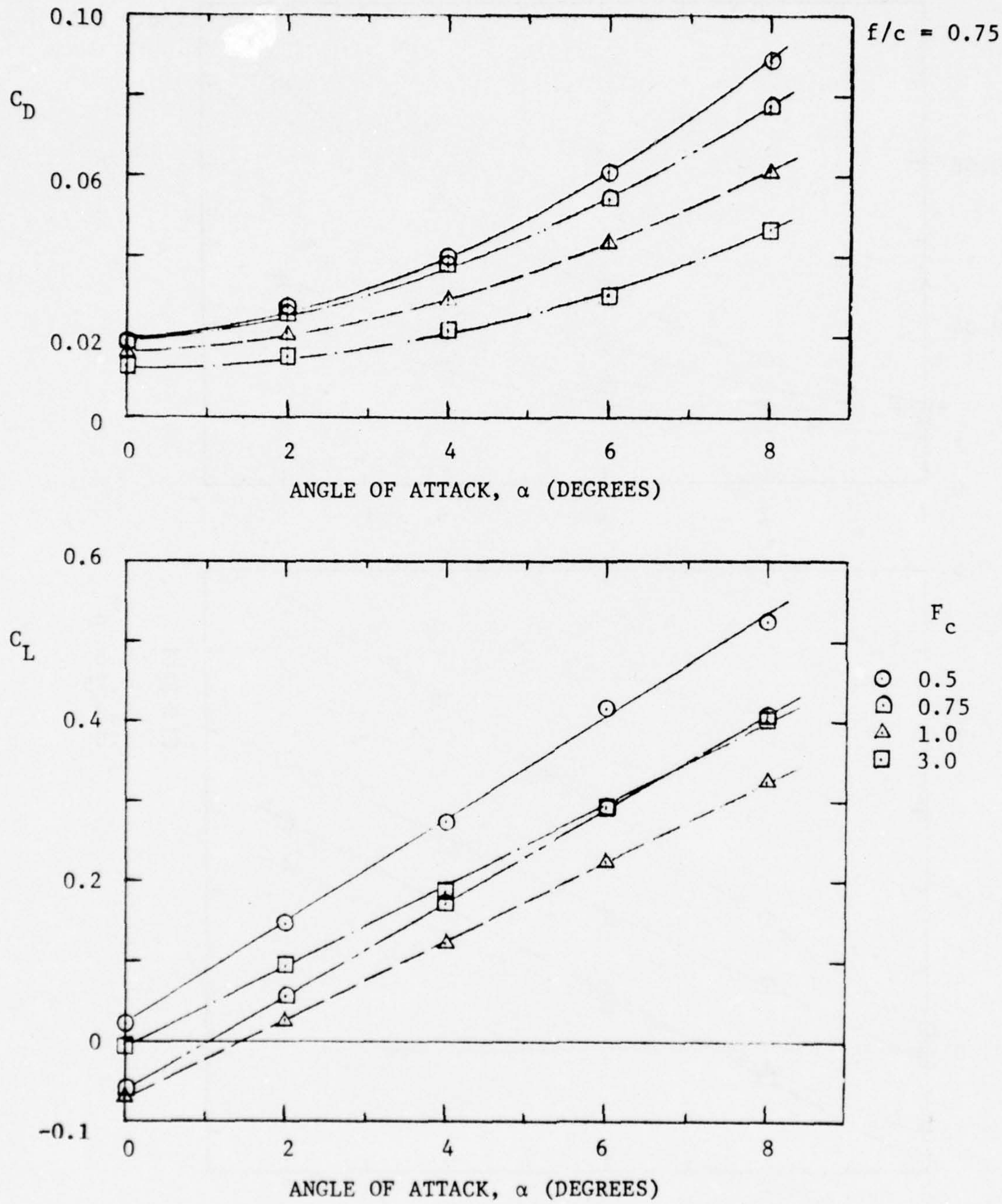

Figure 18 - Measured Drag and Lift Coefficients Versus Angle of Attack for Submergence Ratio f/c = 0.75

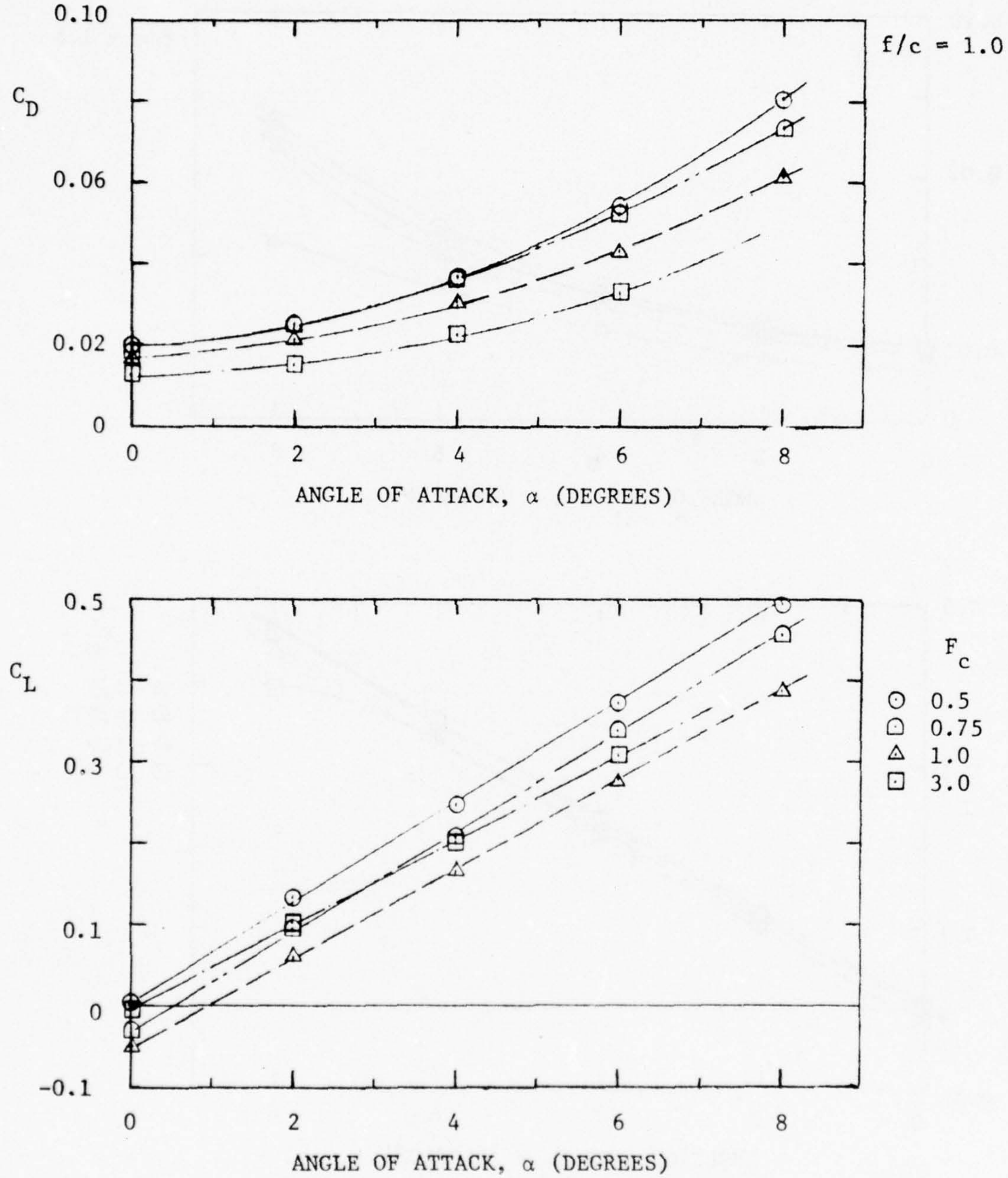

Figure 19 - Measured Drag and Lift Coefficients Versus Angle of Attack for Submergence Ratio f/c = 1.0

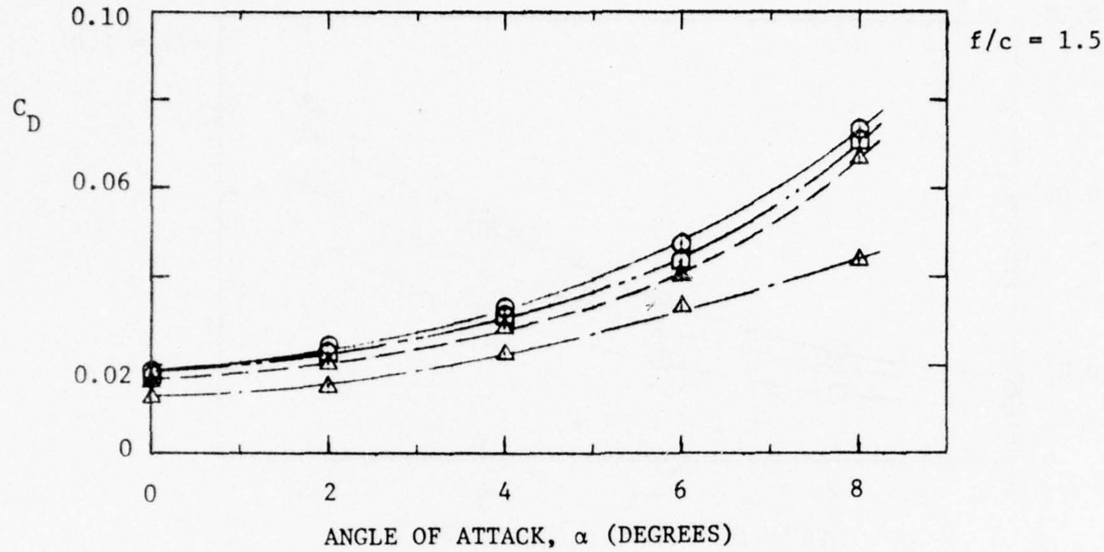

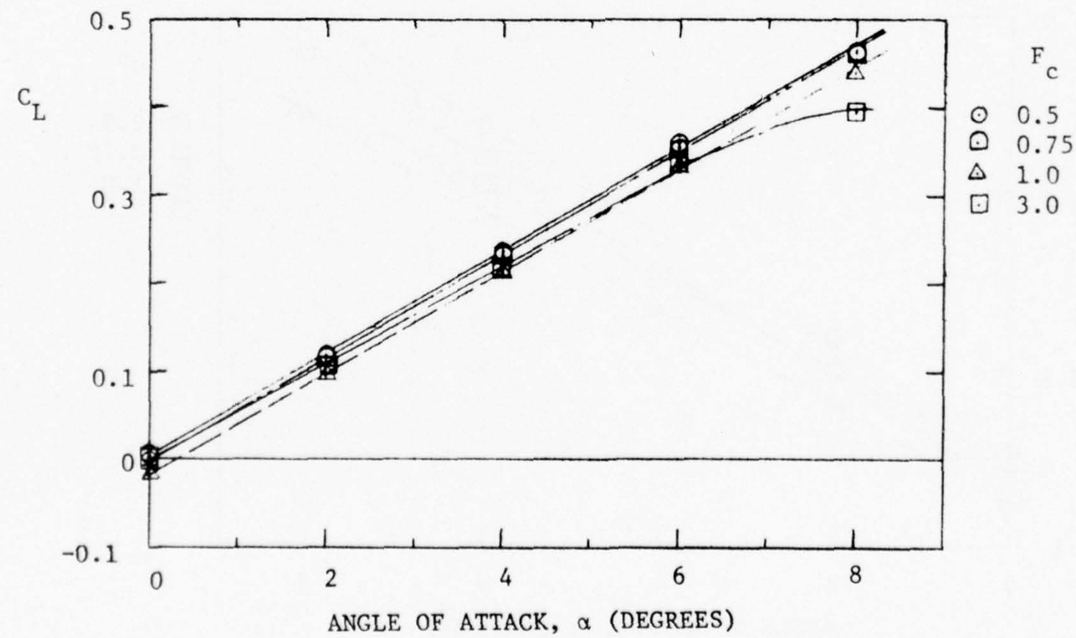

Figure 20 - Measured Drag and Lift Coefficients Versus Angle of Attack for Submergence Ratio f/c = 1.5

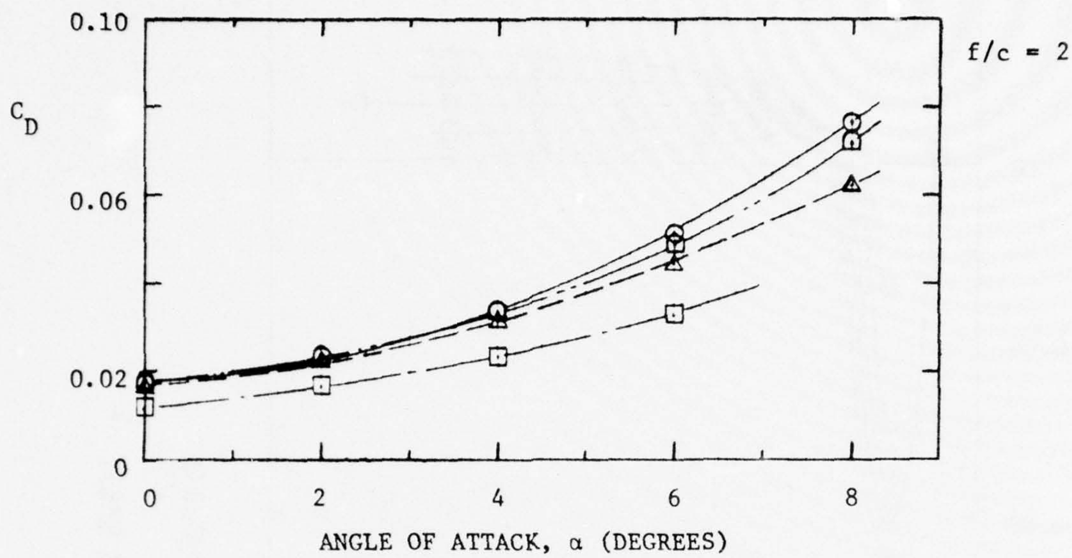

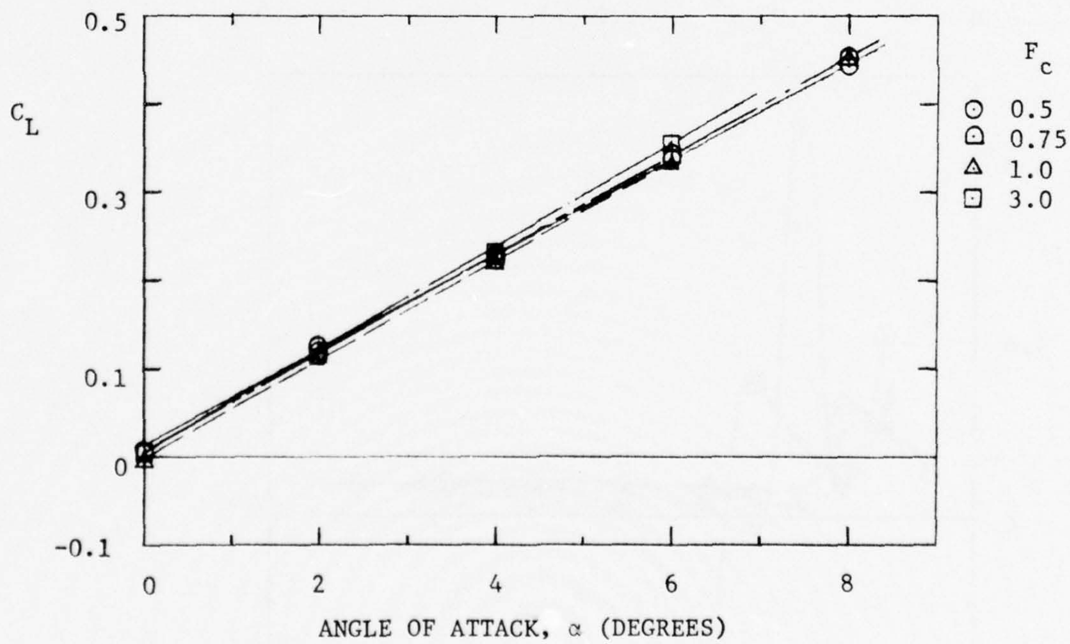

Figure 21 - Measured Drag and Lift Coefficients Versus Angle of Attack for Submergence Ratio f/c = 2.0

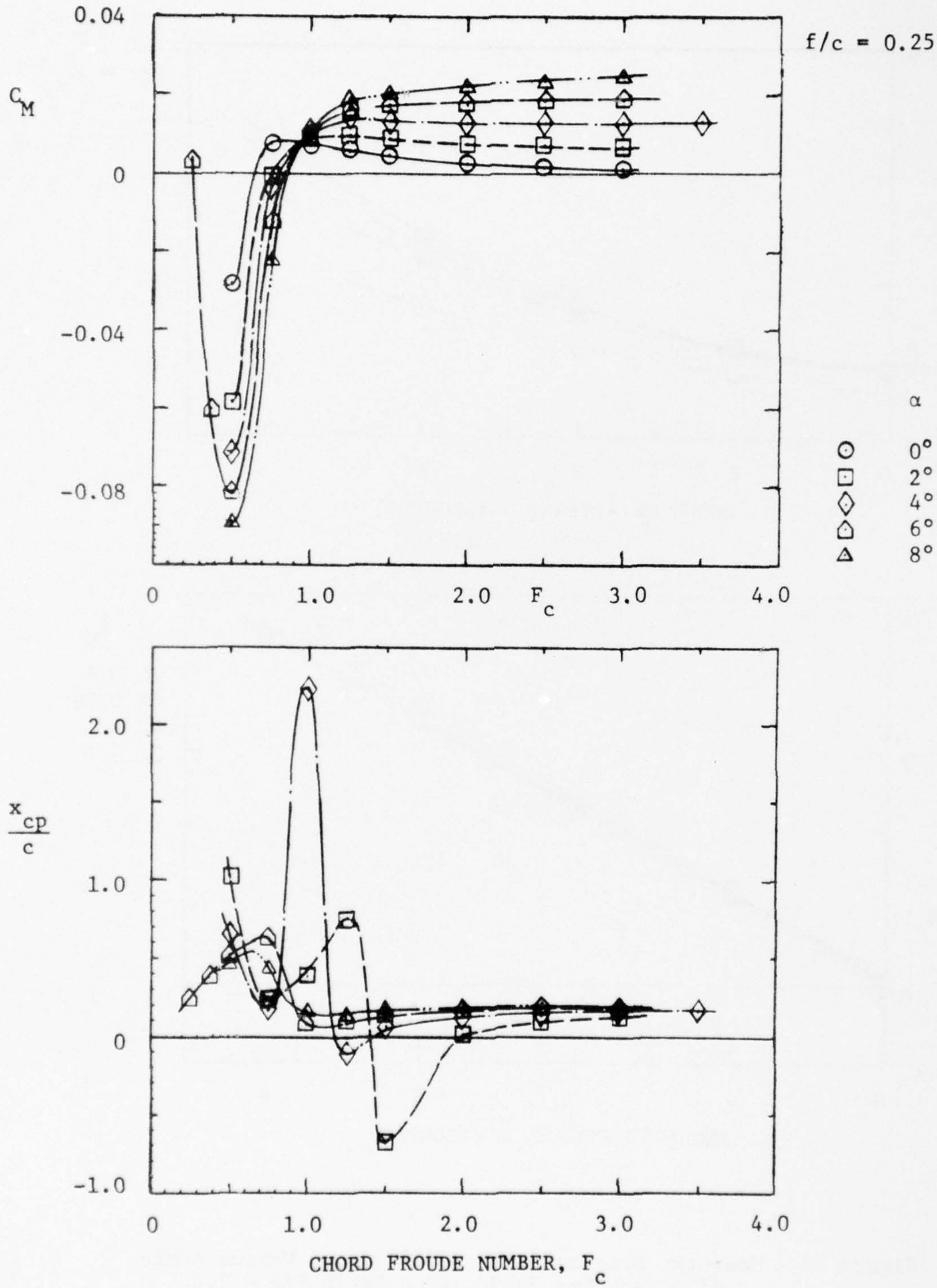

Figure 22 - Measured Pitching Moment Coefficients and Center of Pressure Ratios Versus Chord Froude Number for Submergence Ratio f/c = 0.25

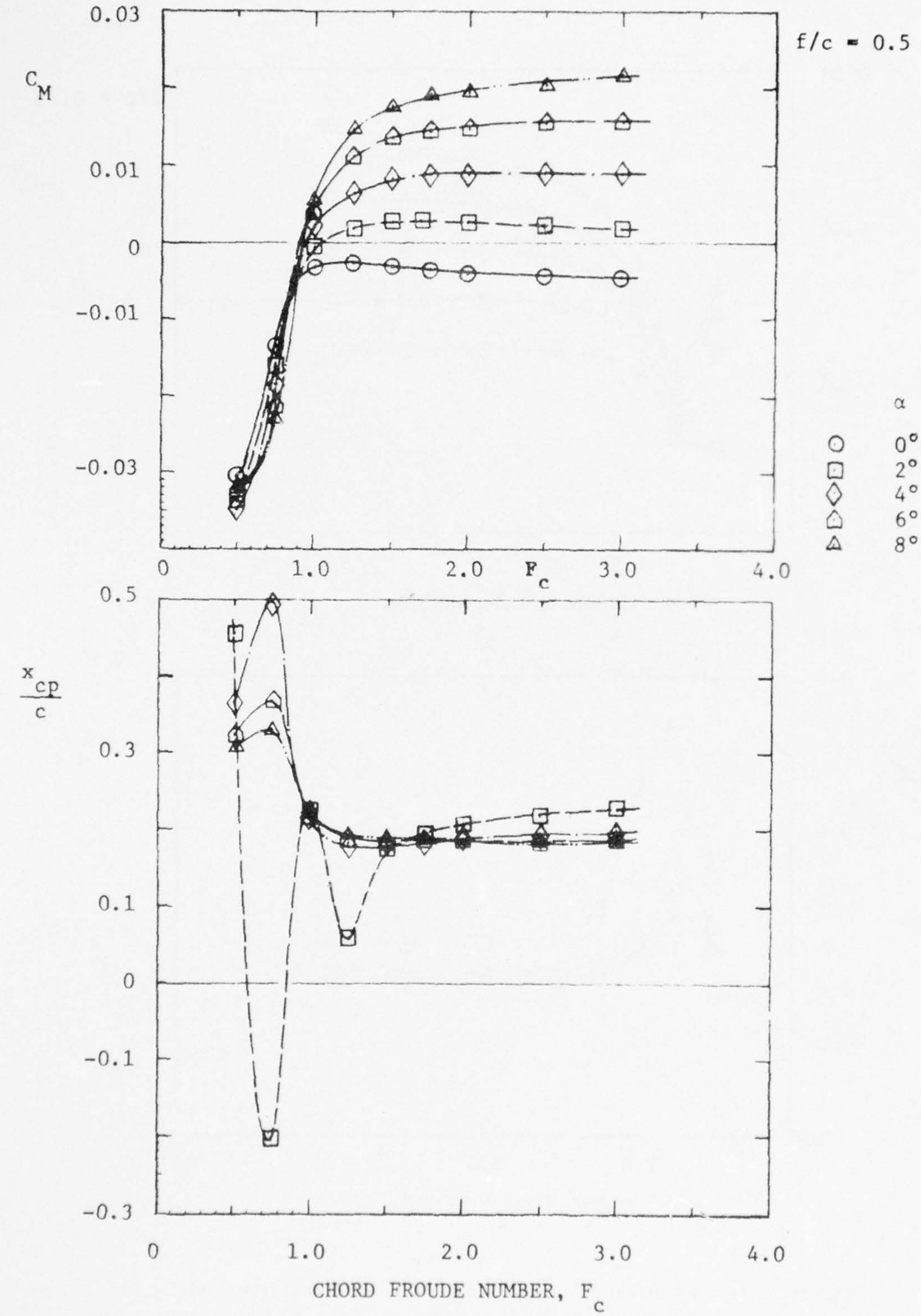

Figure 23 - Measured Pitching Moment Coefficients and Center of Pressure Ratios Versus Chord Froude Number for Submergence Ratio f/c = 0.5

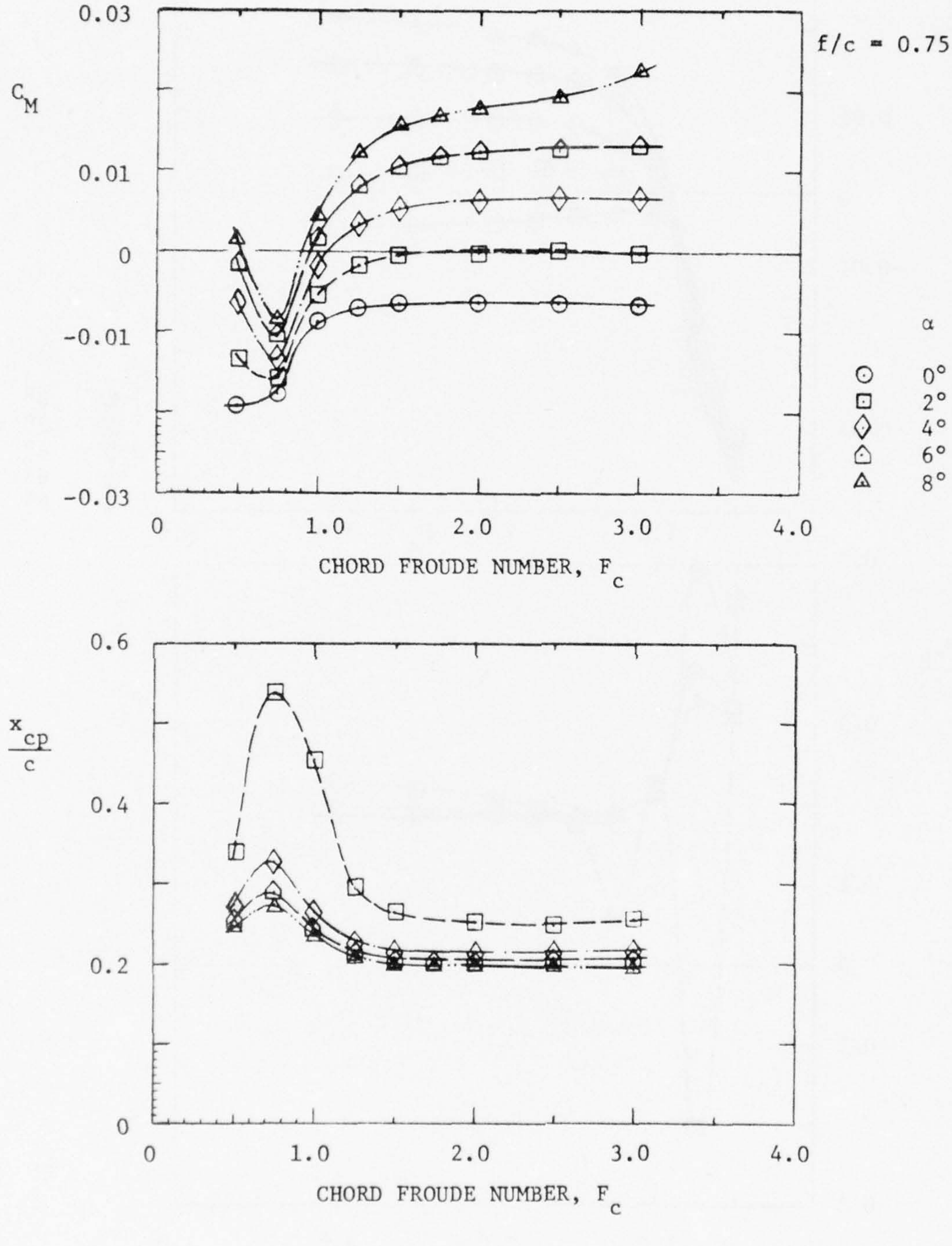

Figure 24 - Measured Pitching Moment Coefficients and Center of Pressure Ratios Versus Chord Froude Number for Submergence Ratio f/c = 0.75

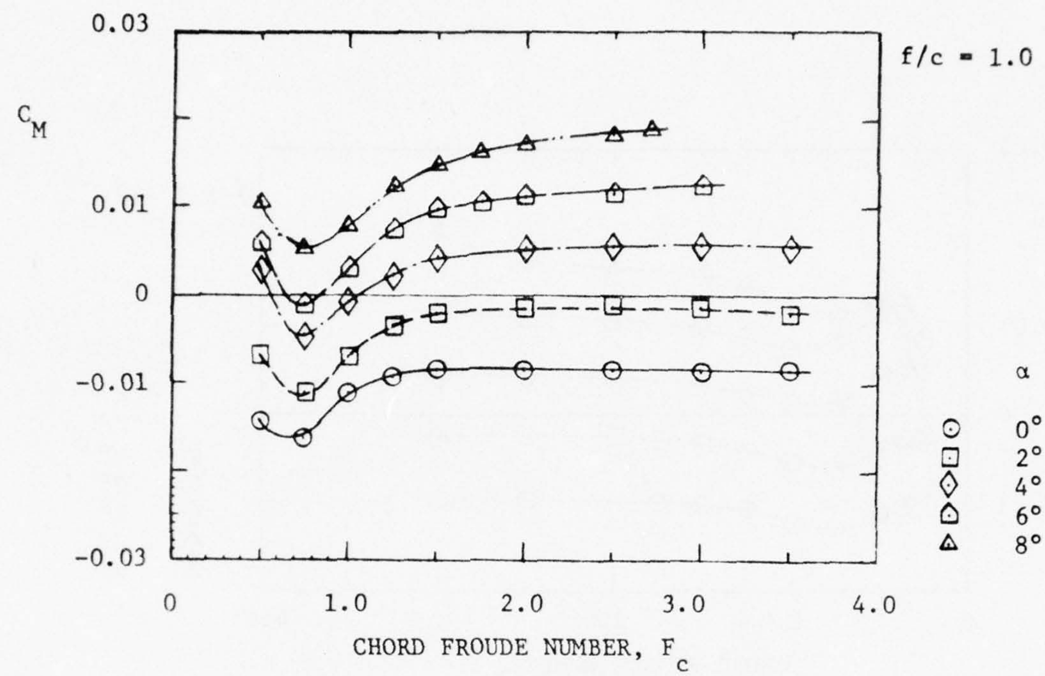

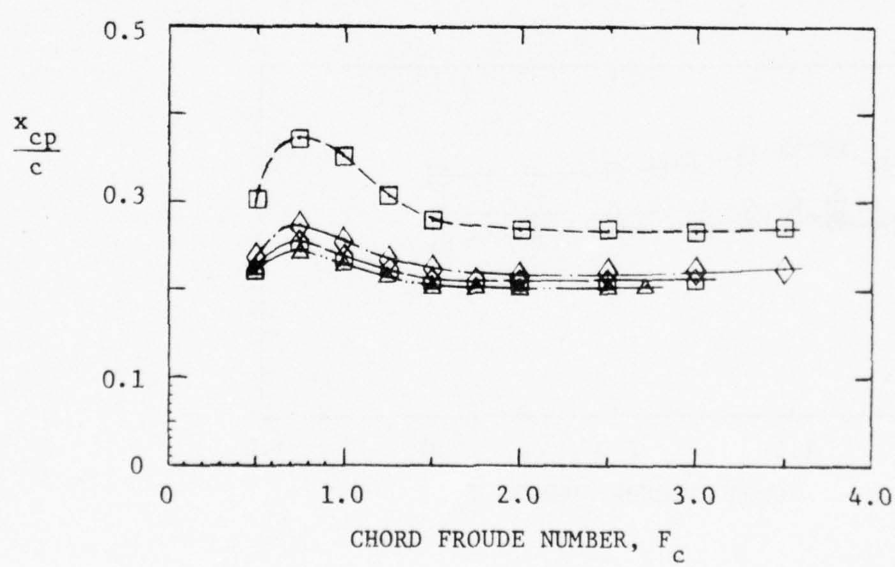

Figure 25 - Measured Pitching Moment Coefficients and Center of Pressure Ratios Versus Chord Froude Number for Submergence Ratio f/c = 1.0

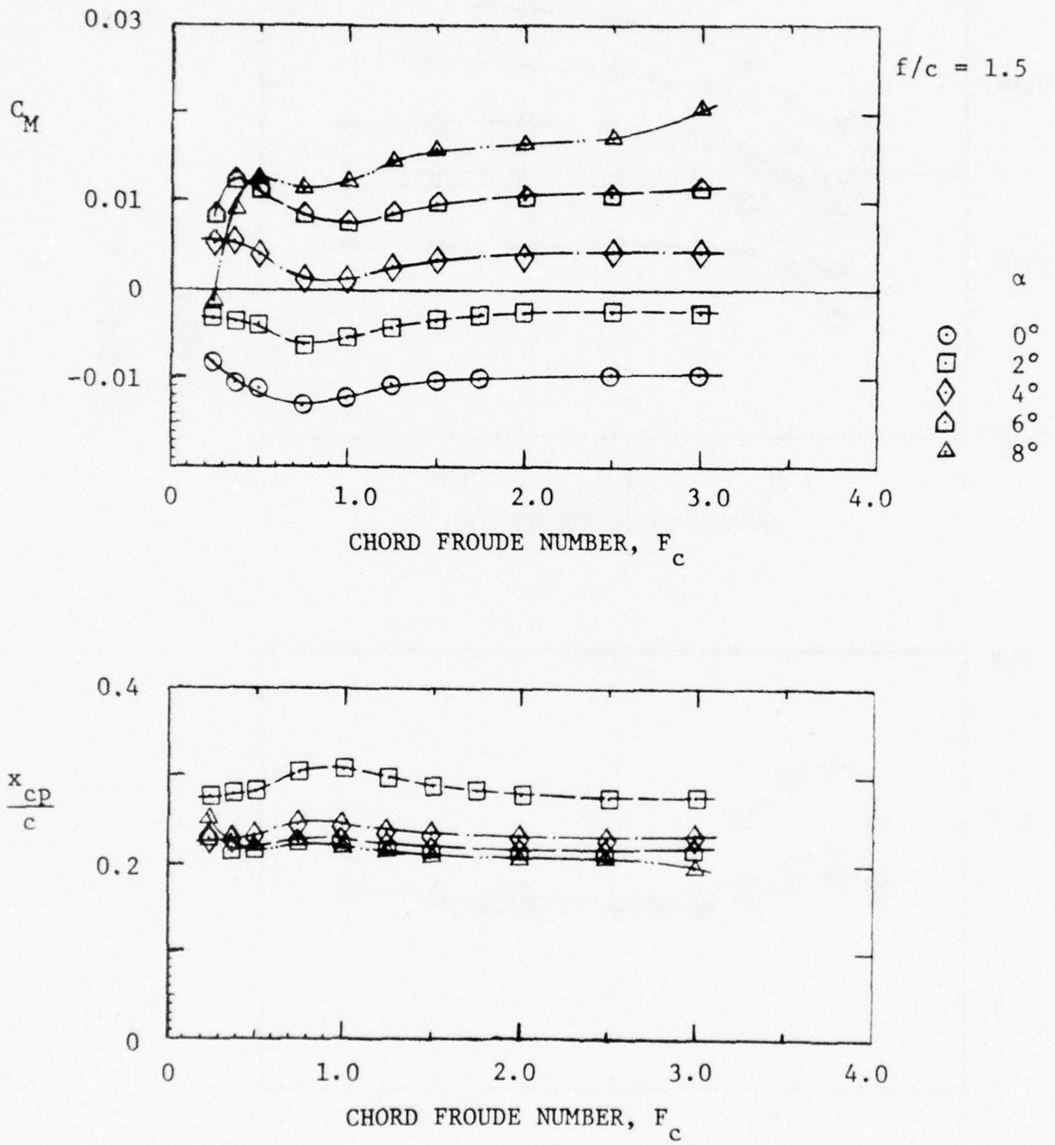

Figure 26 - Measured Pitching Moment Coefficients and Center of Pressure Ratios Versus Chord Froude Number for Submergence Ratio f/c = 1.5

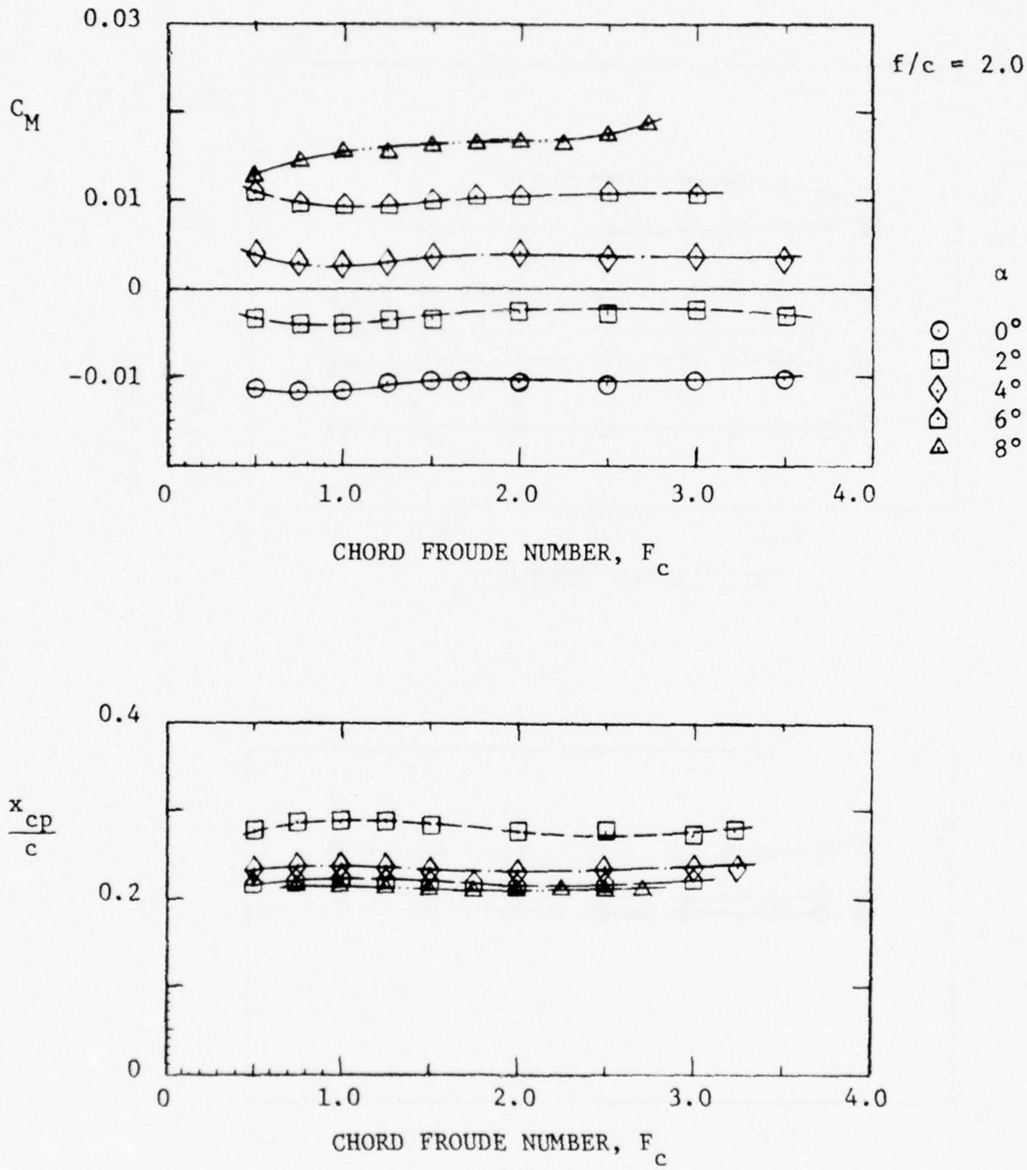

Figure 27 - Measured Pitching Moment Coefficients and Center of Pressure Ratios Versus Chord Froude Number for Submergence Ratio f/c = 2.0

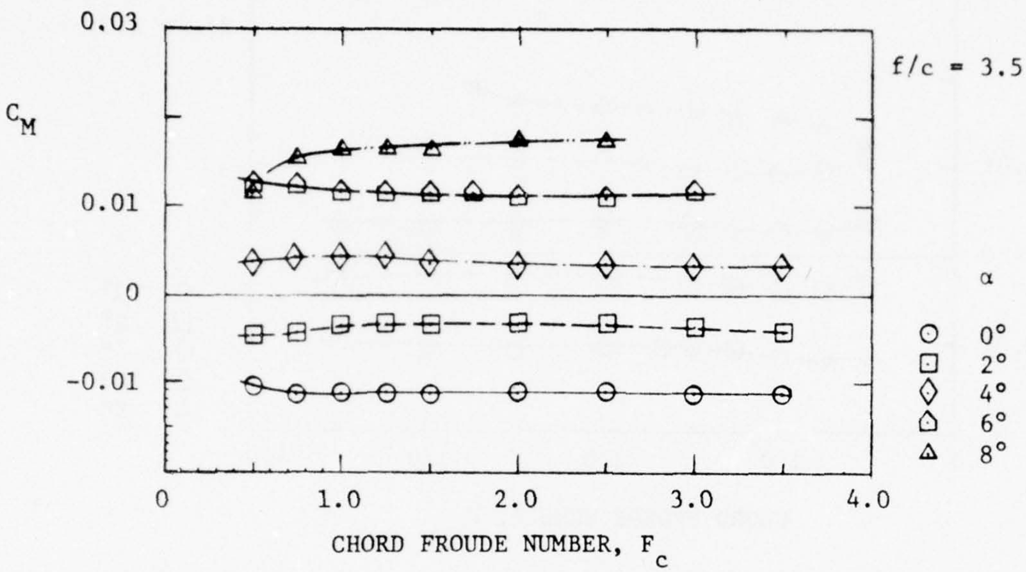

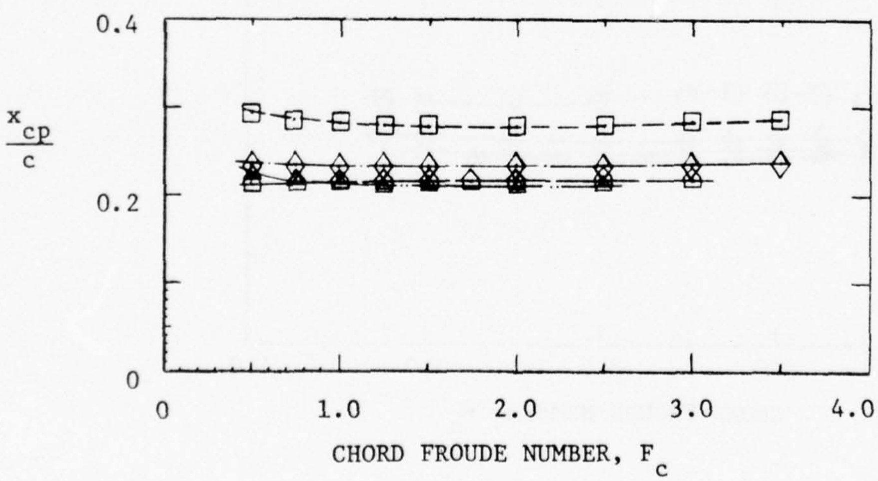

Figure 28 - Measured Pitching Moment Coefficients and Center of Pressure Ratios Versus Chord Froude Number for Submergence Ratio f/c = 3.5

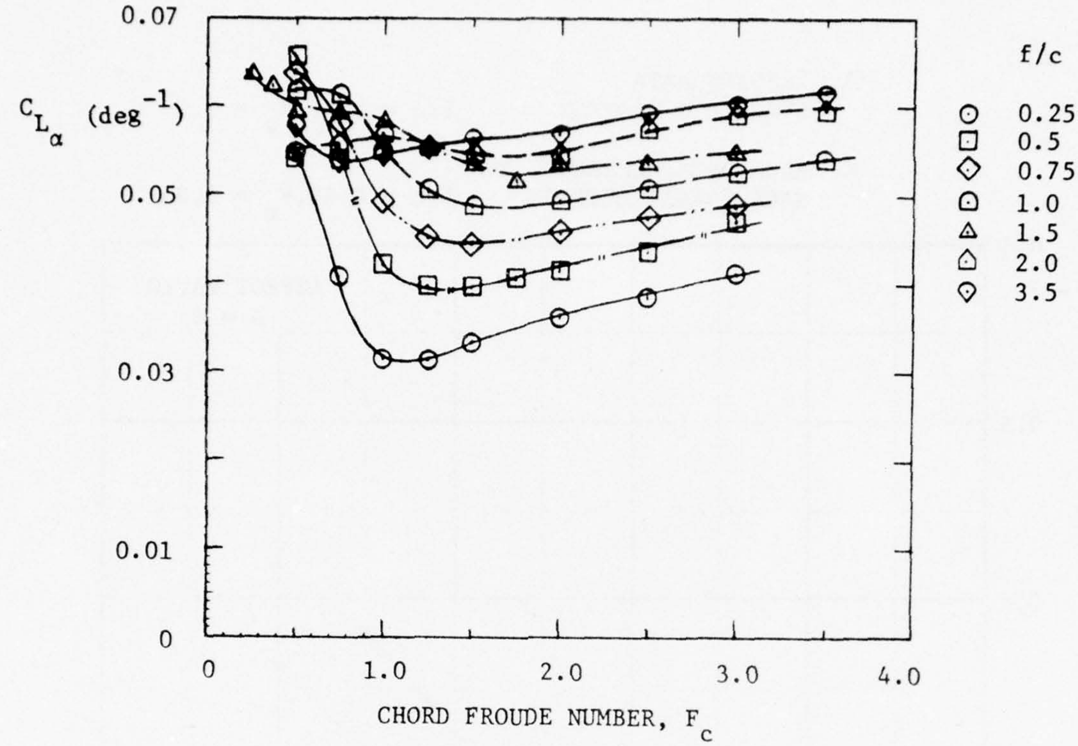

Figure 29 - Lift-Slope Coefficient Versus Chord Froude Number for Various Submergence Ratios

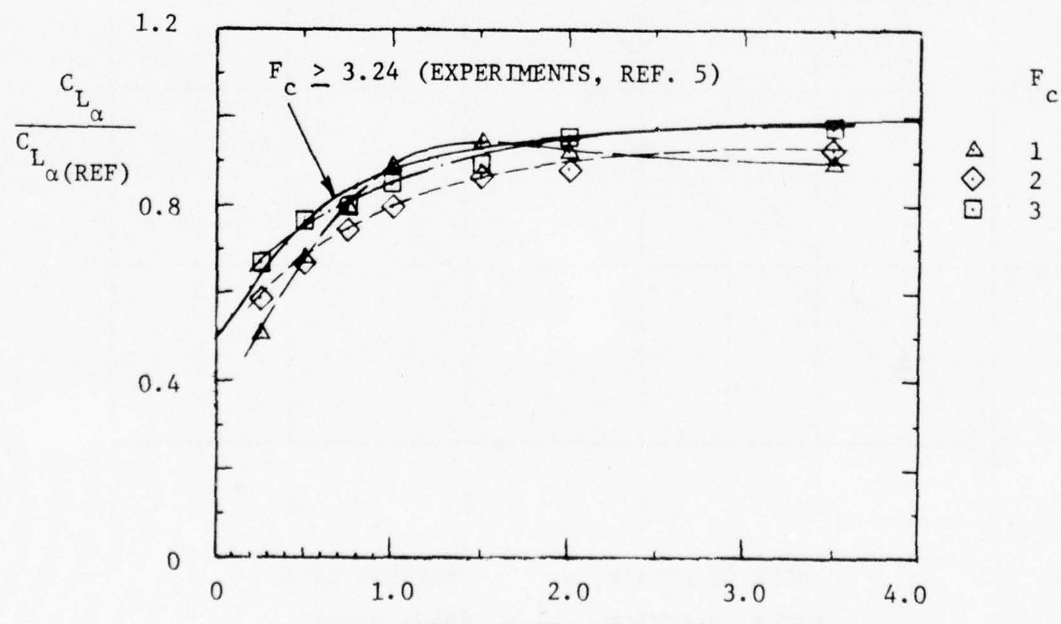

Figure 30 - Relative Lift-Slope Coefficients Versus Submergence Ratios for Several Chord Froude Numbers

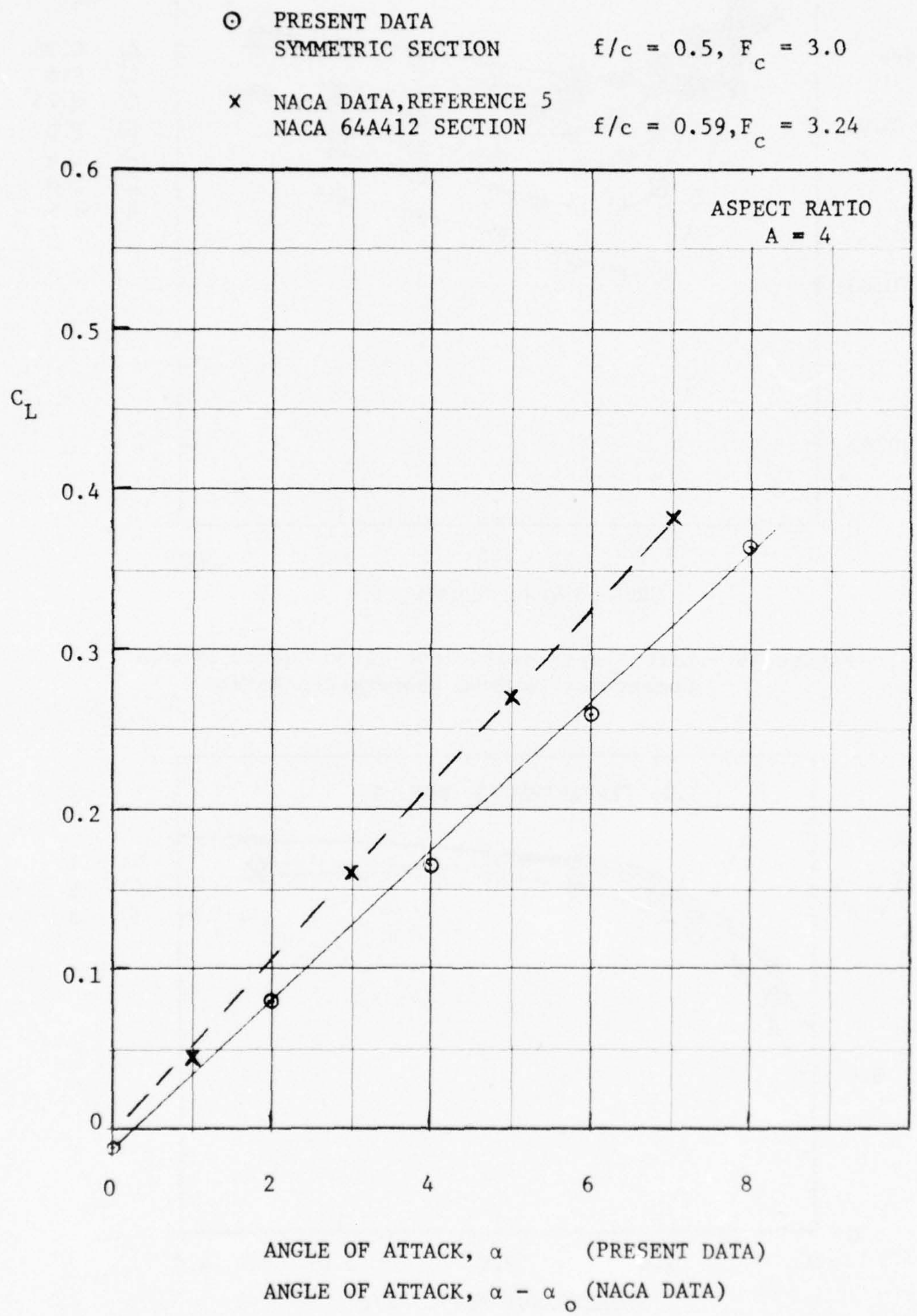

Figure 31 - Comparison of Lift Coefficient Versus Angle of Attack for Constant Submergence Ratio and Chord Froude Number

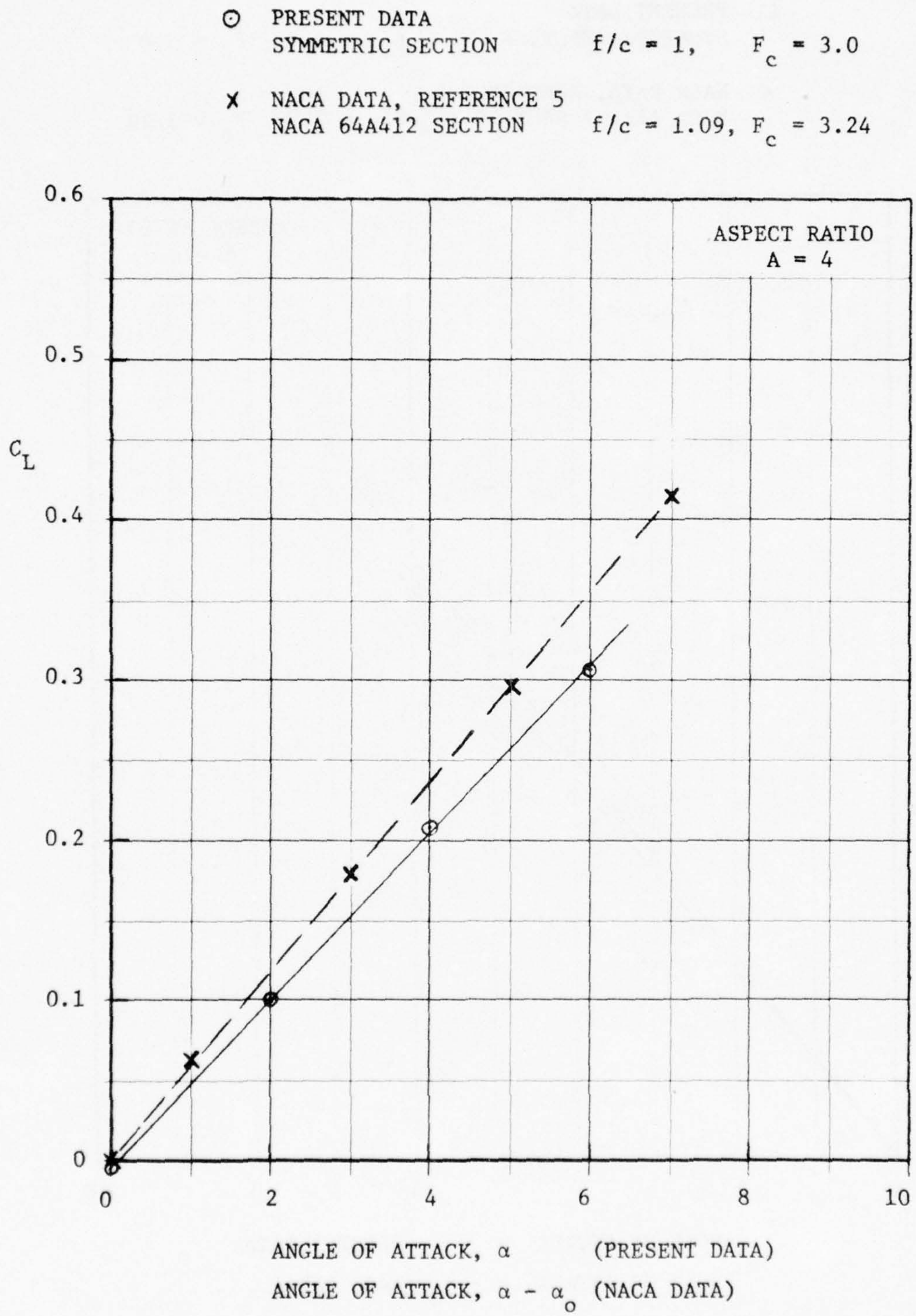

Figure 32 - Comparison of Lift Coefficient Versus Angle of Attack for Constant Submergence Ratio and Chord Froude Number

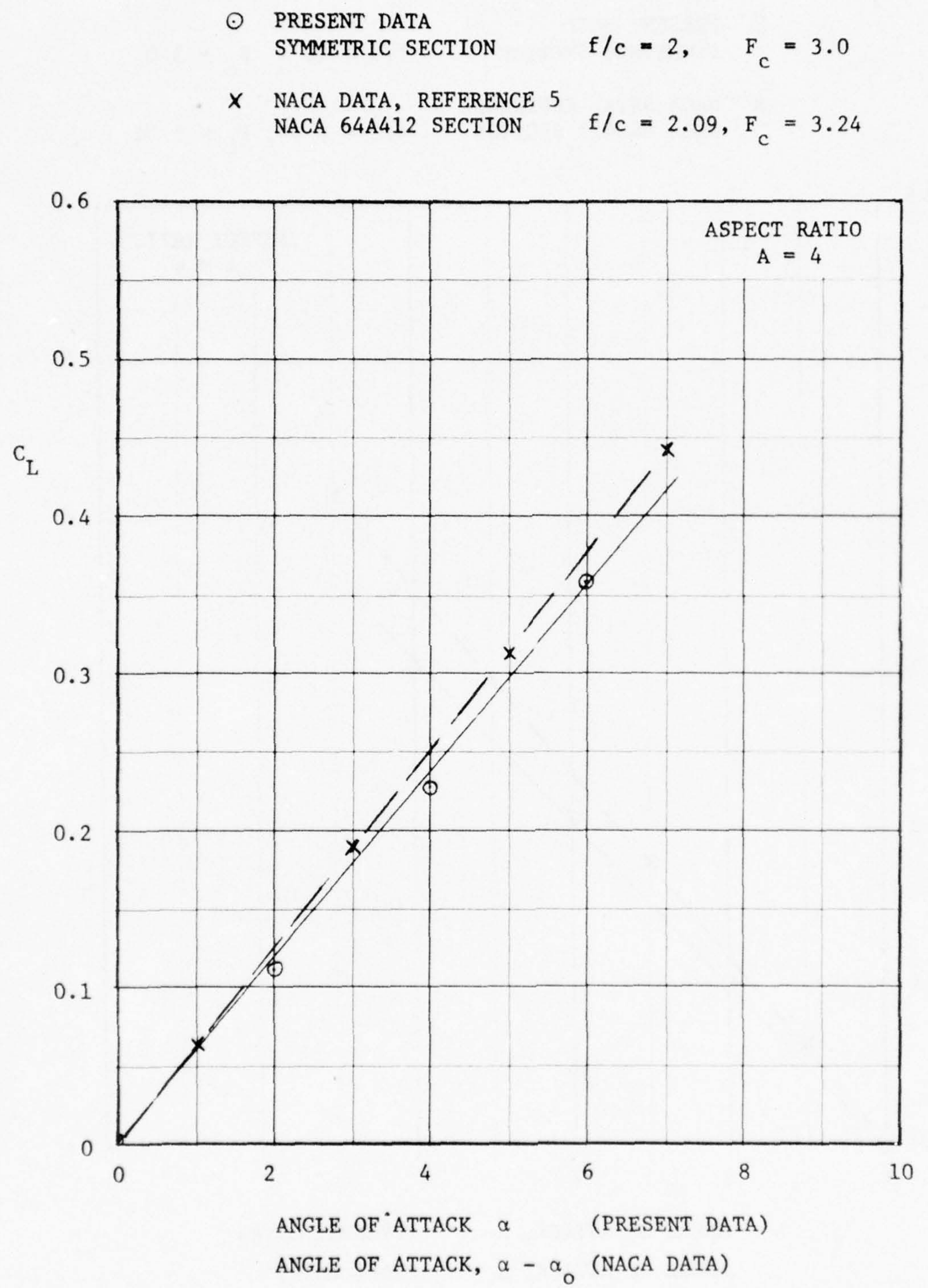

Figure 33 - Comparison of Lift Coefficient Versus Angle of Attack for Constant Submergence Ratio and Chord Froude Number

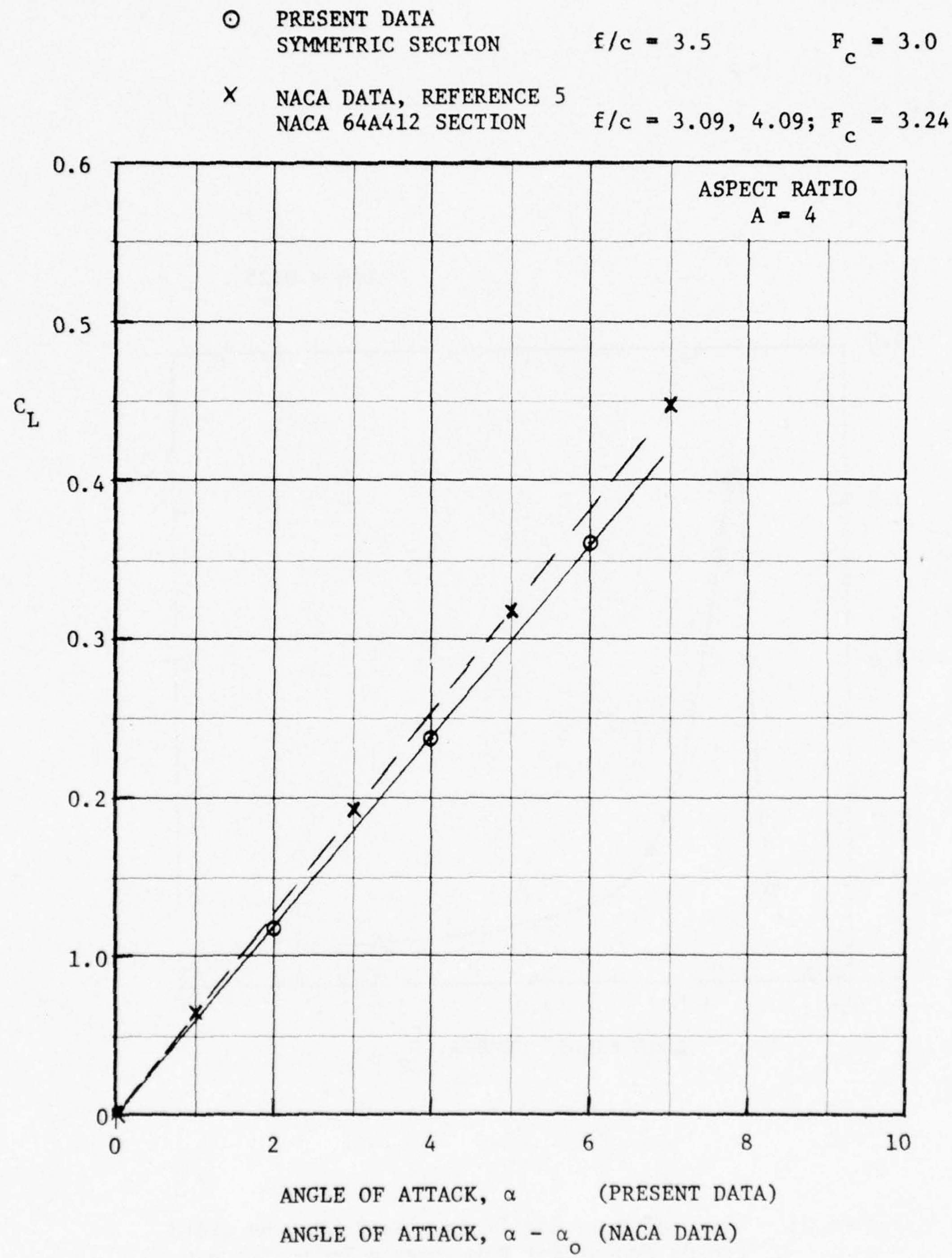

Figure 34 - Comparison of Lift Coefficient Versus Angle of Attack for Constant Submergence Ratio and Chord Froude Number

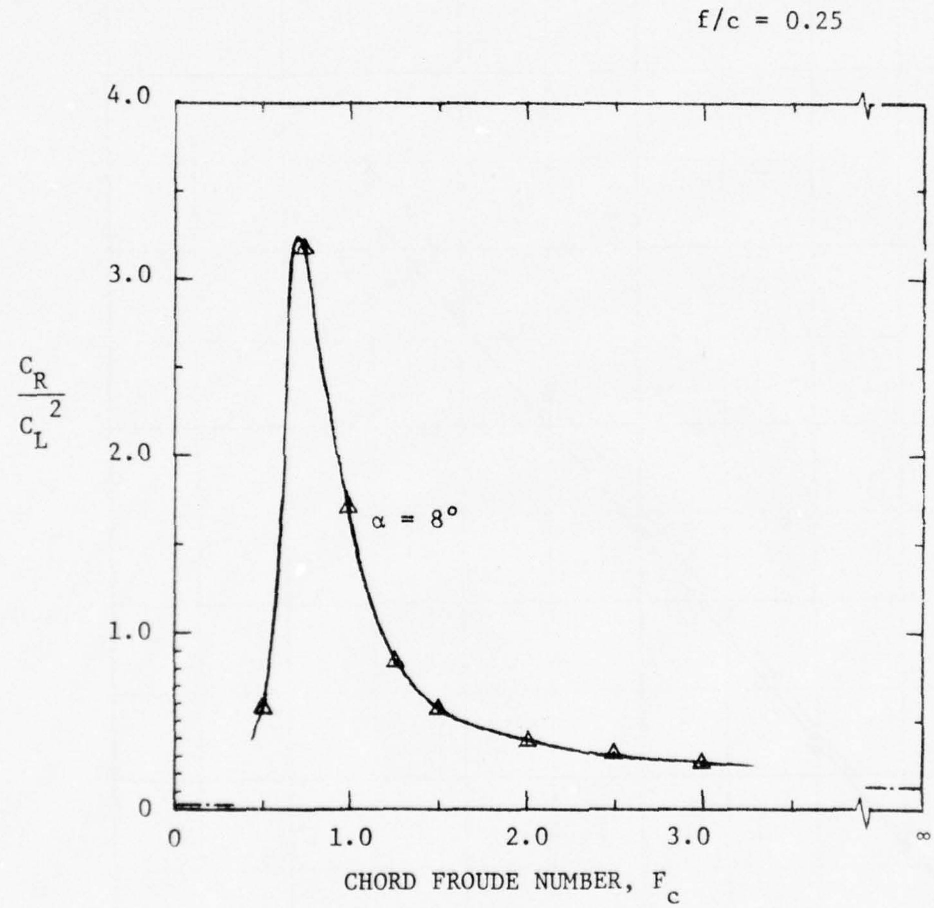

Figure 35 - Residual Drag Coefficient Ratio Versus Chord Froude Number for Submergence Ratio f/c = 0.25

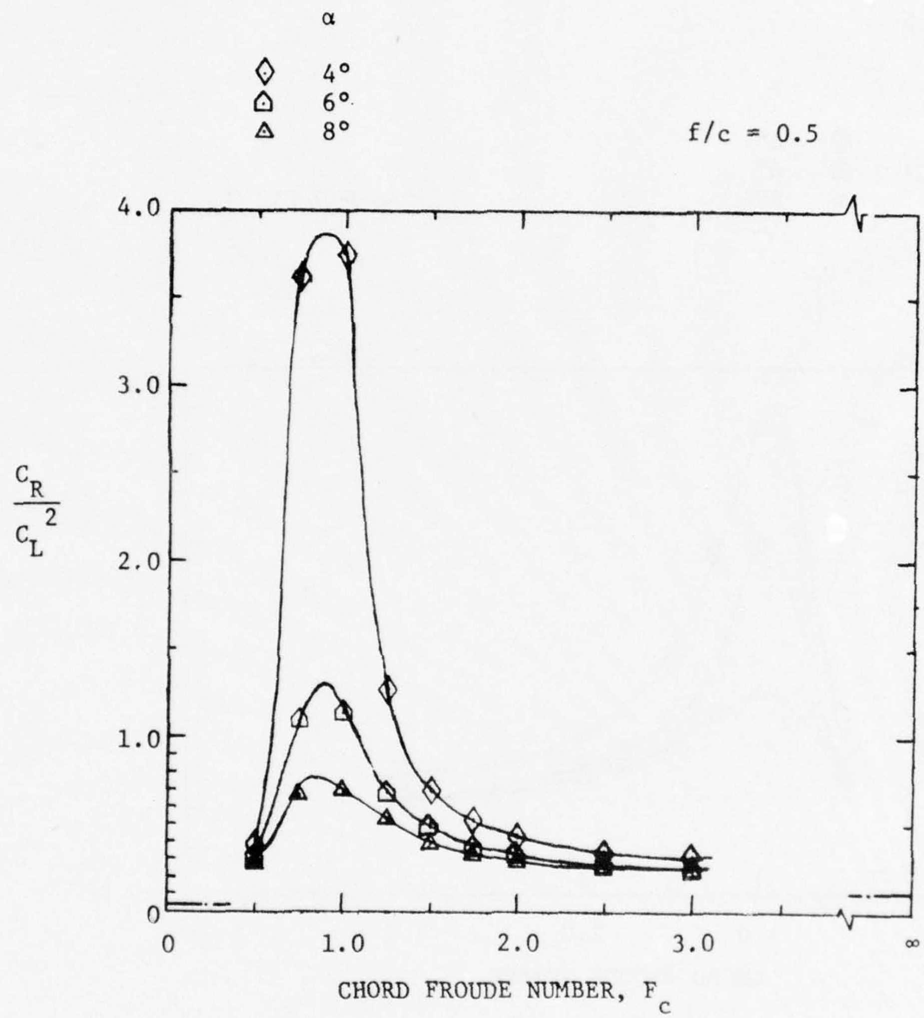

Figure 36 - Residual Drag Coefficient Ratio Versus Chord Froude Number for Submergence Ratio f/c = 0.5

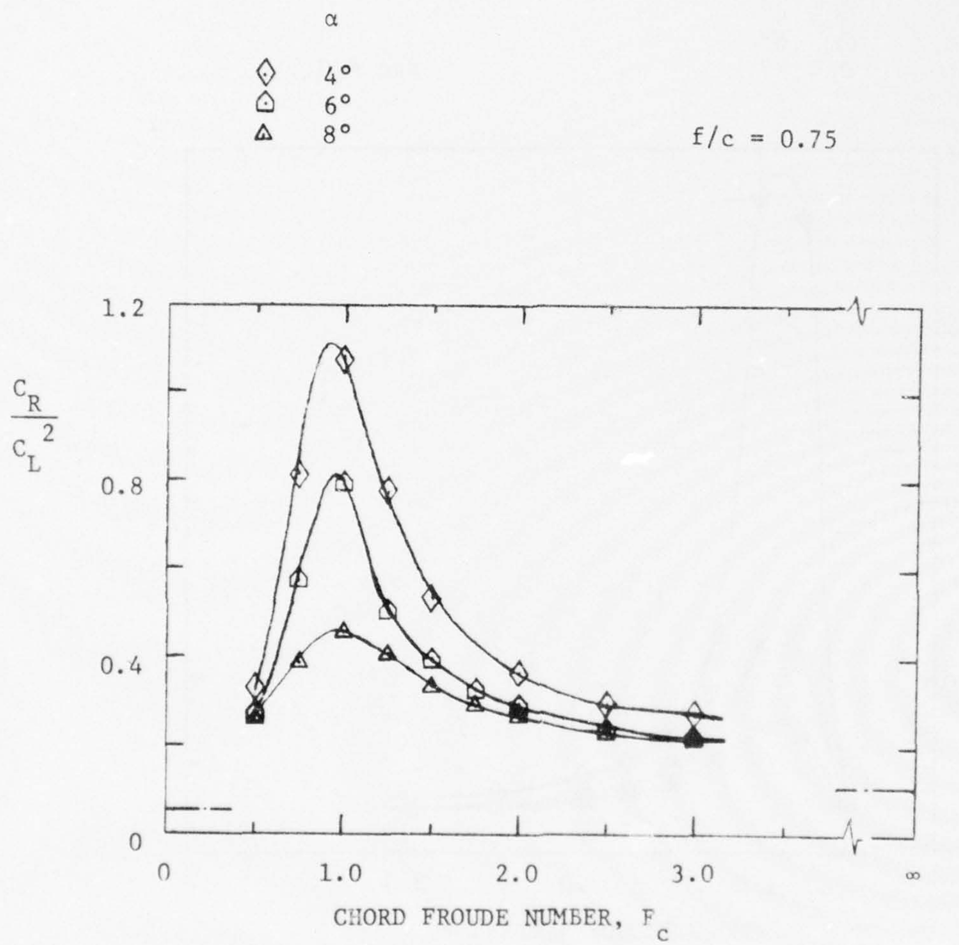

Figure 37 - Residual Drag Coefficient Ratio Versus Chord Froude Number for Submergence Ratio f/c = 0.75

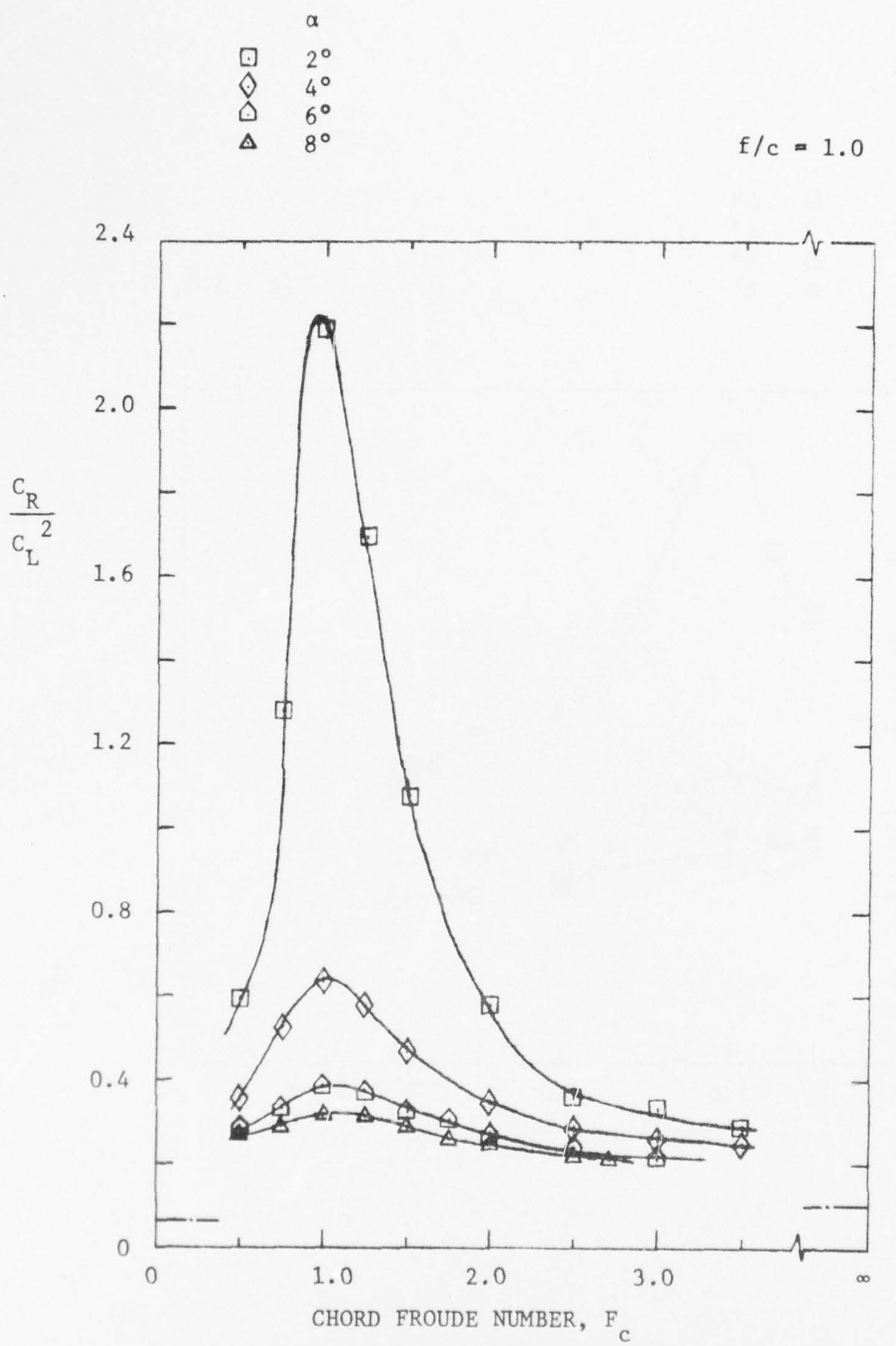

Figure 38 - Residual Drag Coefficient Ratio Versus Chord Froude Number for Submergence Ratio f/c = 1.0

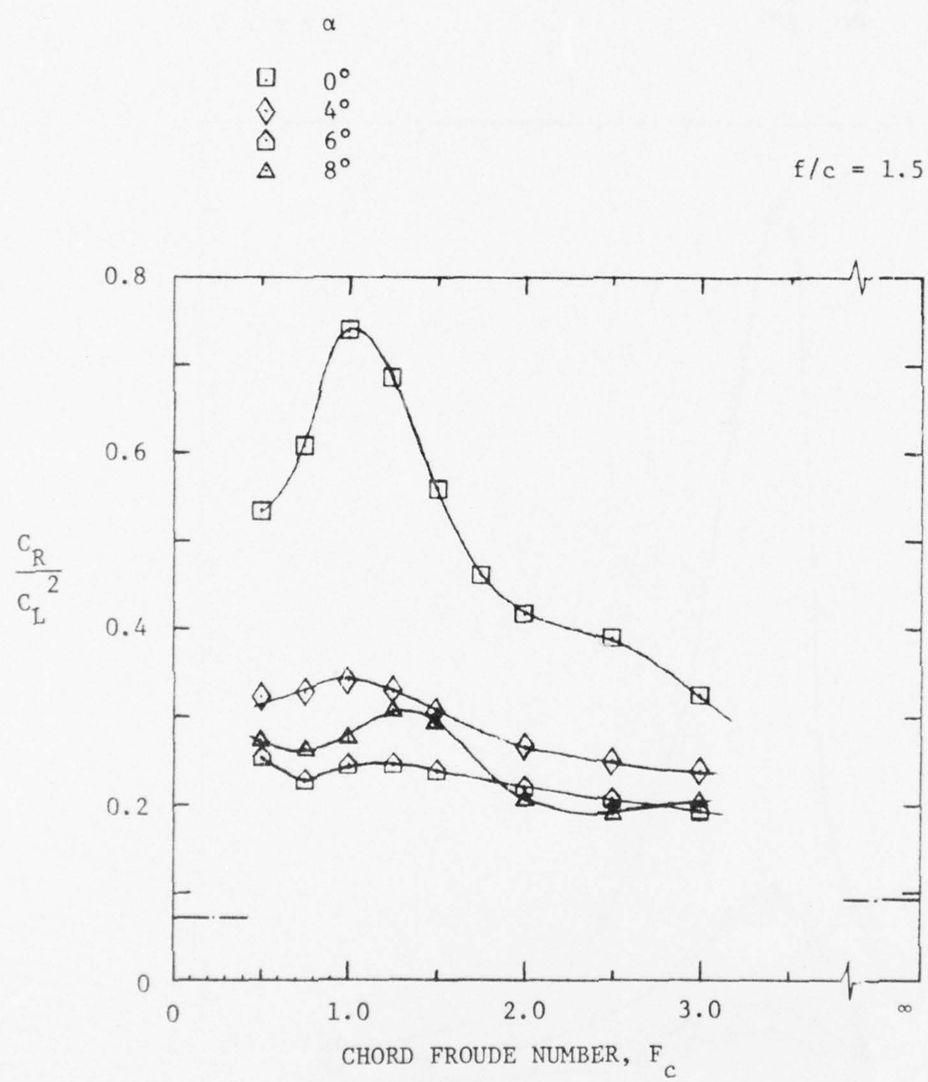

Figure 39 - Residual Drag Coefficient Ratio Versus Chord Froude Number for Submergence Ratio f/c = 1.5

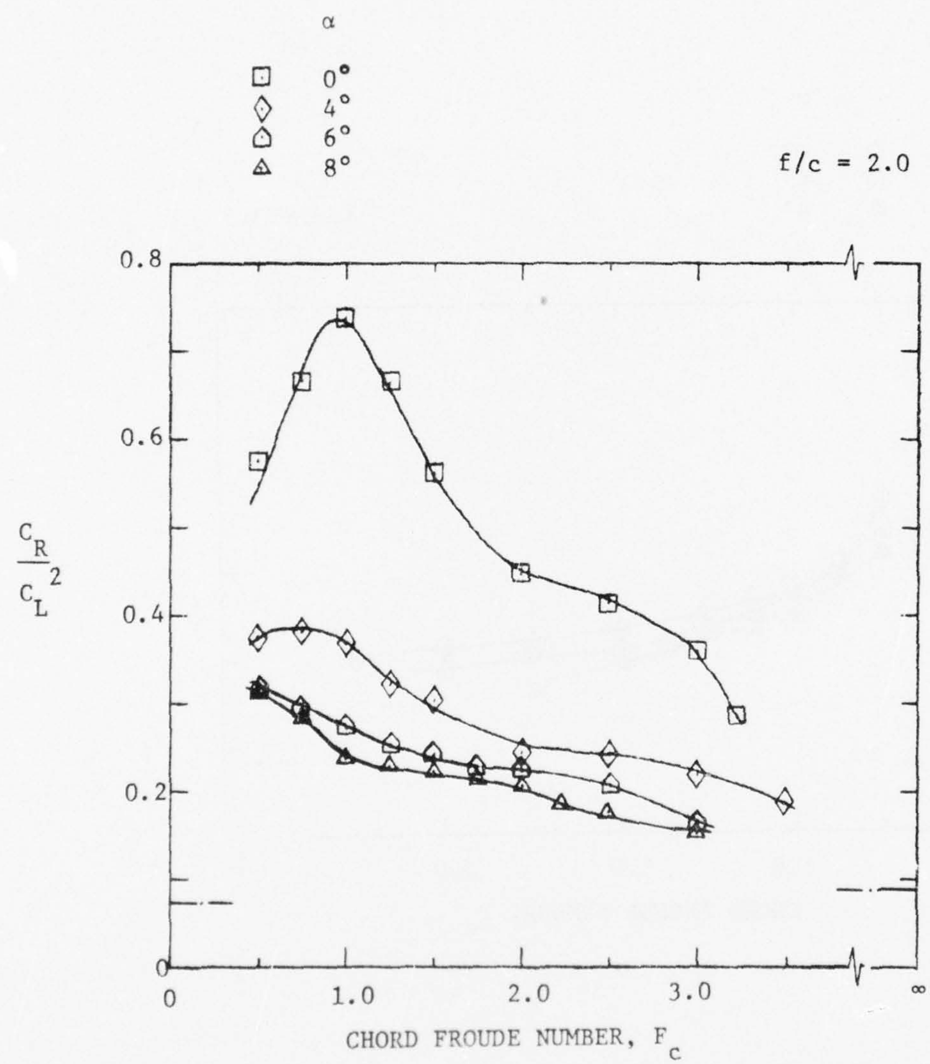

Figure 40 - Residual Drag Coefficient Ratio Versus Chord Froude Number for Submergence Ratio f/c = 2.0

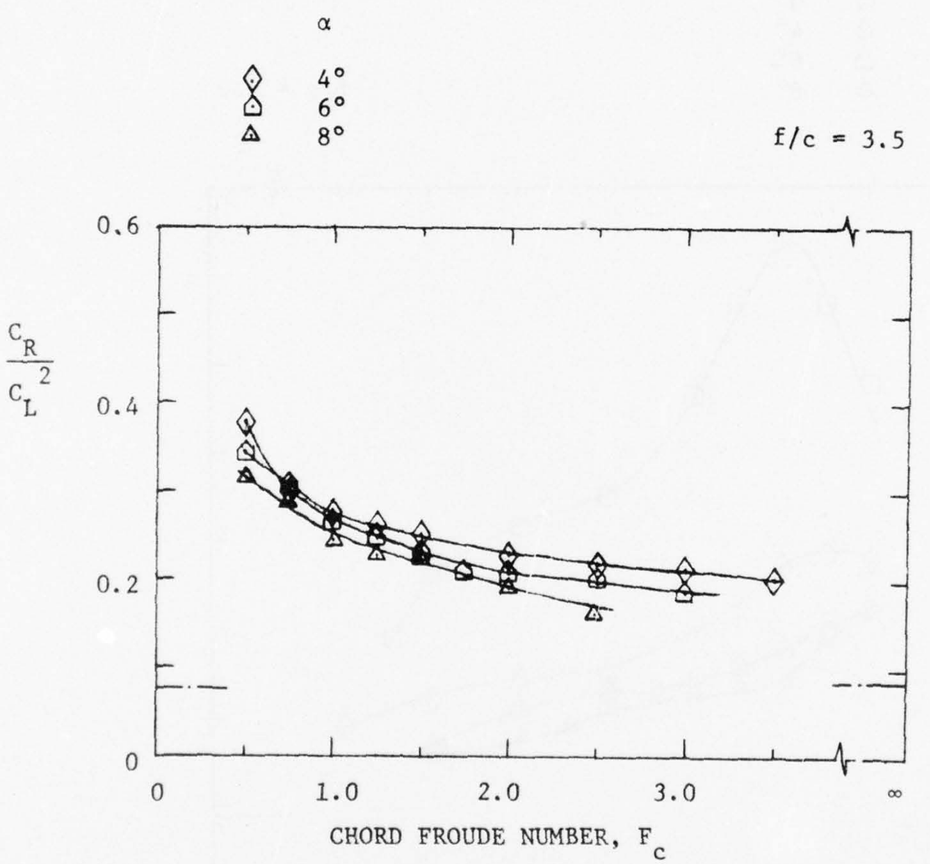

Figure 41 - Residual Drag Coefficient Ratio Versus Chord Froude Number for Submergence Ratio f/c = 3.5

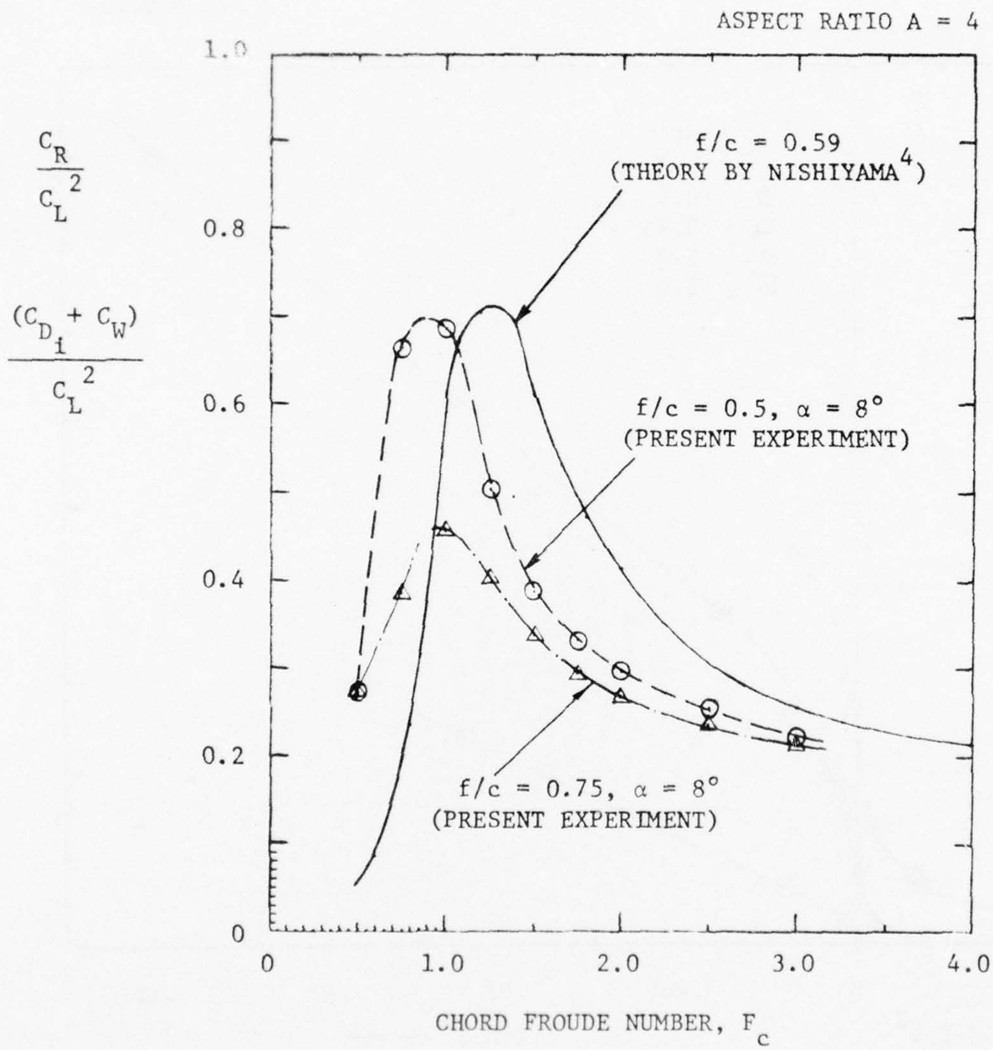

Figure 42 - Comparison of Theoretical Inviscid Drag Coefficient Ratio with Experimental Residual Drag Coefficient Ratio for a Rectangular Hydrofoil

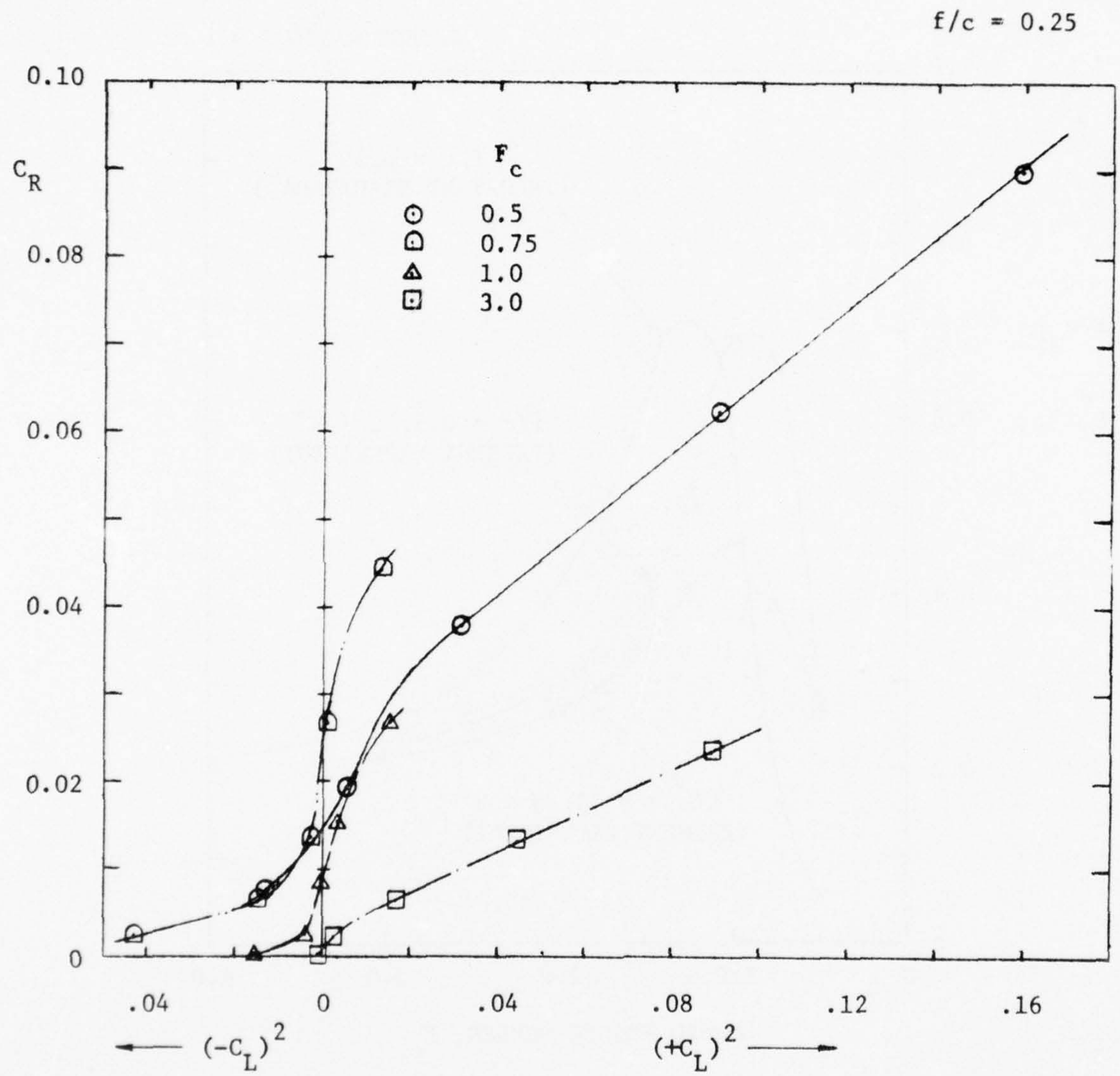

Figure 43 - Residual Drag Coefficient Versus Lift Coefficient Squared for Submergence Ratio f/c = 0.25

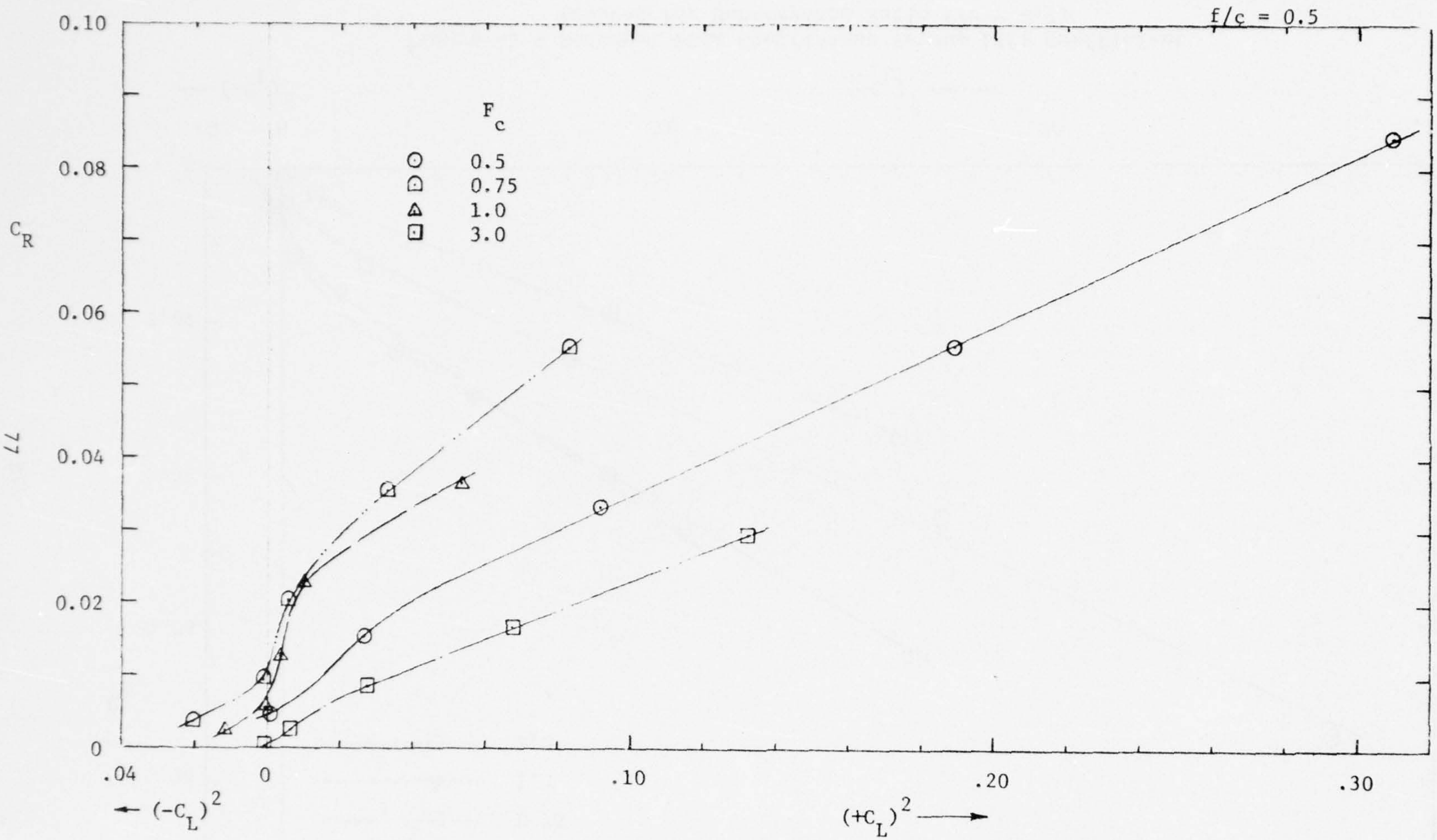

Figure 44 - Residual Drag Coefficient Versus Lift Coefficient Squared for Submergence Ratio f/c = 0.5

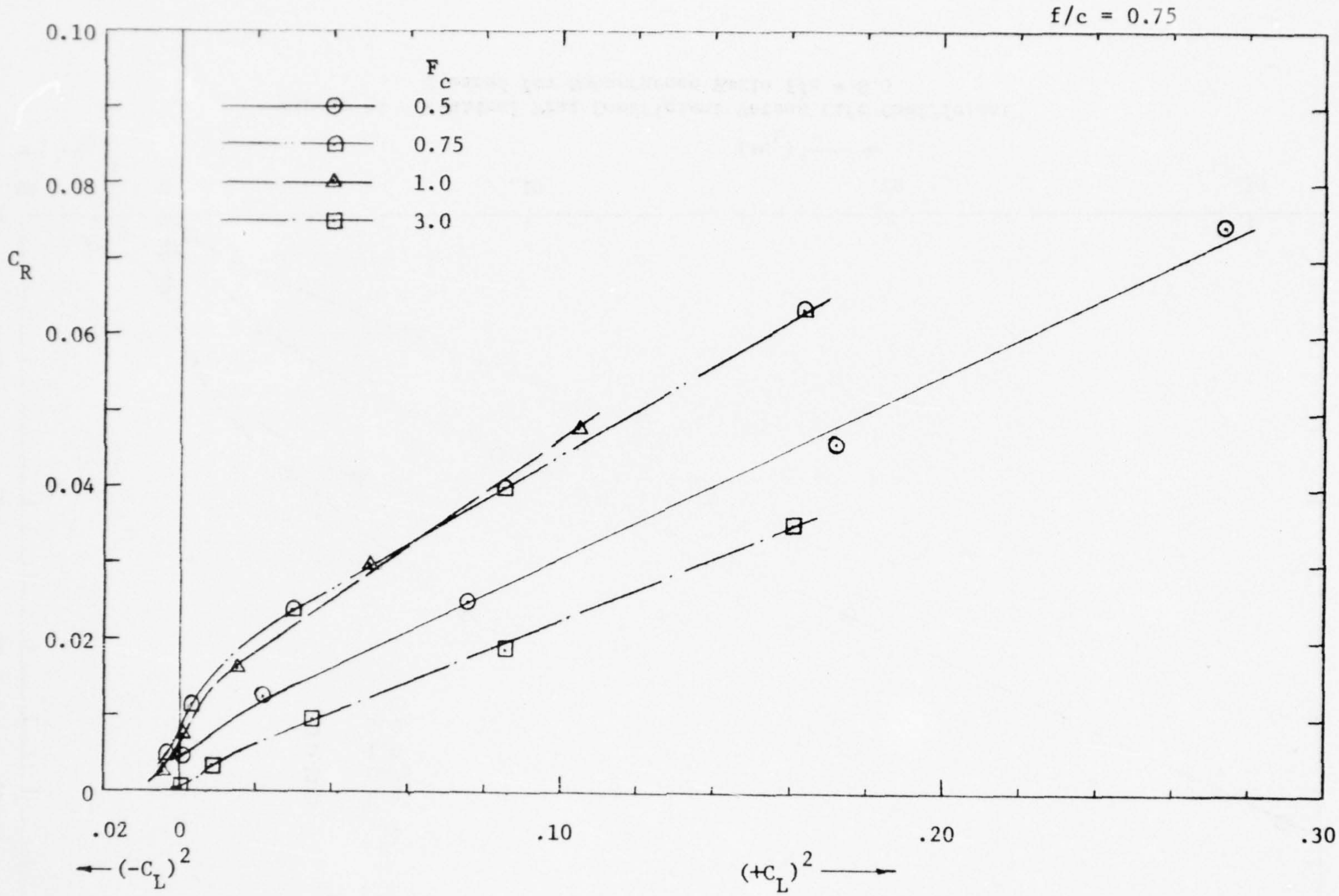

Figure 45 - Residual Drag Coefficient Versus Lift Coefficient Squared for Submergence Ratio f/c = 0.75

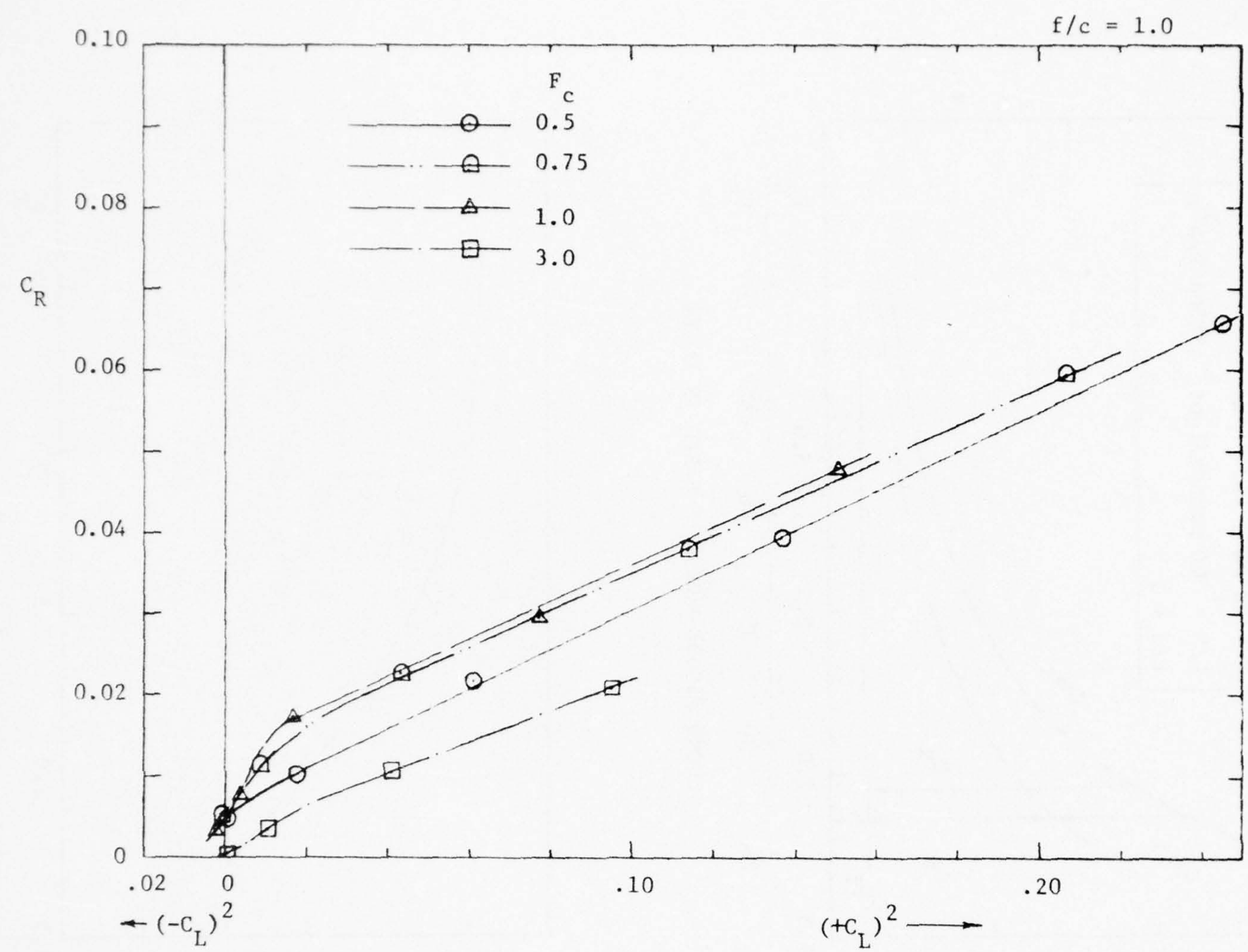

Figure 46 - Residual Drag Coefficient Versus Lift Coefficient Squared for Submergence Ratio f/c = 1.0

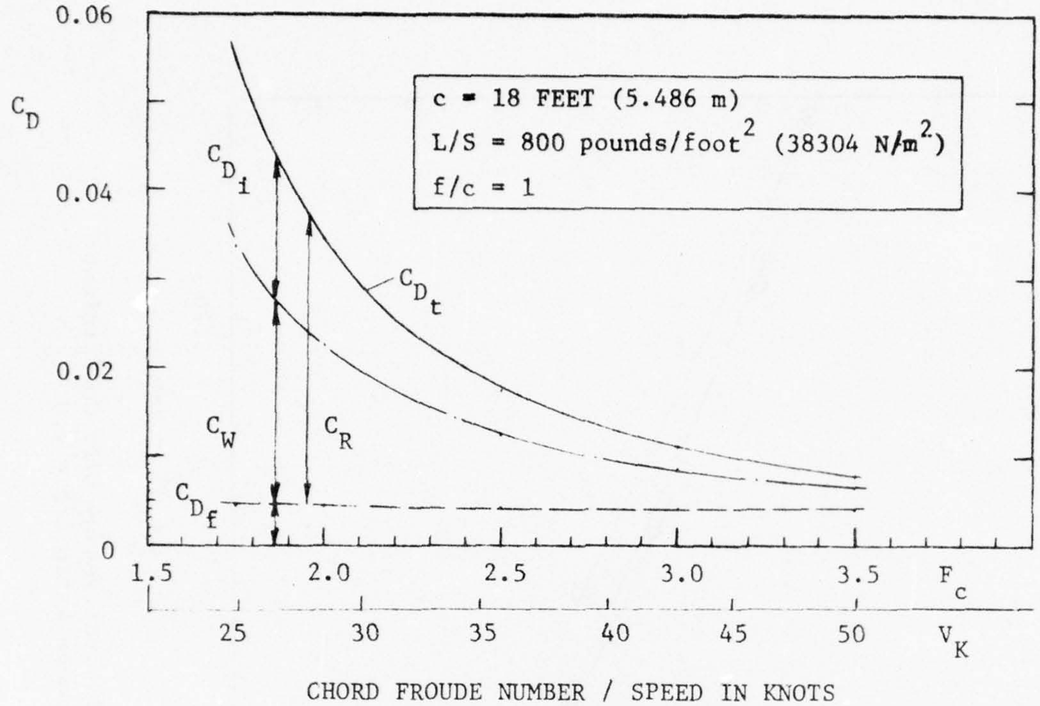

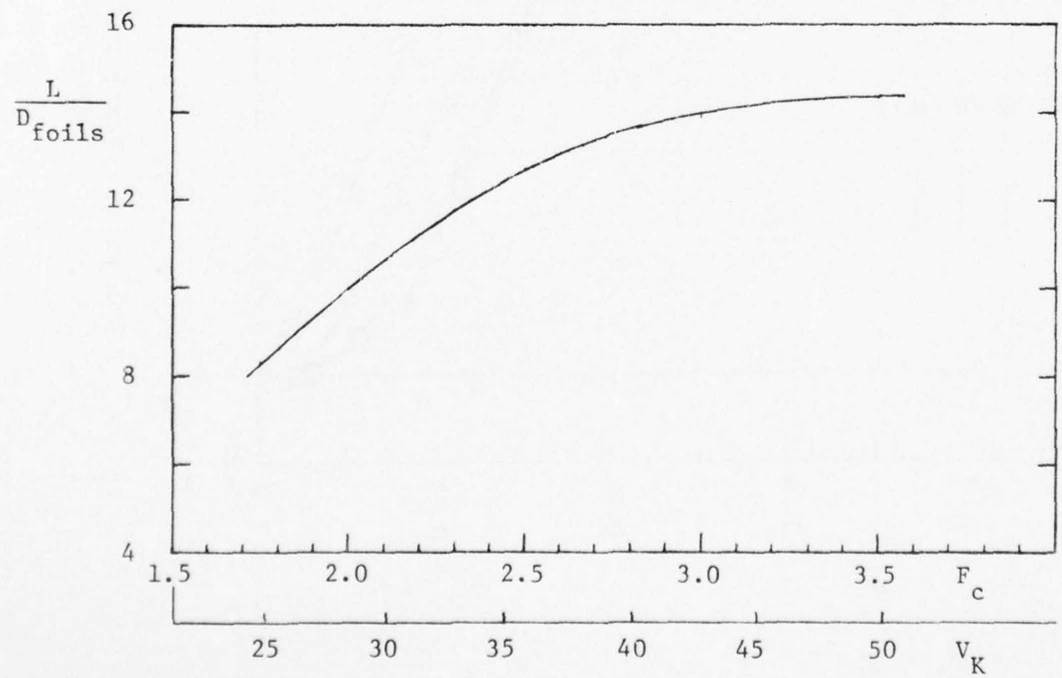

Figure 47 – Projected Drag Coefficient Breakdown and Lift-to-Drag Ratio for an 18-Foot-Chord Hydrofoil at Constant Lift Loading

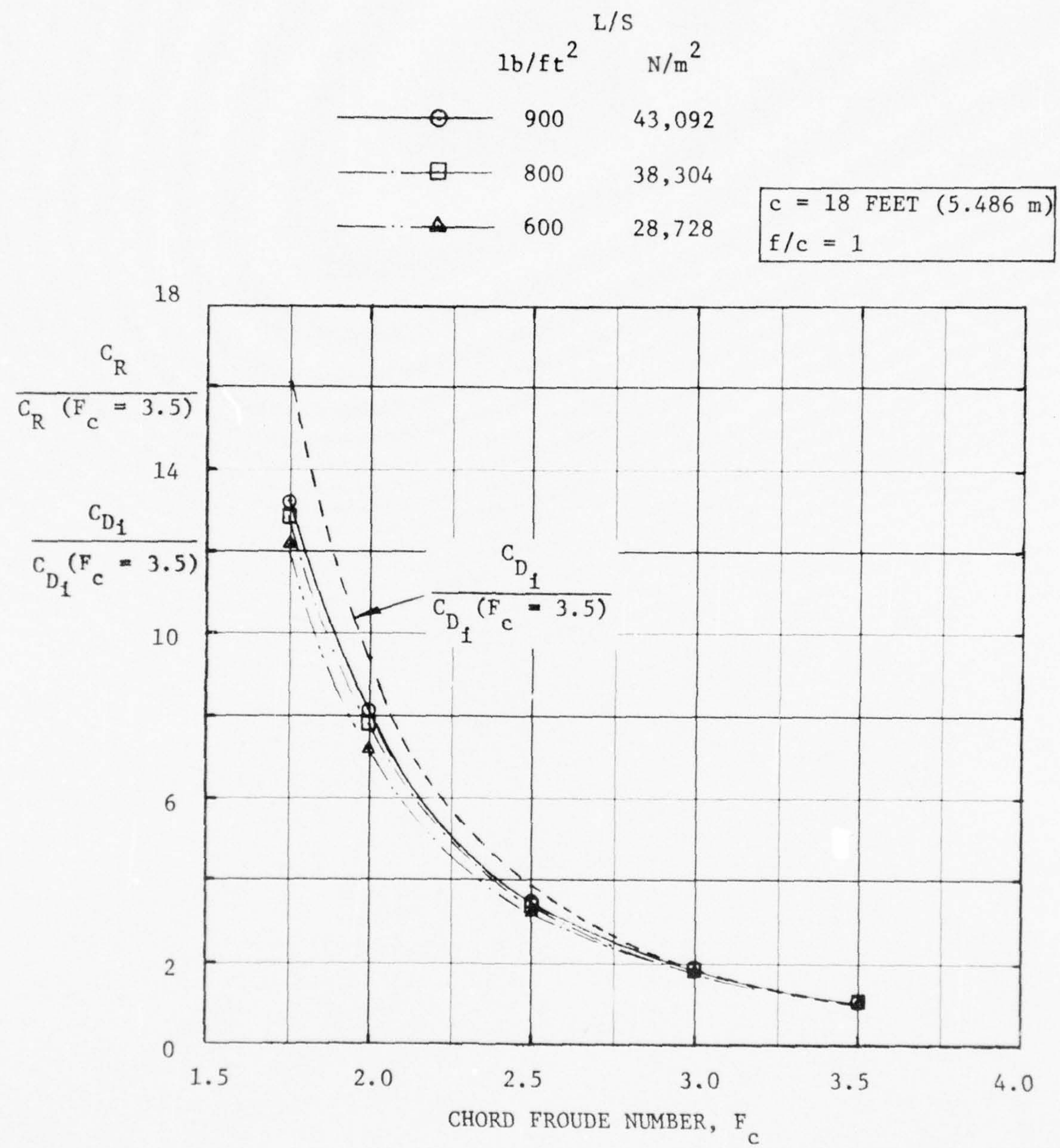

Figure 48 - Comparison of Induced Drag Ratio with Residual Drag Ratio Versus Chord Froude Number at Several Lift Loadings

APPENDIX A - TABLE OF MEASURED FORCES AND MOMENT

APPENDIX A - TABLE OF MEASURED FORCES AND MOMENT						
SUBMERGENCE RATIO $f/c = 0.25$						
ANGLE OF ATTACK α DEGREES	NOMINAL SPEED U FT/SEC	MEAS'D F_c	C_L	C_D	C_M	$\frac{x_{cp}}{c}$
0	4	.5	-.1106	.02253	-.02838	
	6	.746	-.2076	.0165	.007956	
	8	.997	-.1249	.01358	.007866	
	10	1.25	-.08057	.01289	.005971	
	12	1.5	-.0562	.01236	.0045	
	16	1.99	-.03916	.01221	.002336	
	20	2.48	-.03199	.01195	.00148	
	24	2.98	-.02906	.01199	.001085	
2	4	.5	.07537	.03432	-.05835	1.024
	6	.746	-.11903	.02017	-.000852	.2428
	8	.997	-.06299	.01609	.003101	.3[illegible]45
	10	1.25	-.01939	.01497	.009847	.7578
	12	1.5	.009475	.01423	.008978	-.6975
	16	1.99	.03352	.01436	.007753	.01876
	20	2.48	.04523	.01396	.007263	.0894
	24	2.98	.0521	.0139	.006935	.1169
4	4	.499	.1788	.05292	-.0716	.6505
	6	.745	-.05157	.02805	-.003673	.1788
	8	.997	-.005532	.02181	.01093	2.225
	10	1.25	.03905	.01931	.01411	-.1114
	12	1.5	.07239	.01894	.01346	.064
	16	1.99	.1029	.01888	.01302	.1235
	20	2.48	.1191	.01822	.01291	.1417
	24	2.98	.1306	.01808	.01295	.1[illegible]03
	28	3.47	.1365	.01741	.01309	.1541

APPENDIX A - CONTINUED

SUBMERGENCE RATIO f/c = 0.25						
ANGLE OF ATTACK α DEGREES	NOMINAL SPEED U FT/SEC	MEAS'D F_c	C_L	C_D	C_M	$\frac{x_{cp}}{c}$
6	2	.248	.5305	.07047	.003406	.2436
	3	.374	.4908	.0859	-.06	.3722
	4	.5	.301 [a]	.07722 [a]	-.08181 [a]	.5218 [a]
	6	.746	.03203 [a]	.04086 [a]	-.01234 [a]	.6375 [a]
	8	.998	.06083 [a]	.02895 [a]	.01066 [a]	.07473 [a]
	10	1.25	.1042	.02616	.01695	.08733
	12	1.5	.1418	.02646	.01738	.1274
	16	1.99	.1788	.02603	.01792	.1498
	20	2.48	.1985	.02546	.01824	.1581
	24	2.98	.2115	.0249	.01862	.162
8	4	.5	.399 [a]	.1048 [a]	-.08934 [a]	.474 [a]
	6	.746	.118 [a]	.05826 [a]	-.02214 [a]	.4378 [a]
	8	.997	.1256	.04047	.01024	.1685
	10	1.25	.1695	.03689	.01914	.1371
	12	1.5	.2092	.03756	.02045	.1522
	16	1.99	.2493	.03612	.02218	.161
	20	2.48	.2752	.03551	.0237	.164
	24	2.98	.2986	.03544	.0249	.1666

[a] Average Value

AD-A034 535 DAVID W TAYLOR NAVAL SHIP RESEARCH AND DEVELOPMENT CE--ETC F/G 20/4
LOW FROUDE NUMBER HYDRODYNAMIC PERFORMANCE OF A FLAT PLATE HYDR--ETC(U)
DEC 76 M B WILSON, J R KELLEY

UNCLASSIFIED SPD-743-01 NL

2 OF 2
AD
A034535

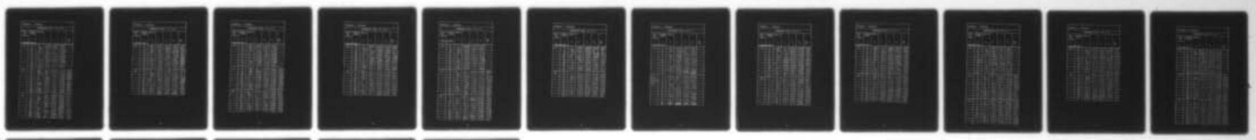

END
DATE
FILMED
2-77

APPENDIX A - CONTINUED

SUBMERGENCE RATIO f/c = 0.50

ANGLE OF ATTACK α DEGREES	NOMINAL SPEED U FT/SEC	MEAS'D F_c	C_L	C_D	C_M	$\frac{x_{cp}}{c}$
0	4	.5	.02204	.01958	-.03042	
	6	.746	-.14359	.01784	-.01363	
	8	.997	-.1092	.016	-.003289	
	10	1.25	-.06783	.01511	-.00299	
	12	1.5	-.0431	.01429	-.003189	
	14	1.75	-.03021	.01367	-.00363	
	16	1.99	-.02461	.01308	-.004083	
	20	2.48	-.01601	.01237	-.004315	
	24	2.98	-.01222	.01217	-.00457	
2	4	.499	.1627	.03029	-.03372	.4573
	6	.746	-.03515	.02328	-.01602	-.2059
	8	.997	-.0265	.01918	-.000626	.2264
	10	1.25	.00946	.01762	.001804	.05925
	12	1.5	.03387	.01649	.002584	.1737
	14	1.748	.04919	.01627	.002715	.1948
	16	1.99	.05725	.01562	.002512	.2061
	20	2.483	.07118	.01433	.002168	.2195
	24	2.98	.0794	.01436	.001901	.226
4	4	.5	.3026	.04838	-.03496	.3655
	6	.746	.07471	.03434	-.01853	.498
	8	.997	.05767	.02604	.002042	.2146
	10	1.25	.08862	.02318	.006361	.1782
	12	1.5	.11426	.02196	.008043	.1796
	14	1.749	.131	.02174	.008829	.1826
	16	1.99	.1409	.02108	.008794	.1876
	20	2.48	.157	.02044	.00902	.1925
	24	2.98	.1662	.02041	.008968	.19605

APPENDIX A - CONTINUED

SUBMERGENCE RATIO $f/c = 0.50$

ANGLE OF ATTACK α DEGREES	NOMINAL SPEED U FT/SEC	MEAS'D F_c	C_L	C_D	C_M	$\frac{x_{cp}}{c}$
6	4	.499	.4348	.07058	-.03247	.3247
	6	.745	.1814	.04964	-.02143	.3682
	8	.996	.1415	.03637	.003893	.2225
	10	1.25	.1666	.03199	.011002	.184
	12	1.5	.1918	.03036	.013503	.1796
	14	1.748	.2132	.0297	.01445	.1822
	16	1.99	.2238	.02901	.014724	.1842
	20	2.48	.2446	.02855	.01529	.1875
	24	2.98	.2594	.02863	.01551	.1902
8	4	.5	.5567	.09913	-.03177	.307
	6	.746	288	.06923	-.02304	.33
	8	.997	.2308	.05015	.005266	.2272
	10	1.25	.2487	.04431	.01459	.19134
	12	1.5	.2735	.04197	.01771	.1852
	14	1.746	.2948	.04136	.01906	.1854
	16	1.99	.3093	.04083	.01954	.1868
	20	2.48	.3324	.04044	.02027	.18902
	24	2.98	.3636	.04121	.02198	.1896

APPENDIX A - CONTINUED

SUBMERGENCE RATIO f/c = 0.75						
ANGLE OF ATTACK α DEGREES	NOMINAL SPEED U FT/SEC	MEAS'D F_c	C_L	C_D	C_M	$\frac{x_{cp}}{c}$
0	4	.499	.02084	.01922	-.01912	
	6	.746	-.0604	.01901	-.01796	
	8	.997	-.07041	.0160	-.00897	
	10	1.25	-.04746	.0148	-.00709	
	12	1.5	-.03074	.01396	-.00654	
	16	1.99	-.01556	.013	-.00654	
	20	2.482	-.00788	.01234	-.006638	
	24	2.98	-.00469	.01229	-.00683	
2	4	.499	.148	.02728	-.01328	.3397
	6	.746	.05546	.02551	-.01595	.5376
	8	.997	.02621	.02067	-.00533	.4535
	10	1.25	.04208	.0187	-.00185	.29397
	12	1.5	.05756	.01754	-.000666	.2616
	16	1.99	.07512	.01619	-.000042	.2506
	20	2.482	.08506	.01541	.000326	.2472
	24	2.98	.09372	.0151	-.00034	.2536
4	4	.5	.27433	.03991	-.006112	.2723
	6	.746	.1711	.03794	-.013247	.3274
	8	.997	.12215	.02964	-.001697	.2639
	10	1.25	.1287	.026	.00339	.2236
	12	1.5	.1449	.0241	.00539	.2128
	16	1.99	.1658	.02245	.00648	.2109
	20	2.48	.178	.02153	.006675	.2125
	24	2.98	.1873	.02152	.00666	.2144

APPENDIX A - CONTINUED

SUBMERGENCE RATIO f/c = 0.75						
ANGLE OF ATTACK α DEGREES	NOMINAL SPEED U FT/SEC	MEAS'D F_c	C_L	C_D	C_M	$\frac{x_{cp}}{c}$
6	4	.5	.4147	.06076	-.00176	.25425
	6	.7457	.291	.05405	-.01082	.2872
	8	.997	.2234	.04333	.001572	.243
	10	1.25	.223	.03808	.0080	.21412
	12	1.5	.2352	.03473	.01052	.20524
	14	1.75	.2486	.03283	.011857	.2023
	16	1.99	.258	.03195	.0124	.2019
	20	2.48	.2757	.03021	.01241	.20477
	24	2.98	.292	.0304	.01301	.20544
8	4	.499	.5233	.08919	.001413	.2473
	6	.745	.4047	.07735	-.008416	.2708
	8	.996	.3229	.06135	.00435	.2365
	10	1.25	.3136	.05292	.01219	.2111
	12	1.5	.3248	.04865	.01577	.2014
	14	1.747	.3405	.04673	.01696	.2002
	16	1.99	.3505	.04543	.01777	.1993
	20	2.48	.3701	.0446	.01904	.1986
	24	2.981	.401	.04688	.02262	.1936

APPENDIX A - CONTINUED

SUBMERGENCE RATIO f/c = 1.0

ANGLE OF ATTACK α DEGREES	NOMINAL SPEED U FT/SEC	MEAS'D F_c	C_L	C_D	C_M	$\frac{x_{cp}}{c}$
0	4	.5	.002444	.01991	-.01434	
	6	.747	-.03315	.01942	-.01618	
	8	.998	-.05143	.0167	-.01113	
	10	1.25	-.04051	.01525	-.00919	
	12	1.5	-.02684	.01436	-.00857	
	16	1.99	-.01447	.01329	-.008594	
	20	2.48	-.008346	.01238	-.008527	
	24	2.98	-.005346	.01233	-.008717	
	28	3.48	-.006046	.0113	-.008631	
2	4	.5	.1314	.02518	-.006998	.3032
	6	.745	.09299	.02517	-.01116	.37
	8	.997	.05944	.02129	-.006	.3509
	10	1.25	.0599	.01925	-.003327	.3056
	12	1.5	.06979	.01794	-.00202	.279
	16	1.99	.08538	.01665	-.00155	.2682
	20	2.48	.0944	.0153	-.001385	.2647
	24	2.98	.1006	.01522	-.00193	.2642
	28	3.47	.1056	.0149	-.002017	.2691
4	4	.5	.247	.03663	.002723	.239
	6	.746	.2076	.03667	-.004535	.2718
	8	.996	.164	.0307	-.0009686	.2559
	10	1.25	.1584	.02767	.002264	.2357
	12	1.5	.1669	.02587	.004252	.2245
	16	1.99	.1802	.02353	.005448	.2198
	20	2.48	.1912	.0226	.005521	.2211
	24	2.98	.2009	.02233	.005678	.2217
	28	3.47	.2099	.02246	.005659	.223

APPENDIX A - CONTINUED						
SUBMERGENCE RATIO f/c = 1.0						
ANGLE OF ATTACK α DEGREES	NOMINAL SPEED U FT/SEC	MEAS'D F_c	C_L	C_D	C_M	$\frac{x_{cp}}{c}$
6	4	.5	.3698	.05404	.005939	.2339
	6	.745	.3376	.05204	-.001	.253
	8	.997	.2779	.04303	.002996	.2392
	10	1.25	.2601	.0385	.007242	.2222
	12	1.5	.2667	.03577	.0098	.2133
	14	1.75	.2747	.03576	.0106	.2144
	16	1.99	.28	.0332	.01108	.2104
	20	2.48	.2924	.03242	.01155	.2105
	24	2.98	.3083	.03263	.01231	.2101
8	4	.5	.495	.08065	.01047	.2288
	6	.745	.4548	.07343	.004256	.2406
	8	.996	.3877	.06136	.007724	.2301
	10	1.25	.3618	.05491	.01237	.2158
	12	1.5	.3627	.0506	.01497	.2037
	14	1.75	.3732	.04879	.01622	.2065
	16	1.99	.3787	.04742	.01713	.2048
	20	2.48	.3974	.04683	.0182	.2042
	22	2.72	.4108	.04766	.0189	.204

APPENDIX A - CONTINUED

SUBMERGENCE RATIO f/c = 1.5

ANGLE OF ATTACK α DEGREES	NOMINAL SPEED U FT/SEC	MEAS'D F_c	C_L	C_D	C_M	$\frac{x_{cp}}{c}$
0	2	.247	-.0025	.01987	-.008015	
	3	.374	-.001093	.0187	-.0105	
	4	.5	.004281	.01831	-.01108	
	6	.746	-.003569	.0179	-.013	
	8	.99	-.01794	.01643	-.01222	
	10	1.25	-.01867	.01495	-.01073	
	12	1.5	-.01306	.01399	-.0103	
	14	1.746	-.007312	.01332	-.010	
	20	2.48	-.002036	.01258	-.009671	
	24	2.98	.000258	.01222	-.00974	

0	2	.248	.02983	.01823	-.008751	
(Without	3	.374	.01308	.01688	-.01159	
Stimulator	4	.5	.01589	.01655	-.01125	
Wire)	6	.746	.00384	.01516	-.01288	
	8	.997	-.01061	.01368	-.01146	
	10	1.25	-.01556	.01234	-.01	
	12	1.5	-.00585	.01169	-.00921	
	14	1.746	-.000652	.01124	-.0088	
	16	1.99	.00174	.0109	-.00894	
	20	2.48	.006308	.01041	-.0088	
	24	2.98	.008903	.01006	-.008763	

APPENDIX A - CONTINUED

SUBMERGENCE RATIO f/c = 1.5

ANGLE OF ATTACK α DEGREES	NOMINAL SPEED U FT/SEC	MEAS'D F_c	C_L	C_D	C_M	$\frac{x_{cp}}{c}$
2	2	.248	.118	.02532	-.003158	.2768
	3	.374	.1193	.02375	-.003514	.2794
	4	.5	.1198	.02263	-.003763	.2814
	6	.745	.1164	.02233	-.00629	.304
	8	.997	.09533	.02026	-.005396	.3066
	10	1.25	.08881	.01857	-.00425	.2978
	12	1.5	.09124	.01753	-.003518	.2886
	14	1.746	.09578	.01689	-.002984	.2812
	16	1.99	.09756	.01641	-.002818	.2789
	20	2.48	.1018	.01616	-.002576	.2753
	24	2.98	.1086	.0157	-.002897	.2767
4	2	.247	.2253	.03359	.005138	.2272
	3	.374	.234	.03331	.005385	.227
	4	.499	.2357	.03289	.004	.233
	6	.746	.2302	.03153	.0011	.2452
	8	.997	.2107	.02864	.00114	.2446
	10	1.25	.1983	.02611	.002528	.2373
	12	1.5	.1981	.02477	.00332	.2332
	16	1.99	.2032	.0234	.00398	.2304
	20	2.48	.2081	.02293	.004343	.2291
	24	2.98	.215	.0229	.004092	.231

APPENDIX A - CONTINUED

SUBMERGENCE RATIO f/c = 1.5

ANGLE OF ATTACK α DEGREES	NOMINAL SPEED U FT/SEC	MEAS'D F_c	C_L	C_D	C_M	$\frac{x_{cp}}{c}$
6	2	.248	.379	.05664	.008251	.2282
	3	.374	.3716	.05093	.01243	.2166
	4	.499	.3595	.04771	.01137	.2184
	6	.745	.357	.04321	.008445	.2263
	8	.996	.3314	.04035	.00765	.2269
	10	1.25	.3131	.03713	.00863	.2224
	12	1.5	.307	.03531	.009854	.2179
	16	1.99	.3126	.03388	.0102	.2174
	20	2.48	.3203	.03321	.01074	.2165
	24	2.98	.334	.0333	.01164	.2151
8	2	.248	.4606	.0851	-.0012	.2526
	3	.375	.4657	.08157	.0092	.2302
	4	.5	.4628	.07334	.01275	.2224
	6	.746	.4642	.07078	.01131	.2256
	8	.996	.439	.06616	.01226	.2221
	10	1.25	.4085	.06448	.01458	.2143
	12	1.5	.4024	.05991	.01598	.2103
	16	1.99	.4186	.04871	.01644	.2107
	20	2.48	.4327	.04762	.01715	.2104
	24	2.98	.3946	.04388	.02091	.1973

APPENDIX A - CONTINUED

SUBMERGENCE RATIO $f/c = 2.0$

ANGLE OF ATTACK α DEGREES	NOMINAL SPEED U FT/SEC	MEAS'D F_c	C_L	C_D	C_M	$\frac{x_{cp}}{c}$
0	4	.5	.007951	.01769	-.011506	
	6	.746	.006032	.01776	-.01188	
	8	.997	-.003686	.0168	-.011594	
	10	1.25	-.006348	.01548	-.01089	
	12	1.5	-.004194	.01445	-.0106	
	13.4	1.67	-.002633	.01408	-.01043	
	16	1.99	-.000617[a]	.01396[a]	-.0107[a]	
	20	2.49	-.003[a]	.0125[a]	-.011[a]	
	24	2.98	.00342[a]	.01161[a]	-.0103[a]	
	28	3.47	.0008	.0119	-.01028	
2	4	.5	.124	.02375	-.00353	.2785
	6	.746	.12	.02366	-.00422	.2852
	8	.997	.1111	.02261	-.004029	.2862
	10	1.25	.1035	.02027	-.003852	.2872
	12	1.5	.1046	.019	-.003531	.2837
	16	1.99	.1052	.01739	-.00272	.2759
	20	2.48	.1084	.01696	-.002928	.277
	24	2.98	.1113	.01633	-.00228	.2705
	26	3.23	.1169	.01565	-.003296	.2782
4	4	.5	.2229	.03359	.00396	.2322
	6	.746	.2265	.0336	.002849	.2374
	8	.997	.2199	.03139	.002267	.2397
	10	1.25	.2154	.02803	.002859	.2367
	12	1.5	.2116	.0264	.003523	.2333
	16	1.99	.2133	.02355	.00401	.2312
	20	2.48	.2188	.0237	.003169	.2355
	24	2.98	.2279	.02326	.003369	.2352
	[illegible]	3.47	.2389	.02233	.003216	.2361

APPENDIX A - CONTINUED

SUBMERGENCE RATIO f/c = 2.0

ANGLE OF ATTACK α DEGREES	NOMINAL SPEED U FT/SEC	MEAS'D F_c	C_L	C_D	C_M	$\frac{x_{cp}}{c}$
6	4	.5	.3375	.05115	.01085	.2179
	6	.746	.3422	.04845	.00976	.2215
	8	.997	.3355	.04417	.009103	.2226
	10	1.25	.3244	.03956	.009184	.2217
	12	1.5	.3219	.03789	.009917	.2192
	14	1.747	.3224	.03636	.01038	.2178
	16	1.99	.321	.03541	.01035	.2178
	20	2.48	.3298	.0346	.01084	.2171
	24	2.98	.3576	.0326	.0105	.2206
8	4	.5	.4437	.07621	.01249	.2218
	6	.746	.451	.07175	.0143	.2183
	8	.996	.4504	.06203	.01552	.2155
	10	1.25	.4387	.05741	.01543	.2148
	12	1.5	[illegible]	.05446	.01604	.213
	14	1.747	.4338	.05243	.01666	.2116
	16	1.99	.4341	.05127	.01675	.2114
	18	2.24	.4499	.04956	.01661	.2131
	20	2.48	.4544[a]	.04895[a]	.01726[a]	.2126
	22	2.72	.4832	.04756	.01869	.2113

APPENDIX A - CONTINUED

SUBMERGENCE RATIO f/c = 3.5

ANGLE OF ATTACK α DEGREES	NOMINAL SPEED U FT/SEC	MEAS'D F_c	C_L	C_D	C_M	$\frac{x_{cp}}{c}$
0	4	.5	.00142	.01632	-.0102	
	6	.745	.00288 [a]	.01718 [a]	-.0114 [a]	
	8	1.0	.00253 [a]	.0162 [a]	-.0111 [a]	
	10	1.25	.00034 [a]	.01514 [a]	-.011 [a]	
	12	1.5	.00064 [a]	.01434 [a]	-.0111 [a]	
	16	1.99	.00087 [a]	.01373 [a]	-.0111 [a]	
	20	2.49	-.00006 [a]	.01296 [a]	-.0111 [a]	
	24	2.98	.00057 [a]	.01262 [a]	-.0112 [a]	
	28	3.48	-.00137 [a]	.01192 [a]	-.0113 [a]	
2	4	.5	.1178	.02103	-.004847	.2917
	6	.744	.1208	.01968	-.00414	.2843
	8	1.0	.1179	.01954	-.003567	.2803
	10	1.25	.1155	.01903	-.003392	.2794
	12	1.5	.1149	.01806	-.003349	.2791
	16	1.99	.114	.01706	-.0033	.279
	20	2.48	.116	.01639	-.00337	.279
	24	2.98	.1175	.0164	-.003772	.2821
	28	3.47	.12	.01629	-.00422	.2852
4	4	.5	.2337	.03566	.003764	.2333
	6	.744	.2347	.03056	.00406	.2327
	8	.998	.2362	.02884	.004116	.2326
	10	1.25	.2334	.02741	.004126	.2323
	12	1.5	.2308	.02624	.003865	.2333
	16	1.99	.2295	.02447	.003854	.2332
	20	2.48	.2292	.02367	.00345	.2349
	24	2.98	.2375	.02376	.00341	.2356
	28	3.47	.2456	.02377	[illegible]	.2376

APPENDIX A - CONTINUED

SUBMERGENCE RATIO f/c = 3.5

ANGLE OF ATTACK α DEGREES	NOMINAL SPEED U FT/SEC	MEAS'D F_c	C_L	C_D	C_M	$\frac{x_{cp}}{c}$
6	4	.5	.3357	.05345	.01257	.2125
	6	.746	.3353	.04851	.01208	.214
	8	.997	.339	.04438	.01161	.2158
	10	1.25	.3404	.04177	.01138	.2166
	12	1.5	.34	.03943	.01141	.2164
	14	1.747	.3477	.03743	.011388	.2172
	16	1.99	.3411	.03676	.011	.2177
	20	2.48	.3442	.0357	.01084	.2185
	24	2.98	.3604	.036	.01162	.2178
8	4	.5	.4631	.08198	.01125	.2257
	6	.745	.444	.07078	.01558	.214[illegible]
	8	.996	.4495	.06296	.01629	.2138
	10	1.25	.455	.06056	.01643	.2139
	12	1.5	.4523	.05869	.01655	.21[illegible]
	16	1.99	.4563	.05223	.01765	.2113
	20	2.48	.4825	.05013	.01749	.2137

APPENDIX B - ZERO AND INFINITE FROUDE NUMBER LIMITS OF HYDROFOIL DRAG DUE-TO-LIFT

APPENDIX B

ZERO AND INFINITE FROUDE NUMBER LIMITS OF HYDROFOIL DRAG DUE-TO-LIFT

The expressions for the drag coefficient due-to-lift in the limits of infinite and zero Froude number given in Equations (8) and (9), respectively, contain the biplane function $\sigma(\lambda)$. This function depends solely on the parameter λ which for rectangular planforms is

$$\lambda = \frac{2}{A} \frac{f}{c}$$

A formula for $\sigma(\lambda)$ valid for elliptic foil loading can be deduced from results discussed by Wu[2]

$$\sigma(\lambda) = 1 - \frac{4\lambda}{\pi} \sqrt{1 + \lambda^2} \; [K(k) - E(k)]$$

where $k = (1 + \lambda^2)^{-1/2}$

K(k) and E(k) = complete elliptic integral of first and second kind, respectively

Approximating formulas for K(k) and E(k) are given by Dwight[16] and have been used to obtain the table values of C_{D_i}/C_L^2 at $F_c \to 0$ and $F_c \to \infty$.

ZERO AND INFINITE FROUDE NUMBER LIMITS OF C_{D_i}/C_L^2

f/c	λ	$\sigma(\lambda)$	Zero F_c: $\frac{1 + \delta - \sigma}{\pi A}$	Infinite F_c: $\frac{1 + \delta + \sigma}{\pi A}$
0.25	0.125	0.6	0.0342	0.1297
0.5	0.25	0.42	0.0485	0.1154
0.75	0.375	0.31	0.0573	0.1066
1.0	0.5	0.232	0.0635	0.1004
1.5	0.75	0.14	0.0708	0.0931
2.0	1.0	0.091	0.0747	0.0892
3.5	1.75	0.0393	0.0788	0.0851

REFERENCES

1. Nishiyama, T., "Linearized Steady Theory of Fully Wetted Hydrofoils," Advances in Hydroscience, Vol.3, Edited by Ven Te Chow, Academic Press, 1966, pp 237-342.

2. Wu, T. Y-t, "A Theory for Hydrofoils with Finite Span," California Institute of Technology Hydrodynamics Lab Report No. 26-8, 1953.

3. Breslin, J. P. , "Application of Ship-Wave Theory to the Hydrofoil of Finite Span," Journal of Ship Research, Vol. 1, No. 1, 1957, pp 27-35.

4. Nishiyama, T., "Lifting-Line Theory of the Submerged Hydrofoil of Finite Span," American Society of Naval Engineers Journal, Aug 1959, pp 511-518.

5. Wadlin, K. L., C. L. Shuford and J. R. McGehee, "A Theoretical and Experimental Investigation of Hydrofoils at Subcritical and Supercritical Speeds," NACA Report 1232, 1955.

6. Feldman, J., "Experimental Investigation of Near-Surface Hydrodynamic Force Coefficients for a Systematic Series of Tee Hydrofoils, DTMB Series HF-1," DTMB Report 1801, Dec 1963.

7. Layne, D., "Lift and Drag Characteristics of NACA 16-309 and NACA 64A309 Hydrofoils," DTNSRDC Ship Peformance Department Report SPD-326-07, Oct 1976.

8. Schlichting, H., Boundary Layer Theory, McGraw-Hill Book Co., 1960

9. Seely, F. S. and J. O. Smith, Advanced Mechanics of Materials, 2nd Edition, John Wiley and Sons, 1965.

10. Acevedo, M. L. and L. Mazarredo, Editors, "Proceedings of Eighth International Towing Tank Conference (1957)," Canal de Experiencias Hidrodinamicas, El Pardo, Spain, 1959.

11. Parkin, B. R., B. Perry and T.Y-t Wu, "Pressure Distribution on a Hydrofoil Running Near the Water Surface," California Institute of Technology Hydrodynamics Lab Report 47-2, April 1955.

12. von Mises, R., Theory of Flight, Dover Publications, New York, 1959.

13. Granville, P. S., "Drag and Turbulent Boundary Layer of Flat Plates at Low Reynolds Numbers," DTNSRDC Report 4682, Dec 1975.

14. Wadlin, K. L., J. A. Ramsen, and V. L. Vaughan, Jr., "The Hydrodynamic Characteristics of Modified Rectangular Flat Plates Having Aspect Ratios of 1.0, 0.25, and 0.125 and Operating Near a Free Water Surface," NACA Report 1246, 1955.

15. Glauert, H., The Elements of Aerofoil and Airscrew Theory, Cambridge University Press, 1959.

16. von Kármán, T. and J. M. Burgers, "General Aerodynamic Theory - Perfect Fluids," Vol. II of Aerodynamic Theory Edited by W. F. Durand, Dover Publications, 1963.

INITIAL DISTRIBUTION

Copies	
10	ANVCE Op 096V, Capt Meeks
1	NAVMAT
	1 0333, Vittucci
11	NAVSEC
	1 6110, Leopold
	1 6114, Johnson
	1 6114P, Kerr
	2 6120, Capt Bress
	Hunley
	3 6136, Keane
	Goldstein
	Conrad
	1 6141B, Graves
	1 6144, Welling
	1 6144E, Lombardi
13	NAVSEA
	1 03
	1 032, Albee
	3 0322, Schuler
	Benen
	Dilts
	1 033
	2 0331, Chaikin
	Miller
	1 035, Sorkin
	1 0351, Peirce
	1 PMS 300, Capt Kurzenhauser
	1 PMS 304.20, Schuldenfrei
	1 PMS 304.31B
12	DDC
8	ABC
2	Boeing Marine Systems, Ray
2	Grumman Marine Systems, Pieroth
2	Stevens Institute of Technology

CENTER DISTRIBUTION

Copies	Code
1	15
1	1507
1	1509
1	152
1	154
1	156
1	1524
1	1532
2	1532, Denny
1	1544
1	11
1	1150
1	1151
1	1153
1	1140
1	1170
1	1180
1	272, Quandt
1	1556, Layne

DTNSRDC ISSUES THREE TYPES OF REPORTS

(1) DTNSRDC REPORTS, A FORMAL SERIES PUBLISHING INFORMATION OF PERMANENT TECHNICAL VALUE, DESIGNATED BY A SERIAL REPORT NUMBER.

(2) DEPARTMENTAL REPORTS, A SEMIFORMAL SERIES, RECORDING INFORMATION OF A PRELIMINARY OR TEMPORARY NATURE, OR OF LIMITED INTEREST OR SIGNIFICANCE, CARRYING A DEPARTMENTAL ALPHANUMERIC IDENTIFICATION.

(3) TECHNICAL MEMORANDA, AN INFORMAL SERIES, USUALLY INTERNAL WORKING PAPERS OR DIRECT REPORTS TO SPONSORS, NUMBERED AS TM SERIES REPORTS; NOT FOR GENERAL DISTRIBUTION.